DOE/BC/14600-10
Distribution Category UC-122

Transient Behavior of Simultaneous Flow of Gas and Surfactant Solution in Consolidated Porous Media

DOE/BC/14600--10
DE91 002249

Topical Report

By
Serge Y. Baghdikian
Lyman L. Handy

July 1991

Work Performed Under Contract No. FG22-90BC14600

Prepared for
U. S. Department of Energy
Assistant Secretary for Fossil Energy

Thomas B. Reid, Project Manager
Bartlesville Project Office
P. O. Box 1398
Bartlesville, OK 74005

Prepared by
University of Southern California
Departments of Chemical Engineering
and Petroleum Engineering
Los Angeles, CA 90089-1211

MASTER

DISTRIBUTION OF THIS DOCUMENT IS UNLIMITED

TABLE OF CONTENTS

LIST OF TABLES vi

LIST OF FIGURES vii

ABSTRACT x

1 INTRODUCTION 1

2 THEORY AND LITERATURE REVIEW 5

2.1 Structure of Foams 5

2.2 Foam Stability and Collapse 6

2.2.1 Foam Stability 7

2.2.1.1 Liquid Viscosity 7

2.2.1.2 Surface Viscosity 7

2.2.1.3 Marangoni Effect 8

2.2.1.4 Disjoining Pressure 8

2.2.2 Foam Drainage 9

2.2.3 Foam Collapse 10

2.3 Foam in Porous Media 12

2.3.1 Effect of Surfactant Properties on Foam 12

2.3.1.1 Type of Surfactant 13

2.3.1.2 Interfacial Tension 13

2.3.1.3 Surfactant Concentration 13

2.3.1.4 Effect of Temperature 14

2.3.1.5 Effect of Surfactant Loss 14

2.3.1.6 Effect of Salinity 15

2.3.1.7 Effect of Alcohol 15

2.3.2 Effect of Gas Properties on Foam 15

2.3.3 Foam Generation Mechanisms 16

2.3.3.1 Leave-Behind 16

2.3.3.2 Capillary Snap-Off 18

2.3.3.3 Lamella Division 18

2.3.4 Foam Coalescence Mechanisms 18

2.3.5 Foam Flow in Porous Media 19

2.3.5.1 Trapped Gas Saturation 19
2.3.5.2 Critical Pressure Gradient 20
2.3.5.3 Pseudoplastic Behavior of Foam 20
2.3.5.4 Gas Velocity 22
2.3.5.5 Liquid Velocity 24
2.3.5.6 Foam Quality 24
2.3.5.7 Foam Texture 25
2.3.5.8 Permeability of Porous Medium 25
2.3.5.9 Relative Permeability 25
2.3.5.10 Fluid Saturations 26
2.3.5.11 Capillary Pressure 26
2.3.5.12 Presence of Oil 29
2.3.5.13 Capillary Number 31
2.3.5.14 Wettability 31
2.3.5.15 Foam Propagation 32
2.3.5.16 Hysteresis 32
2.3.6 Foam in Micromodels 32
2.3.7 Foam in Capillary Tubes 33
2.4 Models for Foam Flow 33
2.5 Review of Foam Application in the Field 34
2.6 Biodegradation of Foaming Surfactants 35

3 EXPERIMENTAL MATERIALS AND PROCEDURES 37
3.1 Experimental Materials 37
3.1.1 Porous Media 37
3.1.2 Aqueous Phases 38
3.1.3 Oleic Phases 38
3.1.4 Gaseous Phase 39
3.2 Experimental Apparatus 39
3.2.1 Flow Set-Up 39
3.2.2 Temperature Monitoring System 42
3.2.3 Data Acquisition System 42
3.2.3.1 Hardware 42
3.2.3.2 Software 43
3.2.4 Extraction Apparatus 43
3.2.5 Spinning Drop Apparatus 43
3.3 Experimental Procedures 45
3.3.1 Flow experiments 45
3.3.1.1 Core Mounting 45
3.3.1.2 Porosity Measurements 45
3.3.1.3 Core Saturation 47
3.3.1.4 Permeability Measurements 47
3.3.1.5 Pressure Measurements 47
3.3.1.6 Foam Start-Up 48

3.3.1.7 Flow Rate Measurements 48
3.3.2 Oil Extraction 48
3.3.3 IFT Measurements 49

4 EXPERIMENTAL RESULTS **50**
4.1 Interfacial Tension Measurements 50
4.2 Oil Recovery with Foaming Solution. 50
4.3 Foam Generation and Propagation in Short Cores 56
4.3.1 Foam Incubation Period 56
4.3.2 Effect of Gas Velocity 59
4.3.3 Effect of Liquid Velocity 60
4.3.4 Hysteresis Effect 61
4.3.5 Effect of Foam Generator 62
4.4 Foam Generation and Propagation in Long Cores 62
4.4.1 Experiments Initiated with a Prefoamer 63
4.4.2 Experiments Initiated without a Prefoamer 65
4.4.3 Effect of Gas and Surfactant Velocities 75
4.4.4 Pressure Distributions with Foam Flow 78
4.4.5 Effect of Foam Generator 82
4.4.6 Hysteresis Effect 84

5 DISCUSSION **87**
5.1 Oil Recovery with Foaming Solution. 88
5.2 Unsteady State Results 91
5.2.1 Foam Mobilization without Prefoamer 92
5.2.2 Foam Mobilization with Prefoamer 93
5.2.3 Foam Mobilization in Short Cores 94
5.3 Steady State Results 94
5.4 Mechanisms of Foam Flow 96
5.4.1 Weak Foam Flow Regime 96
5.4.2 Strong Foam Flow Regime 98
5.4.3 Foam Mobilization Mechanisms 101
5.5 Field Application of Foam 103

6 CONCLUSIONS **106**

7 RECOMMENDED FUTURE WORK **109**

NOMENCLATURE **111**

REFERENCE LIST **113**

Appendix A
DATA ACQUISITION SYSTEM 123

LIST OF TABLES

4.1 Summary of Oil Displacement Results by Gas and Brine Injection. 54
4.2 Summary of Oil Displacement Results by Gas and Surfactant Solution Injection. 55

LIST OF FIGURES

2.1 Principal mechanisms of foam generation in porous media, after Friedmann et al. [43]. 17
2.2 Effect of frontal advance rate on pressure gradient due to foam in Berea sandstone cores, after Friedmann et al. [43]. 21
2.3 Critical velocity for foam generation in Berea sandstone cores during co-injection of nitrogen and surfactant solution, after Friedmann et al. [43]. 23
2.4 Effect of gas fractional flow on gas mobility, after Khatib et al. [72]. 24
2.5 Comparison of unsteady state relative permeabilities measured with and without foaming agent in brine, after Huh [62]. 27
2.6 Effect of liquid flow rate on steady state relative permeabilities (c = 0.2%), after Huh [62]. 28
2.7 Oil recovery under reservoir conditions, after Robin [108]. 31

3.1 Schematic diagram of experimental flow set-up. 40
3.2 Schematic diagram of Dean-Stark extraction apparatus. 44
3.3 Schematic diagram of end plug design, after Huh [62]. 46
3.4 Schematic diagram of core holder design, after Huh [62]. 46

4.1 Interfacial tension of 1% Chaser SD1000 in 2% NaCl with dodecane vs. temperature. 51
4.2 Interfacial tension of 0.5% LTS18 with dodecane vs. temperature. 51
4.3 Effect of time on IFT with dodecane for 1% LTS18. 52
4.4 Effect of temperature on IFT of 1% LTS18 with crude oil. 52
4.5 Steady state gas-brine relative permeability. 53
4.6 Oil saturation as a function of capillary number in oil displacement experiments. 55
4.7 Pressure gradient history with simultaneous flow of gas and surfactant solution without prefoamer. 57
4.8 Pressure gradient history with simultaneous flow of gas and surfactant solution with prefoamer at low gas velocity. 58
4.9 Pressure gradient histories with simultaneous flow of gas and surfactant solution with prefoamer at high gas velocities. 58
4.10 Pressure gradient history with simultaneous flow of gas and surfactant solution with prefoamer at high liquid velocity. 59
4.11 Pressure gradient versus gas velocity at constant surfactant velocity with prefoamer. 60

4.12 Pressure gradient versus surfactant velocity at constant gas velocity without prefoamer or back pressure. 61
4.13 Pressure gradient history in Berea core using a prefoamer with $v_l = 16.2$ ft/day and $v_g = 88.5$ ft/day. 63
4.14 Pressure gradient history in Berea core using a prefoamer with $v_l = 16.2$ ft/day and $v_g = 80.6$ ft/day. 64
4.15 Pressure gradient history in Berea core using a prefoamer with $v_l = 9.90$ ft/day and $v_g = 112$ ft/day. 65
4.16 Pressure gradient history in Berea core using a prefoamer with $v_l = 16.2$ ft/day and $v_g = 104$ ft/day. 66
4.17 Pressure gradient history in Berea core using a prefoamer with $v_l = 16.2$ ft/day and $v_g = 104$ ft/day (early time). 66
4.18 Pressure gradient history in Berea core without a prefoamer with $v_l = 16.2$ ft/day and $v_g = 97$ ft/day. 68
4.19 Pressure gradient history in Berea core without a prefoamer with $v_l = 16.2$ ft/day and $v_g = 97$ ft/day (early time). 68
4.20 Pressure gradient history in Berea core with $v_l = 8.16$ ft/day and $v_g = 103$ ft/day (effect of prefoamer). 69
4.21 Pressure gradient history in Berea core without a prefoamer with $v_l = 16.2$ ft/day and $v_g = 107$ ft/day. 69
4.22 Pressure gradient history in Berea core without a prefoamer with $v_l = 16.2$ ft/day and $v_g = 107$ ft/day (early time). 70
4.23 Pressure gradient history in Berea core with $v_l = 8.16$ ft/day and $v_g = 77.7$ ft/day (effect of prefoamer). 71
4.24 Pressure gradient history in Berea core without a prefoamer with $v_l = 11.8$ ft/day and $v_g = 117$ ft/day. 71
4.25 Pressure gradient history in Berea core without a prefoamer with $v_l = 7.96$ ft/day and $v_g = 195$ ft/day. 72
4.26 Pressure gradient history in Berea core without a prefoamer with $v_l = 7.96$ ft/day and $v_g = 44.2$ ft/day. 73
4.27 Pressure gradient history in Berea core at low velocities without prefoamer (early time). 74
4.28 Pressure gradient history in Berea core without a prefoamer with $v_l = 3.98$ ft/day and $v_g = 41.2$ ft/day. 74
4.29 Pressure gradient versus gas velocity with $v_l = 3.98$ ft/day. 75
4.30 Pressure ditribution inside the core as a function of pore volumes of fluid injected with $v_l = 3.98$ ft/day and $v_g = 41.2$ ft/day. 76
4.31 Normalized pressure gradients obtained at steady state for different gas velocities with $v_l = 25.2$ ft/day. 77
4.32 Pressure gradient versus gas flow velocity in Berea core with and without surfactant for a liquid velocity of 9.7 ft/day. 77
4.33 Cumulative plot of pressure gradient versus gas velocity for different surfactant velocites without prefoamer. 78
4.34 Cross plot of pressure gradient versus liquid velocity at different gas velocitites. . 79

4.35 Pressure distribution in core at different gas velocities for v_l = 7.96 ft/day. . . . 79
4.36 Pressure distribution in core at different gas velocities for v_l = 9.71 ft/day. . . . 80
4.37 Pressure distribution in core at different gas velocities for v_l = 11.8 ft/day. . . . 80
4.38 Pressure distribution in core at different gas velocities for v_l = 16.2 ft/day. . . . 81
4.39 Pressure distribution in core at different gas velocities for v_l = 20.0 ft/day. . . . 81
4.40 Pressure distribution in core at different gas velocities for v_l = 25.2 ft/day. . . . 82
4.41 Pressure distribution in core at different surfactant velocities for v_g = 6.7 - 9.2 ft/day. 83
4.42 Pressure distribution in core at different gas velocities for v_l = 7.96 ft/day with a prefoamer. 83
4.43 Pressure gradient in Berea core at different gas velocites obtained with and without prefoamer for v_l = 7.96 ft/day. 84
4.44 Residual effect of prefoamer on pressure gradient versus gas velocity in Berea core for v_l = 7.96 ft/day. 85
4.45 Pressure gradient versus gas velocity with increasing and decreasing gas velocities at v_l = 7.96 ft/day with a prefoamer. 85
4.46 Pressure gradient versus gas velocity with increasing and decreasing gas velocities at v_l = 7.96 ft/day without a prefoamer. 86

ABSTRACT

With all the technological innovations available today to produce oil from underground reservoirs, no single method or combination of methods is capable of recovering all of the oil in place. Even after applying several different techniques over extended periods of time, more than two thirds of the oil originally in the reservoir remains unrecovered.

During the last two decades, the use of surfactants has emerged as a new enhanced oil recovery (EOR) method. In more recent times, new applications of surfactants include injecting surfactant solutions as steam additives. These surfactants are designed to control the mobility of steam and to make better use of the energy supplied with steam.

Investigations were directed towards the use of surfactant solutions along with a gas phase in order to displace oil from the reservoir. Residual oil can be displaced by increasing the capillary number. This may be accomplished by increasing the pressure gradient and by decreasing the interfacial tension between oil and water.

The main objective of this experimental research was to investigate the mechanisms of foam generation and propagation in porous media. Results obtained give an insight into the conditions of foam generation and propagation in porous media. The rate of propagation of foam is determined by the rates of lamellae generation, destruction, and trapping. Several of the factors that contribute to foam generation have been studied with Chevron Chaser SD1000 surfactant.

Interfacial tension (IFT) measurements were performed using a spinning drop apparatus. The IFT of two surfactant samples of different concentrations were measured with dodecane and crude oil from the Huntington Beach Field as a function of temperature and time. Results show that foaming agents do not reduce IFT values enough to mobilize residual oil.

Foam was used as an oil-displacing fluid. However, when displacing oil, foam was not any more effective than simultaneous brine and gas injection due to the sensitivity of the surfactant used to oil. Foaming did occur as shown by increased pressure gradients but did not produce a high pressure gradient that was capable of displacing the residual oil. The use of foam increased

the pressure gradient by a factor of about ten and reduced the IFT by a factor of about ten. This resulted in an increase in the capillary number by two orders of magnitude.

A series of experiments was performed to study the conditions of foam generation in Berea sandstone cores. Results show that foam may be generated in sandstone at low flow velocities after extended incubation periods. Initially, a weak foam is generated where most of the gas is trapped due to stranded lamellae. This causes little gas mobility reduction. As the pressure gradient increases, lamellae become mobilized which in turn divide and regenerate. Repeated snap-off and lamella division are responsible for the generation of a fine textured foam. Significant gas mobility reduction occurs during this strong foam flow regime. Foam generation and propagation rates are increased and incubation times are shortened with higher flow velocities.

The effect of pregenerating foam before injection into the sandstone was studied. The use of a prefoamer produces small bubbles that enter the core and propagate causing a more rapid pressure response. However, the effect of injecting a pregenerated foam does not extend far from the injected end of the core. Results show that foam propagates as a front in porous media.

Strong foam generation occurs provided the gas and surfactant velocities cause a high enough pressure gradient for foam mobilization. The pressure response due to foam flow is independent of the direction of the fluid velocity change. Therefore, no hysteresis was observed with foam flow in Berea cores.

Steady state foam flow is achieved when foam generation, coalescence and trapping are in balance. As gas velocities are reduced from the strong foam flow regime, foam mobilization decreases and the foam texture coarsens. Gas mobilities increase and liquid mobilities decrease with increasing gas velocities in the strong foam flow regime. Results show that liquid saturations are within a narrow range during foam flow in porous media.

The pressure profiles in the core were monitored using three pressure taps along the length of the core. Pressure distributions as a function of distance in the core are almost linear. With a prefoamer, higher pressure gradients are encountered at the inlet end, whereas without a prefoamer, pressure gradients increase with distance from the inlet end.

A systematic study of foaming with different fluid velocities and foam qualities provides extensive data for foam flow conditions. Results clarify the two foam flow regimes identified as weak foam and strong foam. Such studies under field conditions are necessary prior to foam application in the field. Results indicate that an excessively large number of pore volumes of foam would be necessary to propagate foam deep into the reservoir. Propagation of high pressure gradients away from the wellbore may not be feasible.

Chapter 1

INTRODUCTION

As world oil reserves are limited, more sophisticated oil recovery methods are necessary to recover the remaining oil in reservoirs. Hydrocarbon production is shifting away from the dwindling conventional crude supplies toward heavy oils, bitumen and possibly oil shale [119].

Thermal oil recovery methods are by far the most important enhanced oil recovery (EOR) techniques employed in the oil industry during the past decade. They have particular application in the recovery of heavy oils. In the 1980's, about 80% of the oil produced by EOR methods in the United States has been attributed to thermal recovery methods, mainly steam injection.

The use of steam in oil recovery encompasses two processes:

1. Cyclic steam stimulation, "huff-n-puff": Steam is injected into a well for several days. Then the well is put back on production.

2. Steamflooding: Steam is injected into a well while oil is produced from adjacent wells.

Steamflooding increases oil production through a number of mechanisms such as viscosity reduction, thermal expansion, and steam distillation. Residual oil saturations to steamfloods are generally below 10% in the steam swept zone. However, large amounts of oil are bypassed because of gravity segregation or steam override. Also, permeability heterogeneities reduce areal sweep efficiencies. The application of mobility control foams could help solve these problems.

Foam flooding is an in situ steam mobility control process. Foam in porous media may be defined as a dispersion of a gas in a liquid such that the liquid phase is continuous and at least part of the gas is made discontinuous by thin liquid films called lamellae [57], that are stabilized by the presence of surfactant in solution. Therefore, foam in a porous medium does not exist as a bulk foam.

The approach that treats foam simply as a fluid of modified viscosity is inadequate to explain the characteristics displayed by foam flowing in a porous medium. The sizes of the bubbles generated in sandstones are of the same order of magnitude as the pore sizes. Therefore, the flow of bubbles in porous media is affected by bubble-pore wall interactions. This causes lamellae to deform, break down, and regenerate. The liquid moves through the porous medium primarily through the interconnected liquid filled channels, which are mostly the smaller pores. Gas moves progressively through the system by bubbles breaking and reforming throughout the length of the flow path.

Oil recoveries obtained experimentally in linear steam floods tend to be excessively optimistic. Such successful oil recoveries have not been achieved in field tests because gas channeling causes most of the oil in the reservoir to be bypassed. Foam is a possible solution to the problem. It diverts steam towards areas of the reservoir not contacted by heat.

A common problem in gas-driven EOR processes is the severe gas channeling in the reservoir due to high gas mobility. In two-phase gas-water flow tests in porous media, the presence of a surfactant in the aqueous phase lowers the mobility of gas significantly. Foams are used:

- to reduce gravity override, which is the segregation of vapor and liquid phases due to the large differences in fluid densities,
- to reduce gas fingering which results from the large contrast in fluid viscosities,
- to block high permeability streaks, thereby, obtaining better sweep efficiency.

While foam is used to accomplish these tasks, it works as a driving fluid as well. When the fluids travel in the oil depleted zone, high gas velocities promote the formation of lamellae. A high pressure gradient develops in the reservoir causing oil to be displaced. The effects of using a foaming agent are two-fold. First, the foaming agent can cause an increase in the pressure gradient due to the formation of a series of lamellae. Second, it is capable of reducing the interfacial tension between oil and the aqueous phase and, thereby, mobilizing the oil. During steamfloods, low residual oil saturations are obtained in the areas effectively swept by steam. When surfactants are injected along with steam and nitrogen, the sweep efficiency may be increased at the pore level due to reduction of interfacial tension. Also, the steam additives reduce the mobility of the gas phase in the steam-swept zone due to an increase in the apparent fluid viscosity and thus improve the sweep efficiency.

Surfactants present in the liquid phase reduce gas mobility by stabilizing the liquid lamellae that form in porous media. Properties of the surfactant contribute to the stability of the foam.

Surfactant loss onto the porous medium surface as well as to the oil phase may cause the foam to collapse. A low IFT between the surfactant solution and the oil phase helps mobilize the oil.

Interest in the application of foams for mobility control increased at the beginning of the nineteen eighties due to high oil prices. Effort was directed towards improving steam injection efficiency. However, applications were limited due to an inadequate knowledge of foam generation and propagation mechanisms.

Important results of numerous studies on foam flow in porous media can be summarized as follows:

- Gas phase permeability is reduced by several orders of magnitude in the presence of foaming surfactants when compared to cases where no surfactant was present [5, 19, 43, 44, 59, 60, 62, 88, 107].
- Gas saturation during foam flow is high relative to that in the absence of surfactant under similar gas flow rates due to the presence of a high trapped gas saturation, that is, gas which does not participate in the flow process [5, 6, 43, 60, 88, 92, 101, 107].
- Gas breakthrough is delayed when foaming solution is present in the liquid phase flowing through a porous medium due to the build-up of a high trapped gas saturation [44, 62].
- Gas permeability increases with applied pressure gradient and flow rate [60, 62].
- In high permeability cores, larger permeability reduction occurs than in low permeability ones [5] and foam propagates faster due to selective foam blocking [44].
- Liquid relative permeabilities remain relatively unchanged in the presence of foaming agent when compared to gas-water systems at similar saturations [6, 19, 62].
- Liquid and gas saturations do not change significantly with changing flow rates under steady state conditions [6, 19, 36, 43, 60, 88, 97, 101, 107]. Liquid saturations are constant at slightly above connate saturation, independent of flow rate.
- During simultaneous gas and liquid flow at a given gas saturation, the liquid flows primarily through the same paths irrespective of surfactant concentration [6, 60].
- The mobile gas moves via a network of bubbles separated by liquid lamellae which form and break continuously [44, 60].
- The presence of oil has a destabilizing effect on foam with most foaming surfactants [5, 6, 18, 25, 44, 60, 67, 78, 81, 86, 106].

In field operations, it is desirable that foam generated near the wellbore region propagate deep in the reservoir. Systematic studies in well characterized systems are necessary to characterize better foam behavior in porous media. Investigation of the mechanisms of foam flow in porous media and the feasibility of generating and propagating foam deep in the reservoir are the main objectives of this study.

Chapter 2

THEORY AND LITERATURE REVIEW

In general, the term foam is used for the state of aggregation of two phases, liquid and gas, such that these two phases form a dispersion that consists of gas bubbles separated by liquid films. The term foam may also be used for dispersions of gas in solids such as polyurethane foam. In true foams, the films separating the bubbles are liquid or solid and bubbles are not interconnected. The gas phase is discontinuous, the continuous phase being liquid or solid [8]. Foam can also be considered as a type of emulsion in which the inner phase is a gas and the dispersion medium is a liquid with some surfactant component present to add stability [1]. The dispersion system with a small gas volume fraction where bubbles are not interacting is called gas emulsion or "kugelschaum" (from German meaning sphere foam [80]). Foams that contain mostly gas phase, separated by thin liquid films, are called "polyhedral foam," or "polyederschaum" (also from German) because of their structure.

2.1 Structure of Foams

The laws of bubble geometry have been formulated by Plateau [99]. These principles hold for bubbles in equilibria, based on the minimizing of surface area of liquid films as a result of the tension of liquid surfaces. The principles that determine foam structure are:

1. Three, and only three, foam lamellae (faces of a polyhedron) meet to form a liquid channel (edge of a polyhedron) known as "Plateau's border". These lamellae foam equal angles of 120° between them.

2. Four, and only four, of these edges come to one point and foam tetrahedral angles of 109° 28' 16".

Plateau's border plays an important role in the mechanism of film drainage. The high curvature of the boundaries around the border indicates a considerable capillary pressure between the gas and liquid phases which causes the liquid to be "sucked" from the film into the border. The presence of lamellae in a porous medium increases the importance of capillary pressure, as discussed in Section 2.3.5.11.

Matzke's [85] extensive statistical investigations of the geometric features of foam confirmed the above principles. Gibbs [48] analyzed the problem of filling space with different regular geometrical bodies. The most probable number of faces in a polyhedron and the face shape can be determined by using stereochemical theorems from Euler and Plateau's principles. A regular pentagonal dodecahedron is the most widespread polyhedron in foams and the maximum number of face angles is five [21, 85, 120].

The shape of the polyhedrons and the number of films that separate bubbles change considerably during foam collapse. Bubbles acquire tetrahedral form before disappearing due to transfer of gas from small bubbles to large ones by diffusion through the films [120].

The three main physicochemical parameters that characterize foam structure are:

1. Gas-liquid ratio. This can be quantified as the foam quality, the fraction of gas in the gas-liquid mixture, or expansion factor, the ratio of foam volume to liquid volume. Foams with quality greater than 90% are called dry foams.

2. The average bubble size, referred to as foam texture or dispersivity.

3. The bubble size distribution.

2.2 Foam Stability and Collapse

Coalescence of two bubbles is preceded by the formation of a thin liquid film. The behavior of this film is important in determining the stability of foam. When two bubbles interact with each other, electrostatic forces become important. Derjaguin et al. [20] introduced the concept of "disjoining pressure" to measure this thermodynamic interaction between bubbles separated by a thin liquid film of thickness smaller than 100 nm.

The modulus of surface elasticity E, the reciprocal of film compressibility, is a rheological property important in lamella stability [48]. Under static conditions, E is defined as:

$$E = 2\frac{d\sigma}{dlnA} = -2\frac{d\sigma}{dlnh} \tag{2.1}$$

where σ = surface tension, A = lamella area, and h = lamella thickness.

2.2.1 Foam Stability

The theories pertinent to the stability of a simple film are applicable for foam stability. Surface tension effects cause liquid surfaces to contract. However, foams tend to have a measurable lifetime due to several stabilizing factors such as high liquid and surface viscosities, Marangoni effects and disjoining pressure.

2.2.1.1 Liquid Viscosity

High liquid viscosity retards liquid motions including drainage and rupture of lamellae. With very viscous foaming solutions, foam formation is as slow a process as foam collapse. The inner layer of a film has the same viscosity as the bulk liquid. High bulk viscosity, therefore, decreases the liquid drainage rate from the lamella increasing its stability [8]. The effect of high liquid viscosity is important with thick lamellae, or lenses, where the amount of liquid in the lamellae is substantial. However, with thin lamellae, the surface viscosity is more important.

2.2.1.2 Surface Viscosity

High surface viscosity retards drainage and surface deformations, increasing the life of lamellae. Surface viscosity, as identified by Plateau [98], plays an important role in film stability. The surfaces of a lamella that are adjacent to the gas phase are much more viscous than the bulk liquid. In general, this surface viscosity increases with surfactant concentration. The relationship between surface viscosity and foam stability is not well understood. Adamson [1] describes two types of surface viscosity, dilational and shear.

1. Surface dilational viscosity relates to the rate of surface density increase of a film with applied pressure. The increase of the surface tension σ of an adsorbed surface layer of area A that is subjected to an increase at a rate of dA/dt is:

$$\Delta\sigma = \kappa_s \frac{dlnA}{dt} \tag{2.2}$$

   where κ_s = surface dilational viscosity and has dimensions of viscosity.

2. The force f required to move a line element of length l in a surface relative to another with a velocity gradient dv/dx is given by

$$f = \eta_s l \frac{dv}{dx} \tag{2.3}$$

where η_s = surface shear viscosity.

2.2.1.3 Marangoni Effect

The Marangoni effect is the departure from equilibrium surface tension produced by dilational deformation of the interface to resist lamella deformation. Bulk material is carried through movements induced by surface tension effects. In liquids containing surface active agents, the surface tension of the solution is lowered. Thus, these surface active molecules accumulate at the surface. It is one of the main causes of film stability. When a film is stretched, the surface area increases causing a reduction in the surfactant concentration at the local level. The resulting higher surface tension tends to restore the deformation by liquid movement to the stretched region of the lamella. The Marangoni effect takes place due to the slow diffusion of surface active agents [8]. This restoring force is the direct result of the difference between static and dynamic surface tension. Therefore, the Marangoni effect operates whenever the surface tension of the solution is considerably smaller than the surface tension of the solvent and the diffusion of the surface active solute is slow enough.

Surface active components tend to concentrate near the surface causing a surface excess [1]. Under static conditions, Gibbs adsorption equation defines this surface excess Γ as follows:

$$\Gamma = -\frac{C}{RT}\frac{d\sigma}{dC} \tag{2.4}$$

where Γ = excess of solute present in the surface layer, C = bulk concentration, R = gas constant, T = absolute temperature, and σ = surface tension of the solution.

If $d\sigma/dC$ is negative, then Γ is positive and there is a surface excess. Otherwise, there is a surface deficiency of solute.

2.2.1.4 Disjoining Pressure

The mutual repulsion of electric double layers stabilizes foam lamellae. An electrical double layer is the region between two homogeneous interfaces (e.g. the surface of a lamella), such that the charge constituents have been separated and each side of the interface is electrified. Also, the charges on the two sides are equal and opposite making the region electrically neutral

[66]. When these two layers approach each other, a repulsion force develops hindering further thinning of the lamella.

Proposed by Derjaguin and co-workers [20], the disjoining pressure is defined as the pressure in excess of the external pressure, that must be applied to the medium between the lamella faces to maintain a given separation. The disjoining pressure may be regarded as a net of several attractive and repulsive intermolecular forces.

Jimenez and Radke [68] have quantified the effect of the disjoining pressure in foam in porous media. The driving force for liquid movement in lamellae was found to be $P_c - \Pi$, where P_c is the capillary pressure and Π is the disjoining pressure defined as:

$$\Pi = -\frac{A_H}{8h^3} + \frac{2\pi q_l^2}{\epsilon} csch(\kappa h) \tag{2.5}$$

where A_H = Hamaker constant, q_l = lamella surface charge density, h = film thickness, κ = inverse Debye length, and ϵ = permittivity constant.

The first term corresponds to attractive dispersion or Hamaker forces (Van der Waals attraction) and the second term corresponds to the electric double layer repulsion. A typical disjoining pressure isotherm as a function of h is similar to potential energy of interaction between two bodies: it increases, goes through a maximum then declines with distance to a value of zero.

2.2.2 Foam Drainage

Foam drainage is a hydrodynamic phenomenon where the liquid flows in the lamellae and Plateau borders at a rate independent of film stability. This drainage is caused by gravitational forces as well as capillary pressure effects. The thin liquid films drain but this does not cause them to collapse. The thinning of films occurs via a mechanism that involves the formation of thin paths of film at the border. The excess liquid drains from the edges of the film into the Plateau border. The high curvature at the film edges indicates a lower pressure than the body of the film causing the liquid discharge.

The drainage of thick films is similar to viscous flow of liquid in capillaries [1]. The liquid flow velocity is derived from Poiseuille's equation [52]:

$$v_{av} = \frac{\rho M^2 \Delta P}{\alpha \mu L} \tag{2.6}$$

where α = shape factor, L = length of the film, μ = liquid viscosity, M = hydraulic radius defined as $flow\ volume/surface\ area$, ΔP = pressure difference over the length L.

The Plateau borders can be approximated as a cylinder with α=2. Then:

$$v_{av} = \frac{r^2 \Delta P}{8\mu L} \tag{2.7}$$

where r = average radius of the border. Lamellae behave similar to parallel plates with α=3. Then, for a lamella of thickness d:

$$v_{av} = \frac{d^2 \Delta P}{12\mu L} \tag{2.8}$$

where d = thickness of the lamella.

2.2.3 Foam Collapse

Migration of gas from smaller bubbles into the larger ones by diffusion through thin films separating them leads to the disappearance of small bubbles. The driving force is the difference of internal pressures in the bubbles. Since capillary forces are inversely proportional to interface curvature, this internal or Laplace pressure is higher for smaller bubbles. The pressure difference between two bubbles surrounded by liquid of radii R_1 and R_2 ($R_1 < R_2$) is:

$$\Delta P = 2\sigma \left(\frac{1}{R_1} - \frac{1}{R_2} \right) \tag{2.9}$$

This pressure difference provides the driving force for gas to diffuse from the smaller bubble to the larger one. The rate of diffusion is inversely proportional to the lamella thickness [129]. Chambers and Radke [13] measured the time it takes for a typical bubble to disappear by gas diffusion and found it to be about two minutes. This value compares well with the characteristic time calculated from the gas diffusion equation.

The lifetime or persistence of foam can be measured [8]. However, no unique or standard method exists that would determine the foaminess of an agent. The measurement of foaminess is dependent on the apparatus and the procedure employed. The different methods that test foam stability can be classified under two major categories:

1. Static tests: A static test is one in which the rate of foam formation is zero. The foam once formed is allowed to collapse without regeneration by further agitation or input of gas. The typical measurement for a static foam is the rate of foam collapse. Such methods include the beating or whipping method [110] and the method described by ASTM D892 IP 146 test.

The volumetric collapse of foam as a function of time approximates exponential behavior. A foam column decays according to first order kinetics [79]. The rate of foam collapse at any instant is proportional to the volume of foam remaining:

$$V = V_o e^{-k_c t} \tag{2.10}$$

where V = volume of foam in the column at any time t, V_0 = volume of foam at time zero, and k_c = rate constant.

The constants of the equation may be obtained by plotting $ln(V)$ versus time t. The half life of foam is calculated by:

$$t_{1/2} = \frac{ln2}{k_c} \tag{2.11}$$

This first-order kinetics are valid for foam decaying due to mostly drainage of liquid [128]. Zero-order kinetics apply if foam collapse is caused by gas diffusion from the smaller to larger bubbles.

A similar approach may be applied to the volume of liquid drained from a foam column as a function of time [110].

2. Dynamic tests: A dynamic foam is one that has reached a state of dynamic equilibrium between rates of generation and collapse [112]. Foam is generated at a fixed gas and the volume of foam at equilibrium is measured. Its final volume may also be measured after a fixed time of decay. Dynamic tests have been conducted in cylindrical [7, 32] as well as in conical [112, 130] equipment.

In foam stability measurements, the testing method should be tailored according to the specific application of the foam. As Ross and Suzin [112] stated: "There is no right answer. A foam test should produce foam and measure its stability under conditions similar to its ultimate application."

Tait [125] observed that when several bubbles coalesce into a single bubble, the surface area of the latter bubble is less than the sum of the surface areas of the original bubbles. However, as a result of the transformation, the gas expands (ΔV), and the volume of the larger bubble is greater than the sum of the volumes of the original bubbles. The following equation:

$$3P\Delta V + 2\sigma\Delta A = 0 \tag{2.12}$$

describes the decrease of interfacial area (ΔA) resulting from gas transfer between spherical bubbles. P and σ being positive requires that ΔV and ΔA should have opposite signs: as the surface area shrinks, the volume increases. A more general form of the above equation, the equation of state of a foam, was given by Ross [110]:

$$PV + \frac{2}{3}\sigma A = nRT \tag{2.13}$$

where n = number of moles of gas, R = ideal gas constant, and T = absolute temperature.

Other factors that contribute to foam collapse [8] include:

- Stretching: Bubbles resist stretching due to the surface tension effects. The limited elasticity of the film allows it to stretch before rupturing.
- Evaporation: Transfer of solvent from the lamella to the gas phase causes an increase in the bulk surfactant concentration stabilizing the thinning lamella, but making it prone to stretching and collapse.

2.3 Foam in Porous Media

Many of the parameters that affect foam flow in porous media have been studied. In spite of the ample amount of data available in the literature, it is not possible to compare results because foam behaves differently depending on the experimental conditions and the specific nature of the porous medium.

Some of the parameters that affect the flow of foam in porous media include surfactant type and concentration, surface properties of foaming solutions, chemical composition of gas phase, presence and type of oil, gas and surfactant flow rates, foam quality and texture, extent of fluid mixing before injection, absolute permeability and wettability of porous medium, surfactant adsorption, length of injection time, temperature, and pressure gradient.

2.3.1 Effect of Surfactant Properties on Foam

Foam formulation has to be designed based on the field properties to be encountered [75]. Properties of the surfactant solution that influence its effectiveness as a foaming agent are several. Some of the important parameters that affect the performance of foaming surfactants are:

2.3.1.1 Type of Surfactant

The three main classes of surfactants are:

1. Anionic: contain a surface active anion. In an aqueous solution, they give negatively charged surfactant ions. Common examples are fatty acid salts as well as alkyl or alkylaryl sulfates and sulfonates used as detergents. They are mostly produced by sulfonation or sulfation of the desired hydrophobe.

2. Cationic: contain a surface active cation. In an aqueous solution, they give positively charged surfactant ions. Examples include long chain quaternary amines and amine salts, used in connection with wetting and emulsion formation or breaking.

3. Nonionic: contain hydrophilic groups which do not ionize appreciably in aqueous solution, e.g. polyether esters and amides, which are used in household products and insecticides.

2.3.1.2 Interfacial Tension

The interfacial tension between the surfactant solution and the oil phase plays an important role in mobilizing the oil phase. A low IFT would increase the capillary number and thereby mobilize the oil.

IFT measurements of alkylaryl sulfonates with crude oil [134], at temperatures ranging from 150° to 350°F, show no significant effect of surfactant concentration above 0.2% by weight. In general, higher IFT measurements were obtained with higher temperatures. IFT values exhibit sharp minima with varying salt concentration. Increasing temperature increased the salinity requirement for minimum IFT. Isaacs and Smolek [65] obtained low IFTs in a bitumen/aqueous sulfonate surfactant system only in the presence of electrolytes. However, no significant effect of temperature on IFT was detected.

2.3.1.3 Surfactant Concentration

Traces of surfactant are capable of stabilizing foam lamellae [118]. As the surfactant concentration is increased, molecules aggregate into larger oriented groups called micelles. Any further increase in surfactant concentration beyond the point of micellar formation would not increase the concentration of single molecules in solution. This point is called the critical micellar concentration (CMC).

Increased surfactant concentration improves the stability of foam by retarding the rate of drainage of liquid from the lamella. Most studies [15, 17, 70] indicate that concentrations above

the CMC do not improve foam stability any further. However, Huh [62] observed increased foam stability with surfactant concentrations above the CMC. Foam tests by Gray et al. [49] show that foam height does not increase much above the CMC with increasing concentration. Detergent-type surfactants reduce the surface tension of water to about 30 dyne/cm with a CMC range of 50-200 ppm [123].

Rao [105] observed that the drainage time increases with increasing surfactant concentration, reaches a maximum at a concentration close to its CMC, then decreases. The increasing trend below the CMC is attributed to a decrease in the surface tension whereas the decreasing trend above the CMC is due to a decrease in the modulus of elasticity of the films.

2.3.1.4 Effect of Temperature

The CMC of the surfactant solution may increase with increasing temperature. This in turn will be detrimental to foam stability. High temperatures also contribute to a lowering of the surface viscosity of lamellae and thus, to an increasing of the rate of thinning.

Duerksen [30] observed lower pressure drops across a foam generator with increasing temperatures. In a foam flow system in a Boise core, after shutting down the flow, the pressure decay was monitored with time. The pressure in high temperature systems decayed faster than in low temperature ones. Robin [108] encountered reduced foam stability at higher temperatures. Opposite results have been observed in another study [86].

Some foaming surfactants such as petroleum sulfonates, may not be stable at steam temperatures for an extended period of time [133]. Alpha olefin sulfonates are more stable and exhibit less chemical decomposition. Half-lives for these surfactants are of the order of several days at 500°F and several years at 350°F. On the other hand, alkylaryl sulfonates exhibit no detectable chemical degradation at 500°F for up to 15 days.

Petroleum sulfonates decompose according to the following reaction:

$$ArSO_3^- + 2H_2O \rightarrow ArH + SO_4^{-2} + H_3O^+ \tag{2.14}$$

This increases the H^+ ion concentration thus lowering the pH [53].

2.3.1.5 Effect of Surfactant Loss

Surfactant loss has a detrimental effect on foam and may be of two kinds: loss to the solid surface and loss to the oil phase.

Surfactant adsorption onto the porous medium surface depends on several factors such as temperature, salinity, pH, and exchange of divalent ions. Sulfonates, in general, exhibit Langmuir type adsorption isotherms on sands [43, 62, 127, 134]. However, adsorption isotherms of mixtures of surfactants show more complex behavior such as the existense of adsorption maxima [16, 55, 126] and dependence on solids concentration [126]. Adsorption tests on sandstone constituents indicate the following order for adsorption capacity:

montmorillonite > *kaolinite* > *illite*

Surfactant loss to the oil phase changes the surfactant concentration. However, loss of surfactant to the oil-water interface is not very significant and contributes positively by lowering the IFT.

2.3.1.6 Effect of Salinity

In general, an increase in salinity tends to decrease the CMC and to increase the surface viscosity of the surfactant solution. High salinity increases the adsorption capacity of kaolinite [55] and sands [76, 77]. However, some surfactants perform best in the absence of electrolytes [74]. Studies [2, 9, 30, 86] indicate a decrease in foam stability with an increase in aqueous phase salinity. Results by Dilgren and Owens [24] indicate that addition of NaCl is necessary to generate an effective steam foam.

Cation exchange between the surfactant solution and clays having a high divalent-cation content causes an increase in divalent-cation concentration in the aqueous phases, resulting in surfactant precipitation. [76]. Also, adsorption of anionic surfactants onto sandstone is higher in the presence of divalent cations, indicating an electrostatic mechanism of adsorption [82].

2.3.1.7 Effect of Alcohol

Hydrate formation may be inhibited by the addition of small amounts of alcohol in the aqueous phase. Addition of up to 20% by volume of methanol to a foaming solution did not affect foam generation in jar tests [78]. However, foam collapsed when methanol was added onto foam due to a sudden surfactant dilution.

2.3.2 Effect of Gas Properties on Foam

Replacing nitrogen gas with hydrocarbon gas (a mixture of methane through butane) did not prevent foam from generating [78]. However, the mobility reduction factor was lower by a

factor of two. Limited variations in gas viscosities [92] show that the gas flow rate is inversely proportional to gas viscosity indicating Darcy flow.

Steam foam behavior is similar to nitrogen and CO_2 foams. However, it is affected by changes in temperature and by pressure gradients which may cause steam foam to collapse. Therefore, formulating steam foam with a small fraction of nitrogen gas increases its stability [30, 34, 35, 38, 65, 74, 87, 100].

Addition of noncondensable gas to steam in the absence of surfactant increases oil recovery [61]. Simultaneous injection of hot water and noncondensable gas performs well also [27]. The role of the noncondensable gas in steam foam formulations is not only to provide foam stability, but also to provide high gas velocities. This would result in improved displacement of heated viscous oils.

CO_2 foams exhibit lower surface tensions than nitrogen foams by a factor of about one sixth [115, 131]. Also, CO_2 gas has a viscosity about thirty times that of nitrogen, decreasing minimum gas velocities for foam mobilization by the same factor [115].

2.3.3 Foam Generation Mechanisms

Foam forms in a porous medium only if the conditions for generating foam are favorable [104]. The accepted mechanisms of foam generation and flow in porous media [37, 47, 46, 59, 84, 93, 104] are as follows (see Figure 2.1):

2.3.3.1 Leave-Behind

When gas displaces surfactant solution from porous media, often lamellae remain behind in pore necks. This occurs when two gas channels invade two adjacent and communicating pores draining the liquid from the pores and leaving a lamella in between the two pores. These stationary lamellae remain at the pore necks where they were generated. This mechanism of foam generation results in a weak foam as resistance to gas flow increases only moderately due to lamellae blocking flow channels. Also, the gas phase remains continuous as no separate bubbles are formed.

The stationary lamellae, generated by the leave-behind mechanism, are subject to lamella stability factors. The lamellae have the potential of being mobilized, given that enough pressure differential is available across it and provided that they do not rupture. Once a lamella ruptures or is mobilized from its generation site, liquid has to reinvade the two adjacent pores before a lamella can be regenerated by gas invasion [104].

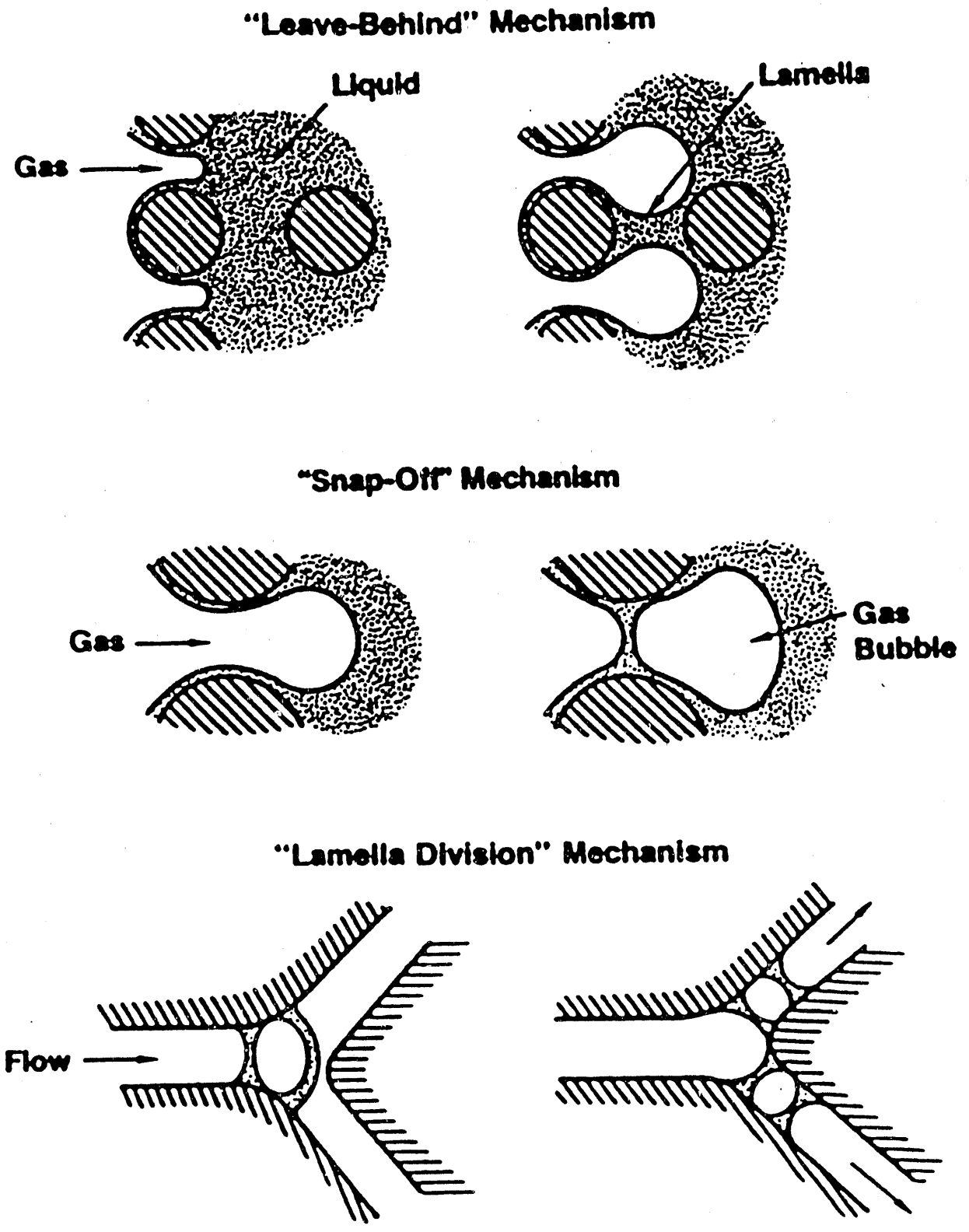

Figure 2.1: Principal mechanisms of foam generation in porous media, after Friedmann et al. [43].

2.3.3.2 Capillary Snap-Off

Roof [109] identified the snap-off process of oil droplets in toroids. The snap-off phenomenon has been applied to foam generation in porous media.

As a gas front advances through a pore throat, it causes a decline in the capillary pressure. This induces flow of liquid from around the bubble back into the constriction. When the capillary pressure drops below a critical value, the liquid in the pore throat bridges and snaps off a gas bubble. This mechanism produces a discontinuous gas phase. Repeated snap-offs increase the degree of discontinuity of the gas. This results in a series of bubbles separated by lamellae that cause an increased resistance to gas flow. This snap-off mechanism, believed to be the dominant foam generation mechanism in porous media, occurs repeatedly at high gas velocities [36, 37, 39, 42, 43, 63, 84, 114].

In a heterogeneous porous medium, lamellae may be generated by snap-off only if the pressure gradient is large enough for the generated lamellae to be displaced from the site [104]. However, snap-off was observed at all velocities at the boundary of a region of low permeability to high permeability in a heterogeneous beadpack [37, 104]. Micromodel observations verify the snap-off mechanism as a dominant mechanism for foam generation [63, 93, 121]

2.3.3.3 Lamella Division

Lamellae that are generated by either of the primary generation mechanisms mentioned above may be mobilized. At a path that branches into multiple branches, one lamella will divide into two or more lamellae [57, 63, 84, 104]. This mechanism requires the presence of mobile lamellae and a branching path. This foam generation mechanism is probably the dominant mechanism near injection wells where velocities and pressure gradients are large.

Lamellae division creates two or more lamellae from a single one. In turn, these lamellae may be mobilized and undergo further division or may block gas flow paths.

2.3.4 Foam Coalescence Mechanisms

Factors that contribute to lamellae stability and collapse have been described previously. With lamellae flowing in porous media, it is only appropriate to stress the importance of stretching of lamellae and capillary pressure induced lamellae drainage. Moving lamella stability depends on the disjoining pressure - capillary pressure balance as well as on lamellae flowing into large pore bodies and stetching [13, 68]. Gas diffusion plays a role in the collapse of stationary

bubbles such as in trapped gas. Steam foam stability is also dependent on evaporation and condensation effects. The presence of an oil phase also contributes to foam collapse.

2.3.5 Foam Flow in Porous Media

Studies of bubbles are important in understanding the basic structure of foam, but not sufficient. Injecting foam into a porous medium causes bubble-pore wall interactions. The sizes of bubbles in porous media are larger than pore sizes in sandstones. Bulk foam does not exist in porous media [22]. Therefore, a thorough study of the parameters and conditions that affect foam flow in porous media is necessary.

2.3.5.1 Trapped Gas Saturation

Foam reduces gas mobility by immobilizing a fraction of the gas. Bernard et al. [6] determined that up to about 70% of the gas is trapped in the presence of foaming agent. An increase in surfactant concentration causes higher gas trapping due to an increase in film stability [15]. Concentration increases above the CMC may not contribute to lamellae stability any further.

The stationary foam does not contribute to the flow of gas and it increases the resistance of the flowing gas by reducing the cross sectional area for flow. Falls et al. [39] estimated the relative permeability component of the gas mobility to be equal to the product of the gas relative permeability in the absence of foam and the fraction of the gas phase that is flowing.

Friedmann et al. [43] have performed tracer studies in Berea cores. The tracer breakthrough was monitored by a gas chromatograph. They determined that the trapped gas saturation is about 85% under steady state conditions of foam flow. What they call trapped gas saturation may not be gas that is permanently trapped. However, it seems that part of the gas may be flowing intermittently at a much lower rate than the rest of the gas that is under constant movement.

Using tracer studies, Nahid [92] had measured the trapped gas saturation to be about 30% under unsteady state conditions. Results were obtained with just gas flowing in the presence of near residual liquid saturations. Such flow experiments occur at very high gas fractional flows.

Results of Radke and Gillis [101] indicate a trapped gas saturation of 70-99% under weak foam flow regime.

2.3.5.2 Critical Pressure Gradient

The observation that some fraction of the foam is stationary while the remainder is mobile suggests that the foam has a yield stress or yield pressure gradient. Rossen [114] included the effects of compressibility, Plateau borders, and foam texture to obtain a model that predicted the critical pressure gradient.

The effect of frontal advance rate on pressure gradient is shown in Figure 2.2. There is a linear relationship on a log-log plot. A power-law model was used for the apparent viscosity of foam [43] as a function of gas velocity with an exponent of -1/3.

Huh [62] observed that the pressure gradient in the porous medium where foam is present is much higher than the rest of the core before a steady state condition was reached.

The normalized pressure square distribution in the core is not linear at low f_g indicating non-Darcy flow. The pressure square distribution is closer to linearity at high gas to liquid ratios [43, 62]. Holm [60] reported increased pressure gradient with distance as inlet pressures were increased. Others [36, 97] have reported linear pressure gradient profiles with steady state foam flow in consolidated porous media.

2.3.5.3 Pseudoplastic Behavior of Foam

Hirasaki and Lawson[59] modeled the apparent viscosity of foam flow in smooth capillaries. Results show that dynamic changes at gas-liquid interfaces are the main factors responsible for the apparent viscosity of foam. Three different factors contribute to the apparent viscosity of bubbles flowing through a capillary:

1. Resistance due to the slugs of liquid between bubbles.
2. Resistance to deforming the interface when a bubble passes through a capillary.
3. The surface tension gradient resulting from an expanding interface at the front and a contracting interface at the back.

Hirasaki and Lawson[59] showed that the apparent viscosity has an inverse 1/3 power dependence on velocity. Falls et al. [39] showed that the dependence of apparent viscosity on velocity for a bead pack where pore constrictions were included ranged from the inverse 1 power at low shear rates, to the inverse 2/3 power with small bubbles (pack-generated) at high shear rates, and to the inverse 1/3 power with large bubbles (controlled-bubble-size) at high shear rates. Note that these results have been obtained in bead packs of absolute permeabilities of several thousands of darcies.

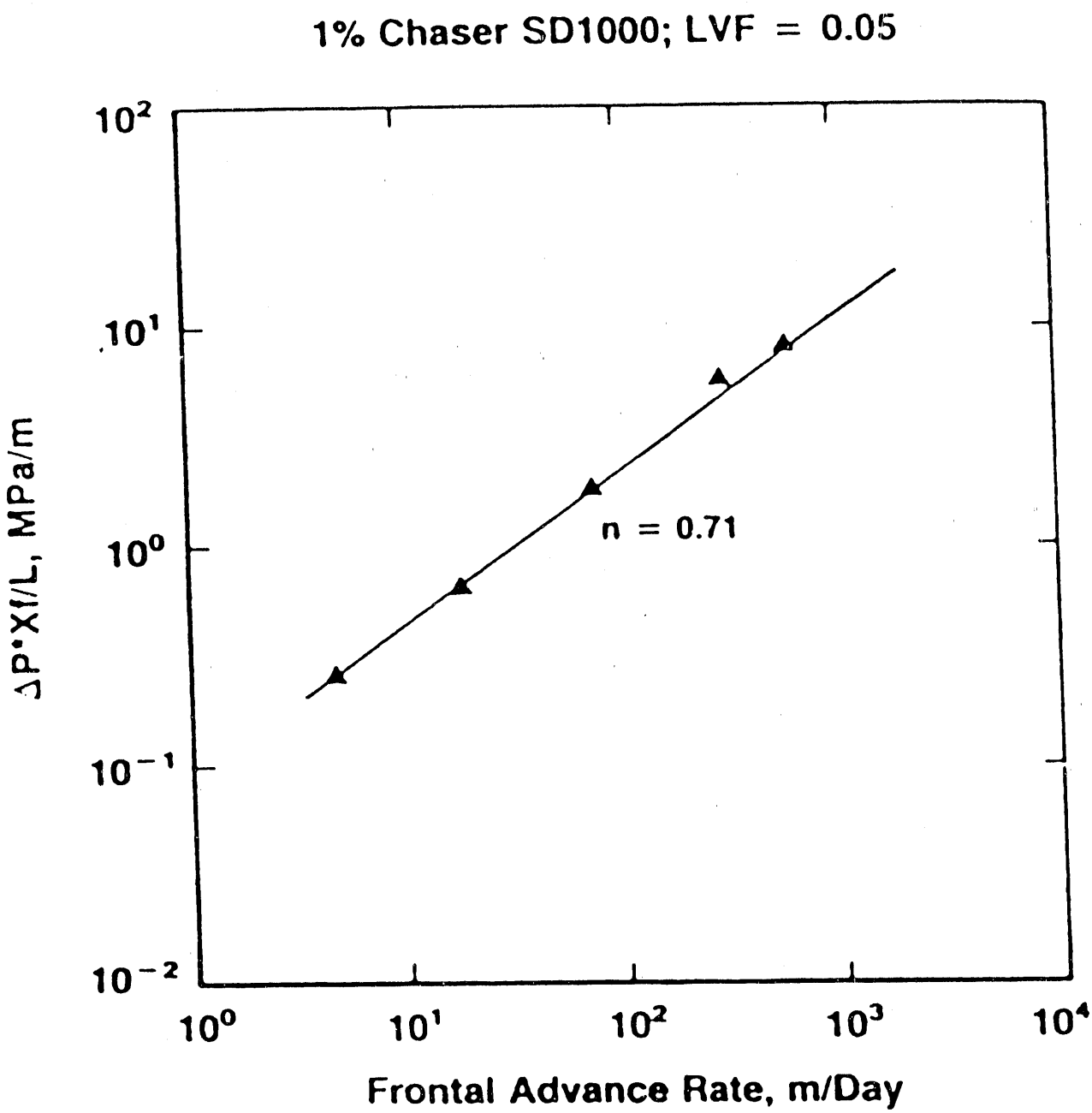

Figure 2.2: Effect of frontal advance rate on pressure gradient due to foam in Berea sandstone cores, after Friedmann et al. [43].

Other studies show that the apparent foam viscosity [36, 43] is proportional to bubble density. In general, results indicate that apparent foam viscosity is inversely proportional to gas velocity with an exponent of 1/3.

Measurements of foam rheology do not uniquely represent a rheological property of foam because oftentimes an important parameter affecting the results is not measured [56]. Apparent foam viscosity measurements provide qualitative guidelines as foam behaves differently depending on the medium or the environment.

2.3.5.4 Gas Velocity

A critical gas velocity for foam generation was measured at constant liquid volume fraction above which bubbles generate in Berea cores [43]. Gas injection rates were increased keeping foam quality constant, until a sudden large increase in the pressure drop along the core was recorded. This pressure increase indicated foam generation by snap-off [115].

Figure 2.3 is a plot of liquid volume fraction versus gas frontal advance rate. There seems to be a critical gas velocity v_c for foam generation as a function of liquid volume fraction LVF:

$$v_c = 1.52(LVF)^{-1.54} \tag{2.15}$$

The effect of gas velocity on bubble size distribution has been studied also. Measurements [36, 44] indicate smaller bubbles are produced at higher gas velocities. However, the pressure drop response in porous media increases only slightly with increasing gas velocities, keeping liquid velocities constant [36, 41, 97].

Results in bead packs by Flumerfelt and Prieditis [41] show a mobilization pressure when gas rates are extrapolated to very low values. The dynamic pressure gradient, defined as $(\Delta P_{total} - \Delta P_{mobilization})/Length$, remained constant at constant gas and liquid rates regardless of the flow history.

Results by Dilgren and Owens [24] show no significant effect of the mode of gas injection on the response of foam drive experiments. Limited experiments were conducted under constant volume and constant mass injection modes.

The experimental results obtained by De Vries and Wit [129] indicate that at a fixed liquid velocity, increasing the gas velocity causes the pressure gradient first to increase, reach a maximum, and then decrease. With low quality foams, increasing the gas velocity would increase the pressure gradient whereas the opposite is true for high quality foams.

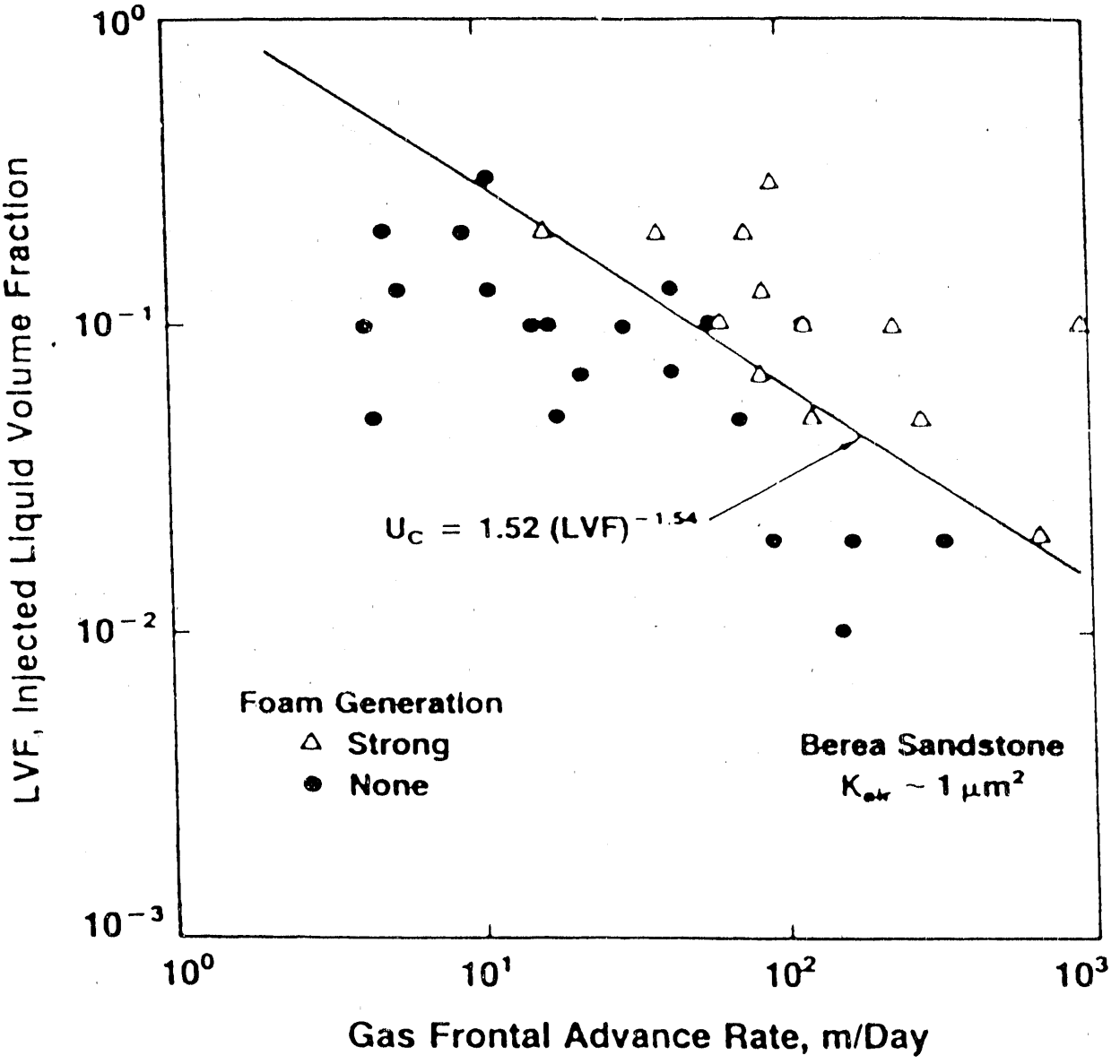

Figure 2.3: Critical velocity for foam generation in Berea sandstone cores during co-injection of nitrogen and surfactant solution, after Friedmann et al. [43].

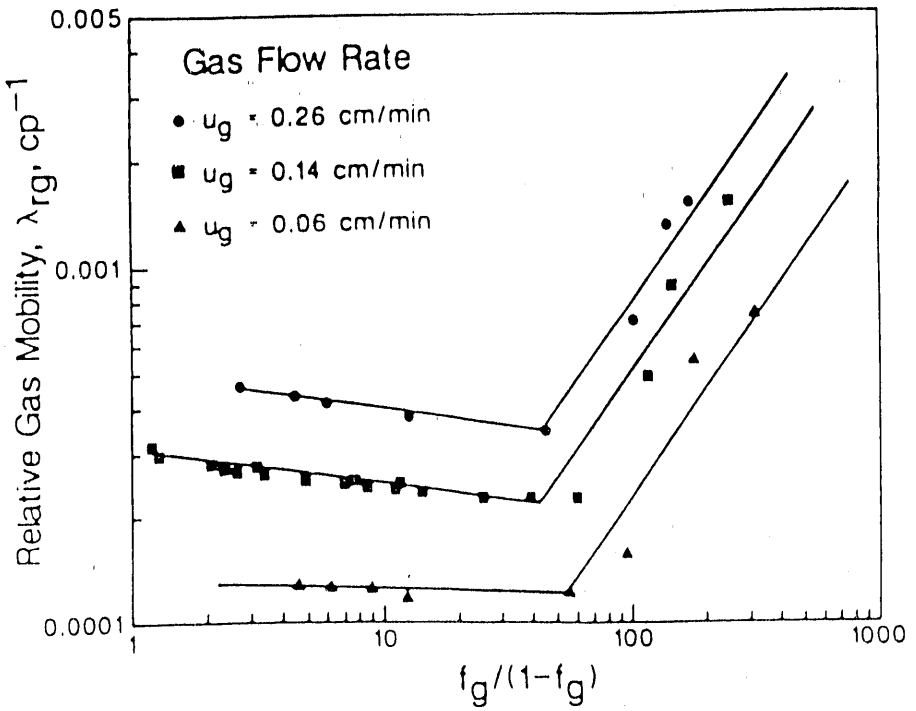

Figure 2.4: Effect of gas fractional flow on gas mobility, after Khatib et al. [72].

2.3.5.5 Liquid Velocity

Increasing the steady state liquid flow velocity with foam flowing in a porous medium increases the pressure gradient across the core [97]. Investigations for foam qualities ranging from 70 to 90% showed that liquid velocity does not change liquid saturations significantly [101]. Higher liquid velocities produce a decrease in foam mobility [92, 118]. Contradictory trends have also been reported in the literature [62, 118].

2.3.5.6 Foam Quality

Foam quality is defined as the volume fraction of gas in the gas-surfactant foam system. Foam quality can be varied by changing gas and liquid flow velocities. Therefore, a study of the effect of the individual velocities would be sufficient. Khatib et al. [72] have shown that at constant gas flow rate, mobility decreases with increasing gas fractional flow for low quality foams and increases with gas fractional flow for high quality foams (Figure 2.4).

Duerksen [30] studied the effect of liquid volume fraction on pressure drop. For increasing LVF, pressure drop increases rapidly then levels off. Effective permeability-apparent viscosity ratio, as calculated by Marsden and Khan [83], decreases linearly with foam quality. Foam quality also affects its propagation rate in porous media. High quality foams were found to propagate better than wet foams [44] and to produce higher pressure gradients [3].

2.3.5.7 Foam Texture

Foam texture or bubble size is an important parameter that affects mobility of foam in porous media. The relationship between bubble size and pore size affects the mechanism of foam propagation. Data available in the literature show that foam pregeneration does not affect foam flow [36, 129] but affects foam propagation [44].

De Vries and Wit [129] reported that varying the texture of the injected foam by varying the properties of the foam generator did not influence the results within experimental error. Pressure drops were monitored in a short section halfway along the length of the porous medium. Therefore, they concluded that the texture of the injected foam is changed by the porous medium to a value independent of the injected texture in a short distance.

However, Friedmann and Jensen [44] observed that different prefoamers generate foams with different bubble size distributions. This in turn affects foam penetration into the porous medium.

Ettinger and Radke [36] observed that bubble sizes at the effluent end of a core are independent of the injection method, that is, whether a prefoamer was used or not.

Chen et al. [15] showed that successive drainage and imbibition cycles cause higher lamella number density.

2.3.5.8 Permeability of Porous Medium

Greater mobility reduction is achieved in higher permeability porous media [5]. Foam propagates faster in high permeability rocks [44]. This makes foam better at controlling channeling due to permeability variation than a fluid with a constant viscosity. Foam formation required a critical gas velocity that was inversely proportional to the absolute permeability [65]. Effluent bubble size measurements indicate that lower permeability porous media generate smaller bubbles [44]. Ransohoff and Radke [104] observed bubble generation by snap-off when fluids entered a high permeability zone from a low permeability one.

2.3.5.9 Relative Permeability

Since a fraction of the gas is stationary, the gas relative permeability is reduced. Further reduction in the gas relative permeability is attributed to an increase in the apparent viscosity of the flowing gas.

Steady [43, 44, 62, 118] and unsteady state [62, 92] relative permeabilities have been measured with and without surfactant in sandstone. The liquid relative permeabilities are not

significantly affected (Figure 2.5). Under steady state conditions, the effect of liquid flow rate on liquid relative permeabilities is insignificant (Figure 2.6). However, gas relative permeabilities are reduced by an order of magnitude or more.

Sanchez et al. [118] show a hysteresis effect on steady state gas relative permeabilities. Drainage relative permeabilities of nitrogen are lower than imbibition relative permeabilities. Results were obtained with trace quantities of surfactant present in solution. Extremely long times were necessary to reach steady state on the drainage cycle. Both increasing [62, 118] and decreasing [92, 118] gas relative permeabilities with increasing pressure drops have been reported. Sanchez et al. [118] attribute these contradictory trends to an initial decrease in gas mobility with increasing pressure drops followed by an increase in gas mobility due to lamellae breaking.

2.3.5.10 Fluid Saturations

Data available in the literature [36, 43, 60, 88, 97] show that, after steady state is reached with foam injection into cores, liquid saturations are about 30-40%. These liquid saturations are independent of flow rates and foam quality. However, even though liquid saturations are within a narrow range, foam flow resistance varies with liquid flow rates. Earlier, Raza [107] had reported liquid saturations of about 20%.

A two-step displacement process has been proposed by Mohammadi et al. [90] for foam injection into porous media: a rapid desaturation to about 65% liquid followed by a slow desaturation process to values of about 30-40% liquid [97].

A set of data generated by DeVries and Wit [129] indicates that high foam qualities (more than 95%) reduce liquid saturations to about 18%. These results were obtained at very high gas velocities (Darcy velocities of 500 ft/day or higher). Under these conditions, extremely high pressure gradients were recorded, of the order of 1500 psi/ft or higher. Even though the relevance of results under these extremely high velocities is questionable, the data do show that liquid saturations during foam flow in porous media vary with velocity. Radke and Gillis [101] obtained liquid saturations of about 20% with only gas flowing.

2.3.5.11 Capillary Pressure

Khatib et al. [72] assumed that during foam flow in porous media, the capillary pressure increases up to a limiting value as the gas fractional flow is increased. With further increases in the gas fractional flow, the capillary pressure remains at its limiting value while the foam

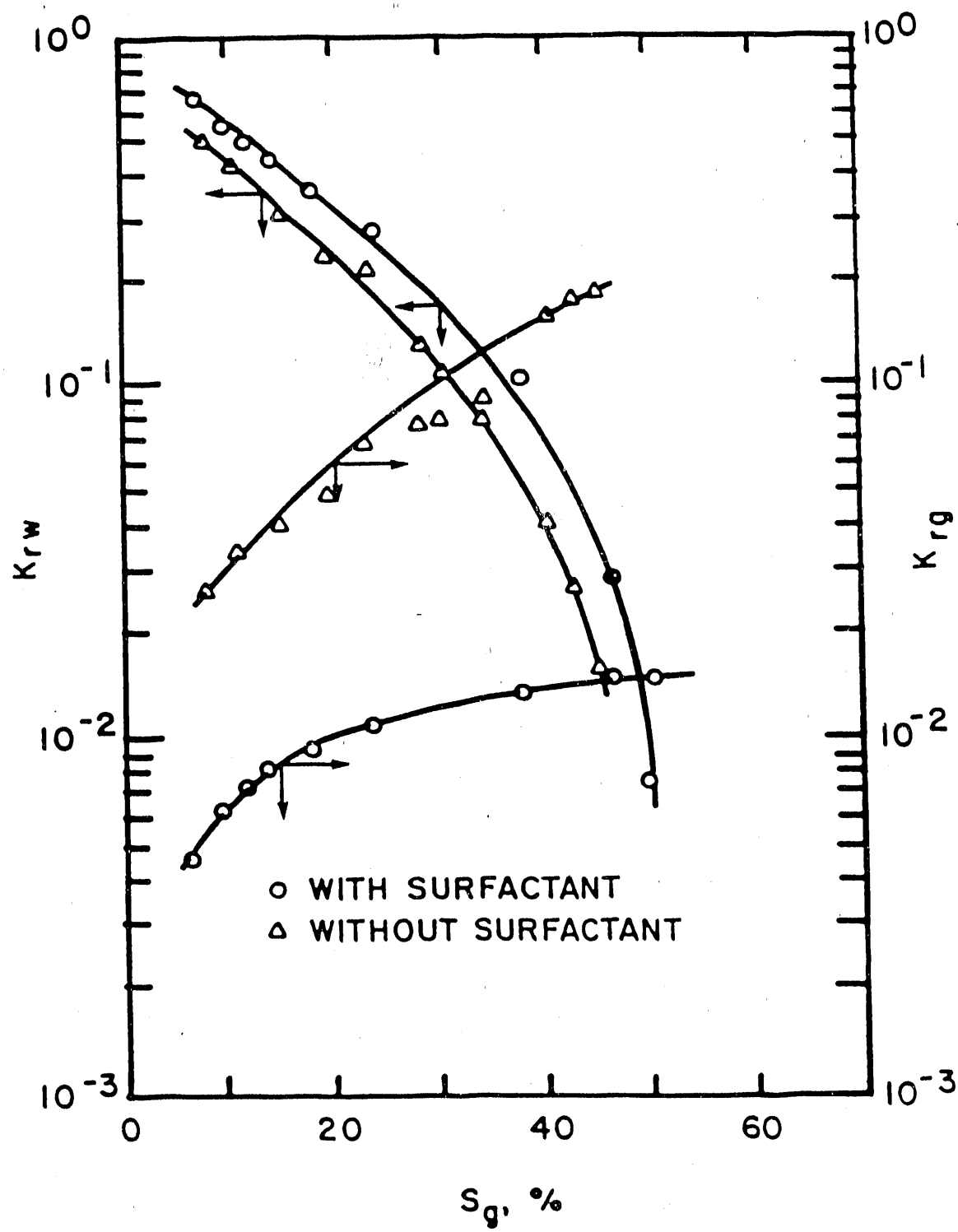

Figure 2.5: Comparison of unsteady state relative permeabilities measured with and without foaming agent in brine, after Huh [62].

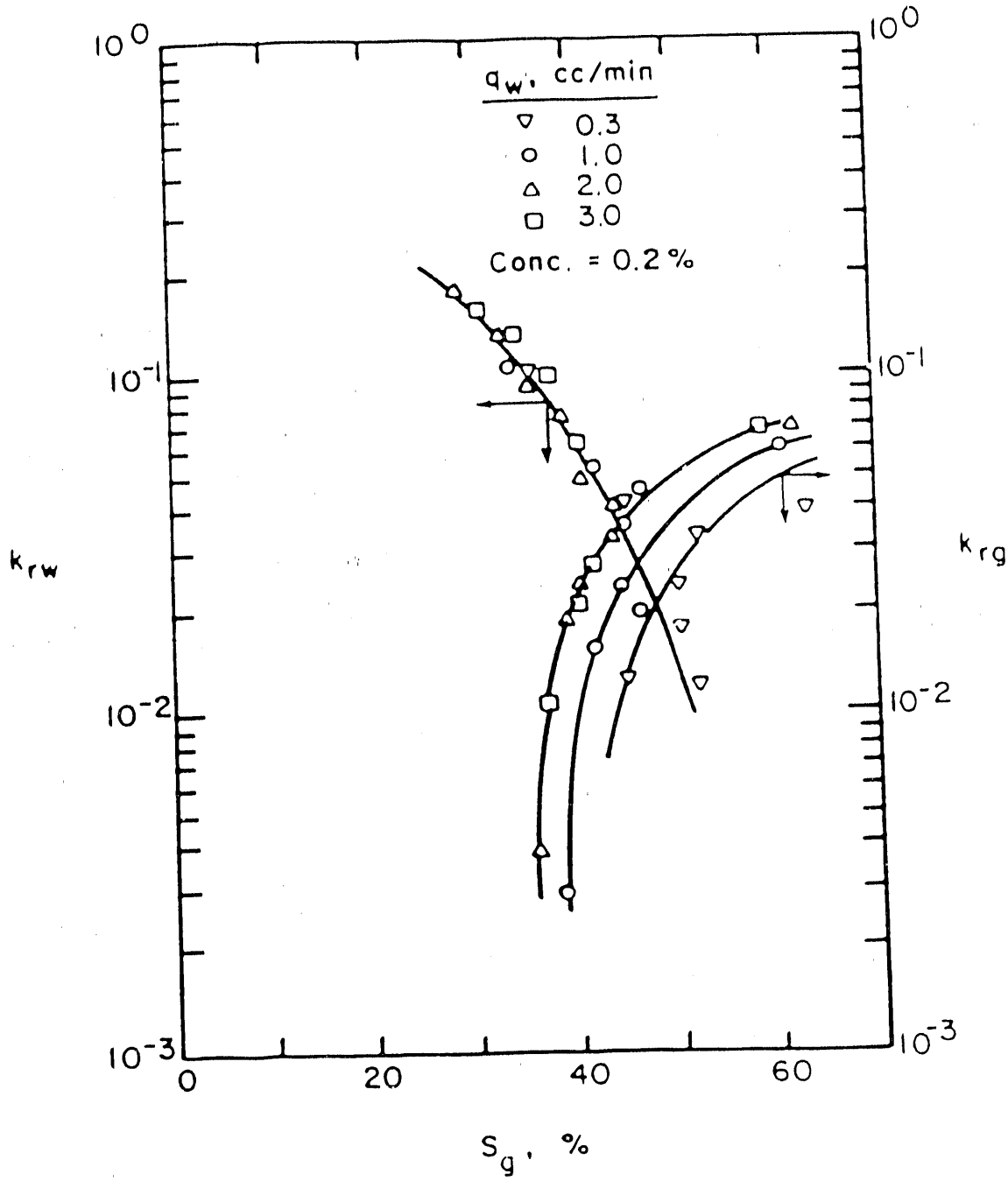

Figure 2.6: Effect of liquid flow rate on steady state relative permeabilities (c = 0.2%), after Huh [62].

texture becomes coarser. Therefore, the gas mobility will become proportional to the gas/liquid ratio above some critical value. The constant of proportionality is the liquid mobility at the saturation corresponding to the limiting capillary pressure.

They also observed that the limiting capillary pressure decreases with increasing absolute permeability. However, their data were obtained for three different packs of permeabilities ranging form 72 to 9000 Darcies. The validity of limiting capillary pressures in low permeability media, obtained by exptrapolation of their correlations, is questionable.

The existence of lamellae depends on pore geometry and fluctuations in capillary pressure [115]. As the capillary pressure falls locally, lenses can form at pore constrictions. These lenses become lamellae as the capillary pressure increases again, draining liquid out of the lenses. The theory of Rossen and Gauglitz [115] describes foam mobilization during an imbibition cycle.

Flumerfelt et al. [40] utilized a network analysis to investigate capillary pressure effects for foam flow in porous media. Semi-quantitative results indicate high trapped gas saturations. High capillary pressures are associated with a fine foam texture and large pore aspect ratios. In broad pore size distribution systems, finely textured foams cause higher capillary pressures and trapped gas saturations [15].

Jimenez and Radke [68] have developed a hydrodynamic stability theory that explains the criteria for foam coalescence in porous media. The maximum capillary pressure that stationary lamellae can endure in a porous medium is determined by the disjoining pressure. Moving lamellae stability is not only subject to this critical capillary pressure, but also to the rate of stretching which is a function of gas velocity.

2.3.5.12 Presence of Oil

The spreading coefficient of oil on water may be defined as the free energy change when a film of oil spreads on water. For non-equilibrated liquids where each phase is not saturated with respect to the other, the initial spreading coefficient [1] can be calculated from:

$$S_{o/w} = \sigma_w - \sigma_o - \sigma_{ow} \tag{2.16}$$

where σ_w and σ_o = surface tensions of water and oil and σ_{ow} = oil-water interfacial tension.

A large positive spreading coefficient is associated with the inhibition of foam formation [113]. This is due to spontaneous spreading caused by a decrease in free energy [1]. However, Ross et al. [111] observed the existence of a correspondence between foam stability and the free

energy of spreading (numerically equal but opposite in sign to the spreading coefficient) of the antifoam on one foaming solution and the lack of correspondence for another system.

The overwhelming majority of data available in the literature confirms that much less gas mobility reduction is obtained in the presence of oil than in its absence [5, 6, 18, 25, 44, 60, 78, 86]. In corefloods, foam propagation is retarded in the presence of oil. Being the non-wetting phase in sands, oil occupies the large pores thus blocking a few of the foam generation sites [44]. Therefore, foam does not propagate until some of the oil is displaced. The destabilization of foam by oil in a porous medium is due to oil penetration of the gas/liquid interface followed by lamellae rupture [106]. Results of Lau and O'Brien [76] show that the presence of a spreading oil slows down foam generation and decreases foam propagation rate. Manlowe and Radke [81] indicated that foam stability in porous media is dependent upon the stability of pseudoemulsion films (liquid films between oil and gas). Collapse of these films causes foam lamellae to rupture.

Friedmann and Jensen [44] reported no significant decrease in the relative permeability to gas in the presence of a 36% oil saturation in sandstone. In the absence of any oil, the relative permeability to gas was reduced by a factor of 10. No pressure increase was observed with foam flowing in the presence of oil. Large numbers of PV's of foam were necessary to reduce the residual oil saturation to a level where foam started generating and a high pressure drop was created.

Jensen and Friedmann [67] reported pressure drops as a function of oil saturation with foam flowing in Berea sandstone cores. Three different kinds of surfactants were used. The pressure drop obtained with the oil insensitive surfactant was not affected by the presence of oil as much as in the case of the other surfactants. The foam was preformed before injecting it at a rate of 14 m/d into the core. There is no mention, however, as to how the data were obtained. Keeping a material balance for oil as a function of pressure drop is fairly difficult because of the production of oil in the form of an emulsion that is hard to break. However, the oil saturation in the cores for all the experiments were determined at the end of the runs by extraction.

Data for residual oil saturation (S_{or}) as a function of capillary number (N_{ca}) were obtained by increasing the surfactant injection rate and thereby increasing the pressure drop. The experiment was performed in a Berea sandstone core at the residual oil saturation to waterflood in the absence of gas. The conclusion was that, since the interfacial tension was similar for all three surfactant solutions, the difference in behavior of the three foaming agents on oil recovery is due to the extent of their foaming ability in the presence of oil. On the other hand, results by Isaacs et al. [65] showed that injection of oil of up to 0.2 volume fraction had minimal detrimental effect on foam mobility reduction.

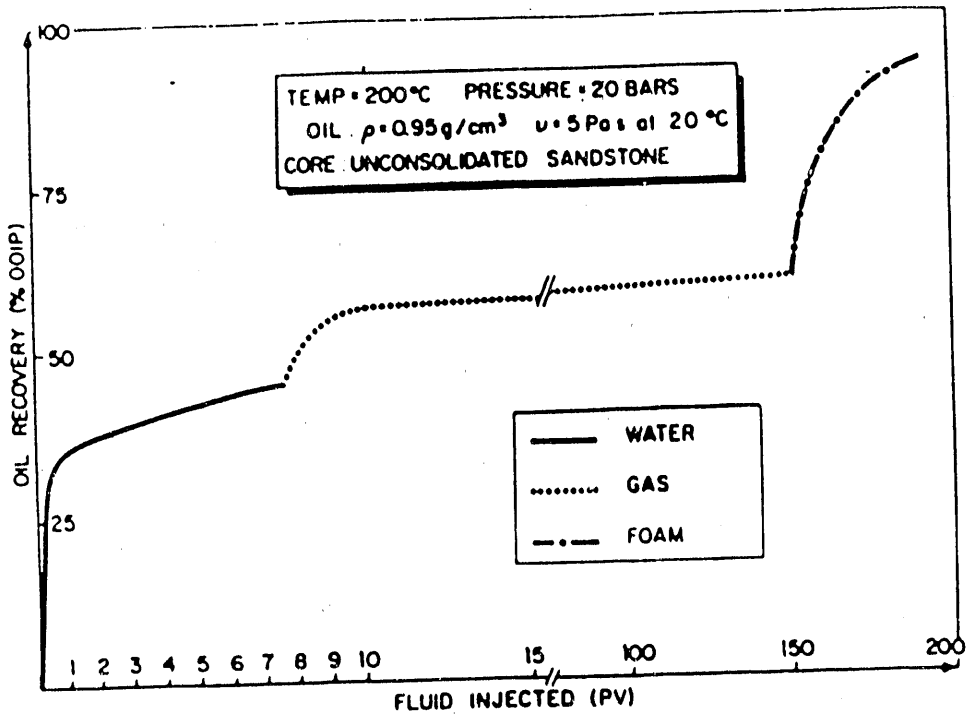

Figure 2.7: Oil recovery under reservoir conditions, after Robin [108].

Robin [108] reported the results of experiments performed in a 12 Darcy sand. The sandpack was first saturated with 100% crude oil, hot water was injected, followed by gas injection and then by foam, as shown in Figure 2.7. Because the core was saturated 100% with oil to start with makes one believe that a high oil recovery was obtained. Also it is worth noting that with the hot water drive, the recovery is still increasing. The injected gas volume was too high and not necessary.

2.3.5.13 Capillary Number

The fact that the surfactant solution is capable of creating a large pressure drop as well as reducing interfacial tension suggests that it is possible to relate the oil recovery efficiency of a foam drive to the N_{ca}. Jensen and Friedmann [67] reported oil-water interfacial tensions by the pendent drop method of around 2-4 mN/m at 275 °F for their system. This is about one tenth of the IFT between oil and water. In their experiment, an increase of about a factor of 10 was enough to reduce S_{or} from 20% down to about 7%.

2.3.5.14 Wettability

Kanda and Schechter [70] observed loss of mobility control in bead packs when the bead packs were silicone coated. Possibly this was because the foam lamella bridging the pores

were unstable as a result of poor wettability. Foam was generated in carbonate cores (k_{air} = 807 md, k_{brine} = 83 md) with several foaming agents. Mobility reduction factors (pressure gradient with surfactant and gas to that of brine and gas) ranged from 8 to 28 [78]. Modifying the wettability of Berea cores to oil-wet caused less mobility reduction to gas [122]. Results by Sanchez and Hazlett [117] indicate that foaming surfactants change the wettability of a system from oil-wet to water-wet.

2.3.5.15 Foam Propagation

Holm [60] used gas and liquid phase tracers to determine that the gas and liquid phases of an injected foam have different residence time. From this, he concluded that liquid moves through the porous medium via the film network of bubbles and gas moves progressively through the system by breaking and reforming bubbles throughout the length of the flow path. High gas saturations were observed even with low quality foams.

Gas breakthrough is found to be substantially delayed when gas is injected into a core in the presence of surfactant in solution [44, 62, 107]. Foam propagation is faster at higher velocities and in high permeability porous media. Pregeneration of foam also contributes to rapid foam propagation [44].

2.3.5.16 Hysteresis

No hysteresis effects were observed between increasing and decreasing gas rates at constant liquid rate [97, 129]. However, Sanchez et al. [118] observed differences in drainage and imbibition cycles with foaming solutions of very low surfactant concentrations. Also, very long times were necessary to reach steady state on the drainage cycle whereas this was not the case on the imbibition cycle.

Chen et al. [15] observed that several drainage and imbibition cycles were necessary to obtain invariant capillary pressure curves.

2.3.6 Foam in Micromodels

Micromodels provide valuable qualitative data from observations at the pore level. However, capillary end effect dominates the fluid distribution and pressure drop in micromodels. Foam is generated at the production end regardless of flow conditions in the micromodel [84]. Also, glass micromodels fail to reproduce reservoir rock wettabilities.

Mast [84] observed that when foam is unstable such as foam obtained with low surfactant concentrations, gas and liquid flow primarily by breaking and reforming lamellae in the constrictions between pores. However, with stable foams obtained with high surfactant concentrations, gas and liquid move mainly as bubbles.

Shirley [121] studied the effect of pore geometry on foam formation mechanisms. Snap-off was the dominant mechanism in highly heterogeneous pore systems. Bubble generation by snap-off causes an increase in the pressure drop across the model [4].

Foam flow studies in etched silicon wafer micromodels provide a visual observation of the different mechanisms for foam flow in porous media [93]. It was observed that snap-off occurs at pore constrictions and that gas flows primarily by lamellae breaking and reforming. Lamellae were found to block the flow paths for gas causing trapping.

2.3.7 Foam in Capillary Tubes

In smooth capillaries with a constriction, the time required for snap-off has been quantified as a function of the time required for bubble movement through the constriction and the time for liquid flow back into the pore throat [13, 103]. Large differences have been observed in the time required for snap-off depending on the geometry of the capillary tube. Studies by Gauglitz et al. [46, 47] indicate no difference in time for bubble breakup between sodium dodecylbenzene sulfonate and Chaser SD1000 surfactant solutions.

Apparent foam viscosity measurements in smooth capillaries have been modeled [57]. The model has further been improved by accounting for capillary pressure and a constricted flow path [37, 39]. Foam viscosities [94] in capillary viscometers were estimated to be about 80 cp.

2.4 Models for Foam Flow

Population balance models have been formulated to try to understand foam flow in porous media [36, 37, 43]. A model that accounts for population balance and mass and momentum conservation predicted bubble generation and trapping [37]. Falls et al. [37] incorporated into their model a critical capillary pressure below which foam generation by snap-off may take place.

The population balance model by Friedmann et al. [43] was incorporated into a conventional thermal simulator. The model predicted foam generation, coalescence and trapping. Foam rheology and texture in porous media have also been accounted for in the model.

Foam generation rates by snap-off are proportional to gas velocity to an exponent [36, 37, 43]. Foam collapse rates are proportional to gas velocity and bubble density. These functions are valid for a particular surfactant provided no saturation and surfactant concentration changes occur.

A steam foam simulation model by Patzek and Myhill [96] could be made to accurately predict incremental oil recovery in the Kern River's Bishop steam foam pilot by adjusting the effective surfactant partition coefficient.

2.5 Review of Foam Application in the Field

Hirasaki [58] described the indications used in evaluating the performance of a steam foam process as follows:

- An increase in the injection pressure due to steam mobility reduction.
- An improvement in the injection profile and vertical sweep.
- A reduction in the steam blow from production wells.
- Increased oil cut and oil recovery or increased oil/steam ratio.
- A minimal amount of surfactant per barrel of incremental oil.

This review of steam foam field tests indicates that less surfactant will be required to control injection profile in a layered reservoir with vertical barriers such as Midway Sunset field than to completely flood a layered reservoir with vertical communication such as Kern River field.

The mode of injection depends on the reservoir properties. For a reservoir with vertical communication, in-depth mobility control can be achieved with continuous injection whereas in a reservoir with vertical barriers, slug injection may be sufficient to improve the injection profile. Also, the addition of noncondensable gas extends the life of foam away from the wellbore [58]. Results by Dilgren et al. [23] indicate that only traces of nitrogen are sufficient to stabilize steam foam.

Steam foam pilot tests in the Kern River [11, 23, 95] and Midway Sunset [26, 28, 29, 45, 90, 100] fields showed increased pressures and improved oil recoveries. Other field tests were undertaken in different fields such as Guadalupe [89], North Kern Front, Painter, San Ardo [29], Cat Canyon [29], South Belridge [25], and Tia Juana [91]. Results indicate increased

oil cuts, improved oil/steam ratios, reduced steam mobility, increased reservoir pressure and temperature, and increased vertical sweep.

Reduction of gas injectivity was observed after foam injection in two different patterns of the Kaybob South Triassic A Pool, a carbonate reservoir in Alberta, Canada. Original gas injectivity was restored by injecting water. Injection of a single slug of high concentration surfactant solution was less effective in reducing gas injectivity than several slugs of lower concentration [78].

Chevron's nitrogen foam field test in the Painter reservoir in Wyoming [73] was not very successful. The pregenerated foam was injected into the low permeability reservoir (7 md). However, pressure-transient analysis showed that the effects of foam were limited to the near-wellbore region and that the foam did not propagate deep into the reservoir.

The cost of the pilot project undertaken by Shell at Bishop in Kern River was about $8-12/barrel of incremental oil [95]. This was evaluated on the basis of 10-15 lbm of surfactant per incremental barrel of oil, including the cost of the surfactant, salt, nitrogen, and foam injection.

2.6 Biodegradation of Foaming Surfactants

Surfactant biodegradation is the destruction of surfactants by the biological action of microorganisms present in various environments.

The most important microorganisms by far are bacteria which are capable of utilizing as food an infinite variety of organic compounds thereby degrading them by oxidation. Bacteria can live, adapt, acclimate and propagate upon such improbable foods as gasoline, benzene, and detergents.

Surfactant biodegradation tests involve parameters such as the type and concentration of bacteria and surfactant, presence of oxygen, temperature, and the analytical methods in use. In biodegradation work, surfactant concentration at or below 10 ppm are of primary interest. A typical result of biodegradation experiment would be a plot of surfactant concentration versus time. In general, a period of acclimation is first observed during which the bacteria adjust and multiply.

It is generally accepted that the surfactant structure is an important factor of its biodegradability [123]:

1. Increased hydrophobe linearity promotes biodegradability whereas branching of the hydrophobe deters it.

2. The nature of the hydrophile is only a minor factor in biodegradation.

3. The rate of alkylbenzene sulfonate biodegradation is increased with larger distance between the sulfonate group and the far end of the hydrophobe group.

Chapter 3

EXPERIMENTAL MATERIALS AND PROCEDURES

The objective of this research program was to investigate some of the important parameters that affect foam flow in porous media. Effort was directed toward studying parameters individually while keeping other parameters constant within experimental limitations. Steady state foam flow experiments were conducted in Berea sandstone cores at room temperature. Most experiments were performed using Chevron CHASER SD1000 surfactant in a system with a back pressure.

Besides some important findings, this systematic analysis contributed to explaining others' results as well as clearing up some of the seemingly contradictory interpretations.

The following sections describe the materials used in the experimental program. A description of the experimental set-up and procedures will also be detailed.

3.1 Experimental Materials

The following sections describe the different materials used in the experimental program.

3.1.1 Porous Media

All experiments were conducted in Berea sandstone cores. Two different sizes of cores were used: 1 inch in diameter, 4 inches in length and 2 inches in diameter, 10 inches in length. All cores were fired in a constant temperature oven overnight at $600^{o}C$ to stabilize clay minerals and minimize their swelling and plugging effects.

The fired short core samples had a porosity of about 27% and single phase permeability to liquid of about 700 md. The fired longer cores had a porosity of 24% and average liquid permeability of about 500 md.

The prefoamer, used in some of the experiments to pregenerate foam, was a sintered stainless steel filter element with a mean pore diameter of 7μm and an effective filter area of 3.5 cm^2.

3.1.2 Aqueous Phases

The surfactants used in the experiments were sulfonates. Chevron Chaser SD1000 was used in all the different types of experimental measurements. In IFT measurements and foam flow experiments, Shell Enordet LTS18 was also tested.

Chevron CHASER SD1000 is an anionic surfactant used as a steam additive in cyclic as well as drive EOR applications. It is an alpha olefin sulfonate dimer based on C_{12}-C_{18} olefin making it a highly branched alkyl sulfonate. It foams with steam or nitrogen gas in porous media where oil saturations are below 10%.

The thermal stability of SD1000 is well above that of other alpha olefin sulfonates. The half-life of this disulfonate at 600°F is about five times longer than that of AOS. It is soluble over a wide range of ionic strengths and a wide variety of brine solutions. It has a molecular weight of about 300. SD1000 is not biodegradable in the ASTM test D2667-82 and is toxic at high concentrations.

Shell ENORDET LTS18, is a linear alkyl toluene sulfonate with an average linear chain of 18 carbon atoms and has a molecular weight of about 460. It is thermally very stable but has moderate solubility in brine. It is a good foamer at steam temperatures.

Surfactant solutions were prepared in 1 % by weight NaCl brine with 0.5 % by weight active surfactant concentration, except in oil displacement experiments where 1 % by weight surfactant concentration was used. The water used to prepare the surfactant solutions was distilled water, filtered through a 2μm filter element.

3.1.3 Oleic Phases

The oil used in the flow experiments was a refined oil, kerosene. In IFT measurements, another refined oil, dodecane and Huntington Beach crude were tested.

At room temperature, the kerosene used in the oil recovery experiments has a viscosity of 1.38 cp and a specific gravity of 0.82.

3.1.4 Gaseous Phase

The gas used in all foam generation experiments was industrial grade nitrogen supplied from tanks through pressure regulators. The gas was filtered through a $2\mu m$ filter before being used in the foam flow experiments.

3.2 Experimental Apparatus

The following sections describe the different equipments used in the experimental procedures.

3.2.1 Flow Set-Up

A schematic diagram of the foam flow apparatus is shown in Figure 3.1. A Hassler type core holder with a rubber sleeve was used for the short cores. A shrinkable Teflon sleeve was used for the long core system. The annular space between the sleeve and the core holder cylinder was filled with liquid before applying the overburden pressure with nitrogen. The overburden pressure prevented fluid bypass between the core and the sleeve. A differential pressure of at least 100 psi was always maintained between the overburden pressure and the fluid pressure in the core.

The long core holder was also equipped with three pressure taps that gave four equal sections of 2.5 inches each. The pressure drop of each section as well as the total pressure drop across the core were recorded using pressure transducers connected to a data acquisition system (DAS) via a demodulator.

Connection lines were either Teflon or Inconel (1/8 inch OD), depending on the pressure level. Stainless steel valves were used throughout the system. The liquids were injected using pulse-free constant rate chromatography pumps. The gas was injected using a gas flow controller which supplied a constant volumetric flow rate regardless of pressure fluctuations in the system. The fluids were mixed either in the tubing right before entry in the core or using a prefoamer which consisted of a sintered stainless steel filter. The system was set at a pressure level of about 100 psig using a back pressure regulator. The effluent was either separated and the cumulative volumes recorded as a function of time or the surfactant solution was recycled in a tank for reinjection.

A brief description of some of the important parts of the experimental set-up follows:

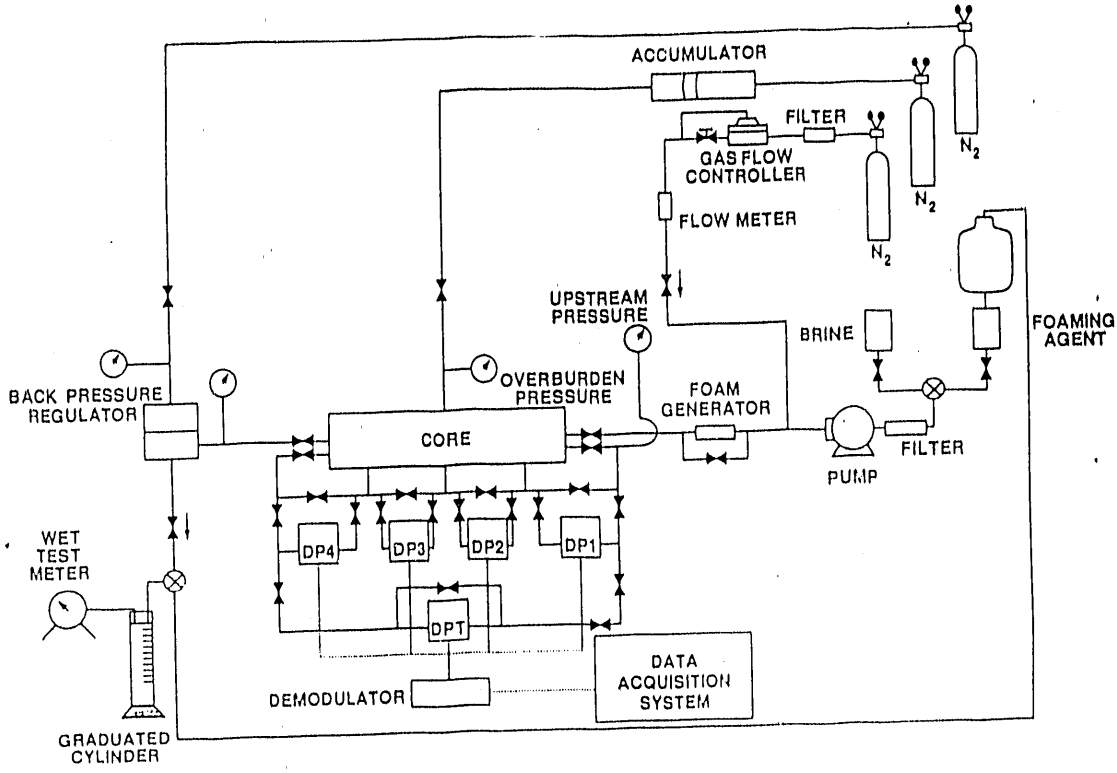

Figure 3.1: Schematic diagram of experimental flow set-up.

- Vacuum Pump: A Welch (Model No. 1400) vacuum pump was used to evacuate the core and saturate it with liquid. A gas drying unit filled with Drierite (anhydrous calcium sulfate) was used in line with the vacuum to prevent moisture from going to the pump.

- Injection Pumps: Two Constametric I liquid chromatography pumps were used to inject the aqueous and oleic phases. These metering pumps, manufactured by LDC/Milton Roy Co., provide a pulse-free constant flow rate irrespective of downstream pressure up to 5000 psi. This is accomplished by the rotation of a motor driven specially designed cam that causes plungers to reciprocate between two pumping chambers. The movement of the plungers is such that the sum of the discharge output is constant. The flow rate is adjustable up to 3.3 ml/min or 10 ml/min, depending on the pump model. Extreme care has to be taken to make sure that large particles are not present in the fluids being pumped. Otherwise, frequent cleaning and repair of the check valves would be necessary, as outlined in the pump's manual.

- Gas flow controller: The Moore 63SD-L constant-differential gas flow controller provided a constant volume flow rate regardless of pressure fluctuations in the core. This is achieved by maintaining a constant differential in the pressures across the external needle valve, making the flow a function of the needle valve opening. This controller yields a fixed foam quality at the inlet end of the core.

- Gas rotameter: The Omega FL-210 flowmeter was used in the gas supply line to obtain a visual reading of the gas flow rate.

- Check Valves: A Nupro (SS-2C-1) check valve was used in the gas feed line just before connecting it to the liquid flow line. This helped start the gas flow in a smooth fashion. Another check valve (SS-2C-10) was used downstream of the back pressure regulator to divide gas expansion from core pressure to atmospheric into two steps. This minimized pressure fluctuations at the downstream end of the core.

- Fluid bottles: Polyethylene carboys were used for the surfactant solutions as well as for the oil phase. The one-gallon bottles had a spigot molded to the base. They were positioned higher than the level of the pumps to supply the liquids by gravity.

- Filters: Even though brine was filtered through a 2μm membrane filter, 2μm in-line filters (NUPRO SS-2F-2) were used between the fluid reservoirs and the pumps. This ensured particle retention before the fluids reached the pumps. Otherwise frequent pump failure would be encountered due to particles lodging in the check valves of the pumps' liquid ends. An in-line filter was also used before the liquids reached the foam generator or the core to minimize any pulses from the pumps.

- Foam generator: A 7μm in-line filter (NUPRO SS-2F-7) was used as a prefoamer in all of the experiments. It had an effective filter area of 3.5 cm^2. It produced a finely textured foam.

- Core holder: Two different stainless steel core holders were used:

  - Hassler type core holder, 1 inch in diameter, that can accomodate a core up to 5 inches in length.

  - Shrinkable Teflon type core holder 2 inches in diameter and 10 inches in length. The core holder had three pressure taps, drilled at equidistants (2.5 inch sections). This core holder was previously used by Huh [62].

- Back pressure regulator: A Grove 90W dome-type back pressure regulator was used downstream of the core to keep the system at a minimum pressure level. The line pressure was regulated by adjusting the pressure applied in the dome with a nitrogen tank .

- Pressure gauges: A Heise gauge was used in the flow system upstream of the core to verify inlet pressure readings. A USG Test gauge was used downstream of the core verifying

the constant downstream pressure. Other gauges were used to measure the back pressure setting as well as the overburden pressure. A vacuum gauge was used to monitor the efficiency of the core vacuuming process.

- Pressure transducers: Validyne DP15 variable reluctance pressure transducers were used to measure the pressure drop across the shorter core as well as across each section of the long core. A flat diaphragm, clamped between symmetrical case halves of the same material, is the pressure sensing element. Diaphragm deflections are sensed by coils embedded in the case halves. Diaphragms of different pressure ratings were used, depending on the pressure drops encountered.

- Demodulator: Two different demodulators were used, one to measure the pressure drop across the core (Validyne CD23) and another to measure the sectional pressure gradients (Validyne CD280). They convert AC signals from the transducers to DC.

- Wet Test Meter: A Precision (Model No. 63115) wet test meter measured cumulative gas volumes produced at atmospheric pressure.

- Timer: A Precision (Model No. 69235) timer continuously recorded the time. This made it easier to calculate gas flow rates as well as to reference all steps and procedures within an experiment from time zero.

3.2.2 Temperature Monitoring System

The room temperature was continuously monitored to correlate with pressure fluctuations. A type J (Iron-Constantan) Omega thermocouple was connected to a thermocouple meter. A Linear 555 chart recorder was used to continuously record the room temperature.

3.2.3 Data Acquisition System

A data acquisition system has two major parts: hardware and software. A plug-in type data acquisition system, Metrabyte DASH-16F board, was installed into an IBM-XT compatible computer. The software used along with the Metrabyte DASH-16F board was Lotus Measure.

3.2.3.1 Hardware

Metrabyte DASH-16F board is a multifunction high speed analog/digital input/output expansion board. It turns the personal computer into a fast high precision data acquisition

instrument. It is capable of providing either sixteen single ended channels or eight differential channels.

3.2.3.2 Software

Lotus Measure provides a data acquisition driver that extends the use of the personal computer. Experimental data can be acquired, transformed and saved in the Lotus 1-2-3 worksheet environment. This gives the user immediate access to data analysis.

Lotus Measure's MBC 16 module works with the DASH-16F board to convert analog signals to digital. Specification of testing conditions under which to collect and convert data is done using the menu-driven module. The user writes the code to convert incoming measurements to engineering units. Measure acts as a dynamic driver for Lotus 1-2-3. The user is able to load it by defining it as part of the 1-2-3 hardware set when loading 1-2-3.

3.2.4 Extraction Apparatus

A Dean-Stark extraction apparatus (Figure 3.2) was used to determine oil saturations in the core at the completion of experiments. The apparatus was designed to accommodate the large cores. A heating mantle provided heat to the 3000 ml round-bottom flask. The heat input was adjusted by regulating the power input to the heating mantle using a rheostat. The sample container has a length of 30 cm and a diameter of 7.5 cm. It has a 81/50 joint on top and a 24/40 joint at the bottom. An adapter covers the sample container and connects the system to the 25 ml water trap which has a Teflon stopcock at the bottom. A 400 mm Liebig condenser is connected to the water trap through a 105° bent adaptor. All joints were 24/40 except for the sample container top joint.

3.2.5 Spinning Drop Apparatus

IFT measurements were obtained by the spinning drop method under different conditions of salinity, concentration, temperature, oil type and time. A detailed description of the spinning drop apparatus and the procedure for measuring IFT's have been discussed in other publications [33, 54, 132].

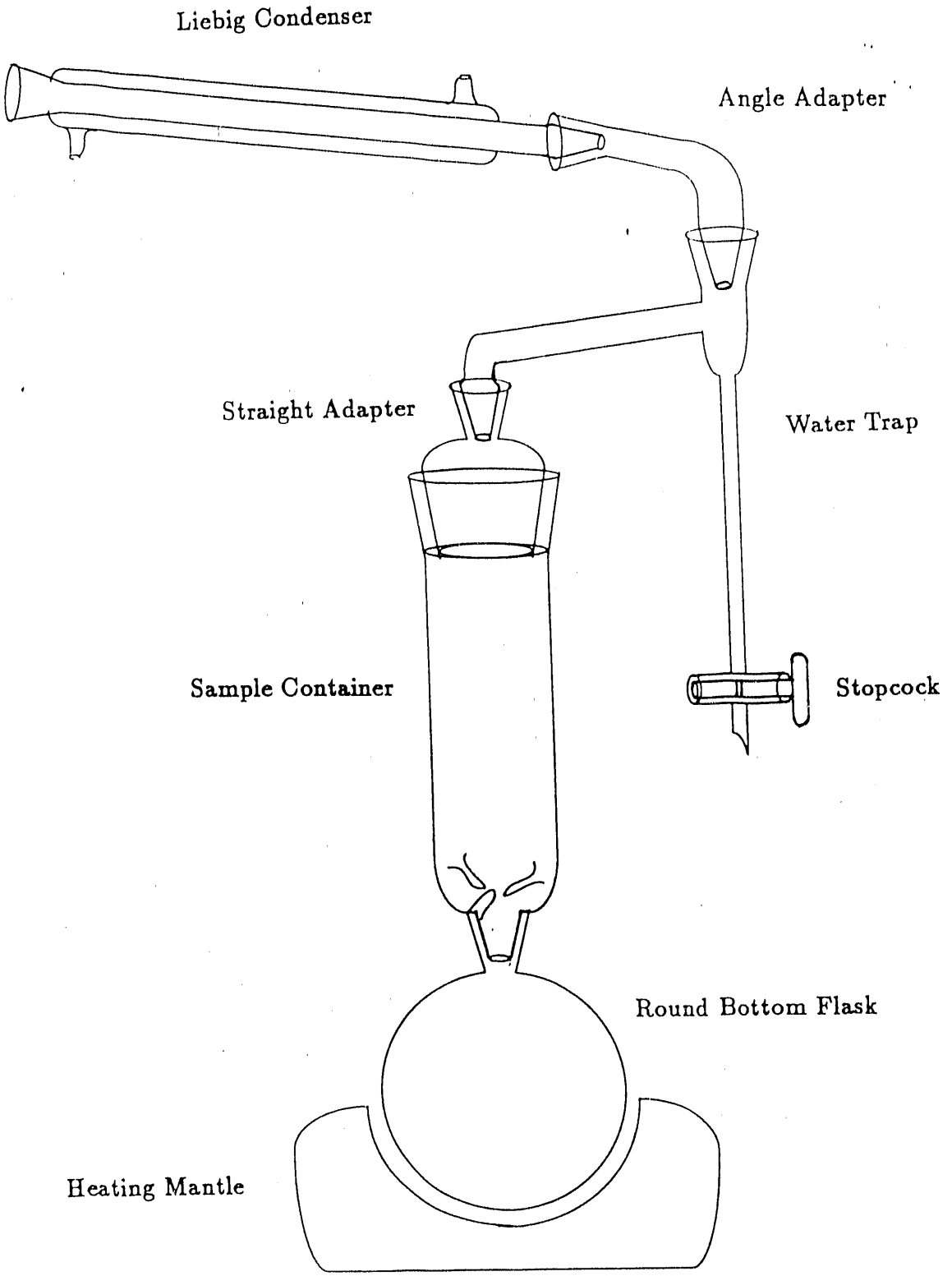

Figure 3.2: Schematic diagram of Dean-Stark extraction apparatus.

3.3 Experimental Procedures

The following sections describe the procedures followed in conducting the different types of experiments and experimental preparations.

3.3.1 Flow experiments

Several procedures have to be completed before foam flow experiments can be conducted. The following sections describe such procedures.

3.3.1.1 Core Mounting

The fired core was mounted in a shrinkable Teflon sleeve using high temperature epoxy and a hot air gun. The sleeve makes it possible to apply an overburden pressure onto the core.

The two inch diameter FEP roll cover was etched with Tetra Etch. This cleans the sleeve and provides a better bonding with the sandstone. It is then washed with warm soapy water and then with isopropyl alcohol.

The lateral edges of the fired core and the end plugs (Figure 3.3) were coated with high temperature epoxy (GE RTV 159). The system was inserted into the roll cover and clamped down. The sleeve has to be about two inches longer than the combined lengths of the core and the two end plugs to account for shrinkage. Heat is applied evenly around the circumference to ensure a surface free of wrinkles or bubbles. The heat gun should be pointed at the rotating roll about one inch away from it and toward the roll end. The heat gun is moved slowly along the rotating roll towards the unshrunk end, always pointed toward the starting end. After completing the shrinking process, the ends of the sleeve are trimmed with a sharp knife.

After mounting the core and letting the epoxy cure overnight, it is inserted into the core holder and end fittings placed and tightened. Viton O-rings were used in the design of the core holder to prevent leaks, as shown in Figure 3.4. The pressure taps were then fitted and holes drilled into the Teflon sleeve through the pressure taps.

3.3.1.2 Porosity Measurements

The core was subjected to an overburden pressure which is monitored to make sure no leaks are present. The core was pressurized with nitrogen gas. While bleeding the gas in steps, produced gas volume and pressure level were recorded. The porosity of the core was calculated

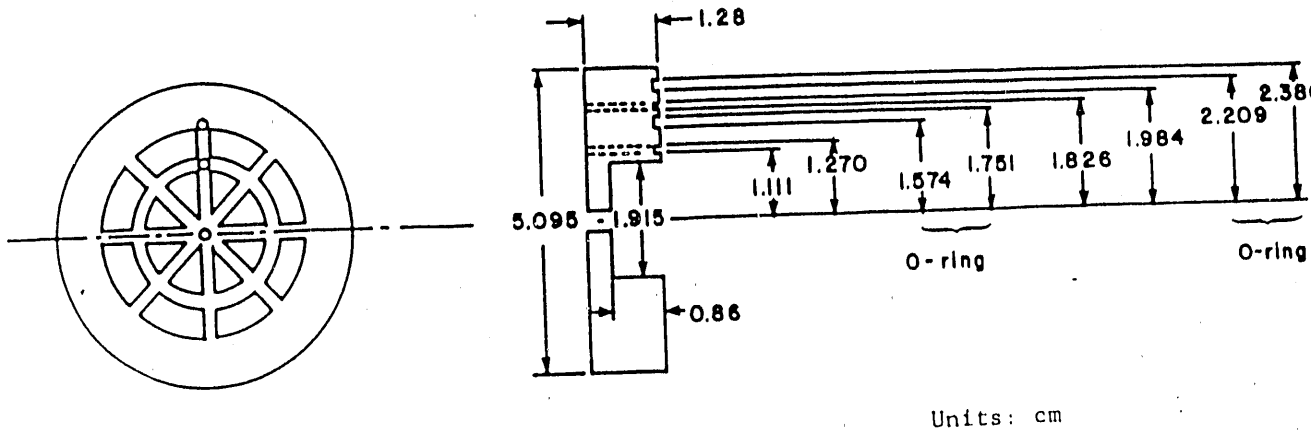

Figure 3.3: Schematic diagram of end plug design, after Huh [62].

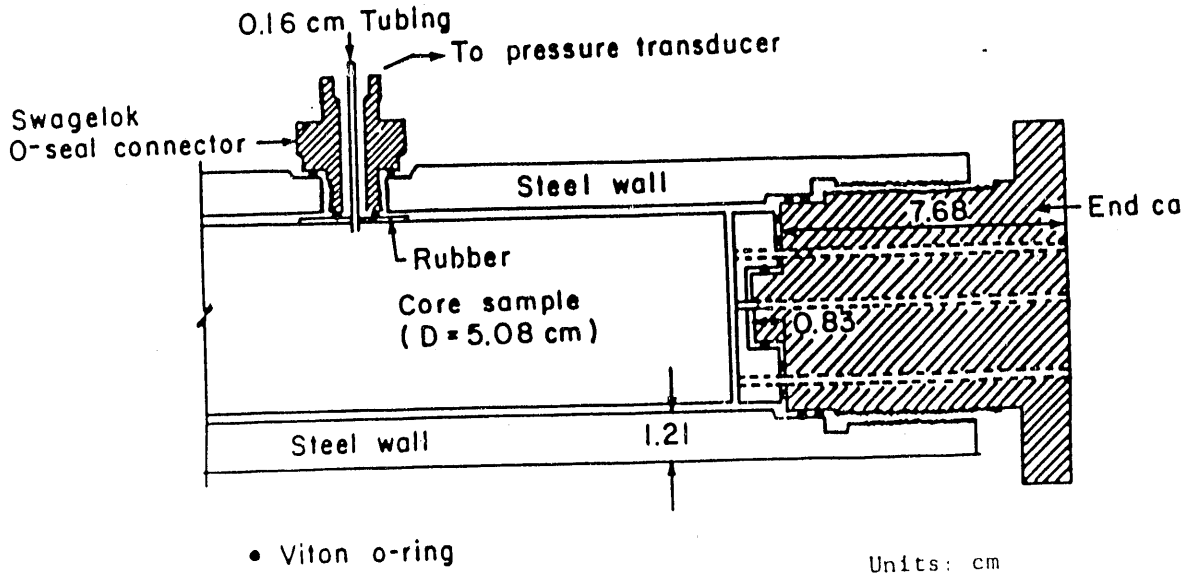

Figure 3.4: Schematic diagram of core holder design, after Huh [62].

by applying Boyle's law. Porosity calculations were verified by measuring the liquid volume intake during saturation of the core, after evacuating it.

Before the core was saturated with brine, absolute permeability to gas was measured with nitrogen injection by applying Darcy's equation. Gas was flowed through the core at a constant rate and the pressure drop across the core recorded, as described below.

3.3.1.3 Core Saturation

The core was evacuated and saturated with 1% brine. The pore volume was determined by measuring the volume of liquid intake, corrected for the amount of dead volume in the system.

3.3.1.4 Permeability Measurements

The single phase gas permeability was measured using Darcy's equation. After the core was evacuated and saturated with brine, several pore volumes of brine were injected at 100 psig pressure to ensure that no changes in permeability would occur. While injecting brine at constant rate, the pressure drop across the core was recorded and absolute liquid permeability calculated using Darcy's equation. Absolute permeabilities were also measured at the completion of experiments. Final values different than initial ones would indicate permeability damage.

3.3.1.5 Pressure Measurements

During single phase liquid flow, pressure drops were recorded using the data acquisition system. In this mode of operation, the DAS was run for a brief period of time, of the order of minutes, depending on the pumping rate. Data was acquired frequently, at least one per second. The pressure profile with time was very useful in detecting pulsation problems with the pump. The pressure cycles indicated check valve leaks as well as liquid end failures.

During unsteady state foam flow experiments, the data acquisition rate was set at one per ten seconds for the first thirty minutes. This ensured detailed data of the early time period. The acquisition rate was then changed to one per minute for the next two and a half hours and then ten or less per hour thereafter. At the end of the experiment, if the rate of pressure change was not very large during early times within a large number of data points, the data set was trimmed in order to keep the files of manageable sizes.

3.3.1.6 Foam Start-Up

All experiments were started with the core evacuated and then saturated with 1% brine. With the system set at a pressure of 100 psig, brine was injected continuously until the pressure gradient across the core was stabilized. This ensured a complete liquid saturation and that no detrimental effects of clay would occur. Injection of about 40 pore volumes of surfactant solution displaced the brine and established equilibrium surfactant adsorption onto the rock surface. Gas flow was initiated while surfactant injection was continued. The data acquisition system was started simultaneously with the gas injection.

No attempt was made to measure gas and liquid pressures individually. Therefore, it is assumed that pressure gradients in the gas and liquid phases are about the same, in view of the level of pressure gradients observed.

In steady state experiments, the gas and liquid flow rates were varied individually or in combination from one experiment to the next. A constant pressure drop over several pore volumes indicated a new steady state was reached. Any minor trends in pressure levels was taken as indicating that the system had not reached steady state. This was particularly justified in the initial drainage cycle, as will be discussed in the results section.

3.3.1.7 Flow Rate Measurements

The effluent foam was either broken down in a separator and cumulative volumes recorded with time or recycled back to the surfactant tank. In experiments where the gas rate was low, the effluent gas was collected in an inverted burette and the volume recorded by water displacement. When the gas rates were high, the effluent gas volume was measured using a wet test meter. Monitoring was continued until the pressure response stabilized.

The liquid flow rate was set by the dial on the pump. Frequent flow rate measurements verified that the liquid flow rate is proportional to the pump dial setting.

3.3.2 Oil Extraction

In oil displacement experiments, continuous material balance calculations provided an estimate of oil saturations in the core. In the absence of surfactant, produced oil and brine were easily separated by gravity and measured. However, with surfactant present, some of the oil was produced as an oil-in-water emulsion. Therefore, oil saturation measurements by material balance were not precise. At the completion of the experiment, the oil was extracted from the core in a Dean-Stark extractor using toluene.

Since kerosene is a light oil, solvents such as methylene chloride or methanol were not necessary to extract it. The core was extracted with toluene until water production stopped. The difference between the initial weight of the core and the weight after extraction and drying equals the weight of fluids recovered from the the core. Subtracting the weight of extracted water yields the weight of oil removed.

3.3.3 IFT Measurements

IFT was measured by the spinning drop method. The procedure consists of filling a glass capillary tube (0.079 inch ID, 6 inches long) with surfactant solution. A droplet of oil is injected into the center of the tube and its end is then sealed with epoxy. The tube rotates at 3600 RPM on the shaft of an electric motor in an insulated box. The temperature was maintained with a heat gun by regulating its power input with a rheostat. The dimensions of the oil droplet are observed under a microscope and recorded. IFT values can then be calculated as follows:

$$\sigma = \Delta\rho\omega^2 y^3/4 \quad (approximate\ solution,\ x_o/y_o > 4) \tag{3.1}$$

where σ = interfacial tension, $\Delta\rho$ = density difference between water and oil (g/cm^3), ω = rotational speed (rad/sec), y = one-half the minor axis of the drop (cm), and x_o/y_o = ratio of length of drop along axis of rotation to length of drop perpendicular to axis of rotation.

Chapter 4

EXPERIMENTAL RESULTS

4.1 Interfacial Tension Measurements

Interfacial tensions were measured using the spinning drop apparatus for two different surfactants which are known to be good foaming agents. Low values of IFT were not obtained with the Chevron Chaser SD1000. Figure 4.1 shows the IFT between dodecane and SD1000 as a function of temperature. The IFT is reduced by a factor of about 10 when compared to the oil-brine IFT.

The effect of temperature on IFT with LTS18 is shown in Figure 4.2. This surfactant reduces the IFT by a factor of 10 when compared to SD1000. However, this surfactant is not a good foaming agent at room temperature. Figure 4.3 shows the effect on σ of measurement time for the spinning drop method. The IFT decreases with time and then increases slightly. The effect of temperature on IFT of LTS18 with Huntington Beach crude oil is shown in Figure 4.4. The IFT increases steadily with temperature.

Results show that foaming surfactants do not reduce the IFT between oil and water enough to displace oil from porous media. Chevron Chaser SD1000 reduced the IFT by a factor of ten and LTS18 by a factor of about 100. However, this reduction in IFT is not sufficient to increase N_{ca} significantly, such that low residual oil saturations can be achieved.

4.2 Oil Recovery with Foaming Solution.

A series of preliminary experiments was performed to study oil displacement from Berea cores by foam injection. A steady state gas-brine relative permeability experiment was conducted in a 540 md Berea core, 2 inches in diameter, 10 inches in length. Nitrogen gas and 0.5% brine were the flowing fluids. The back pressure regulator was set at 210 psig. The results are

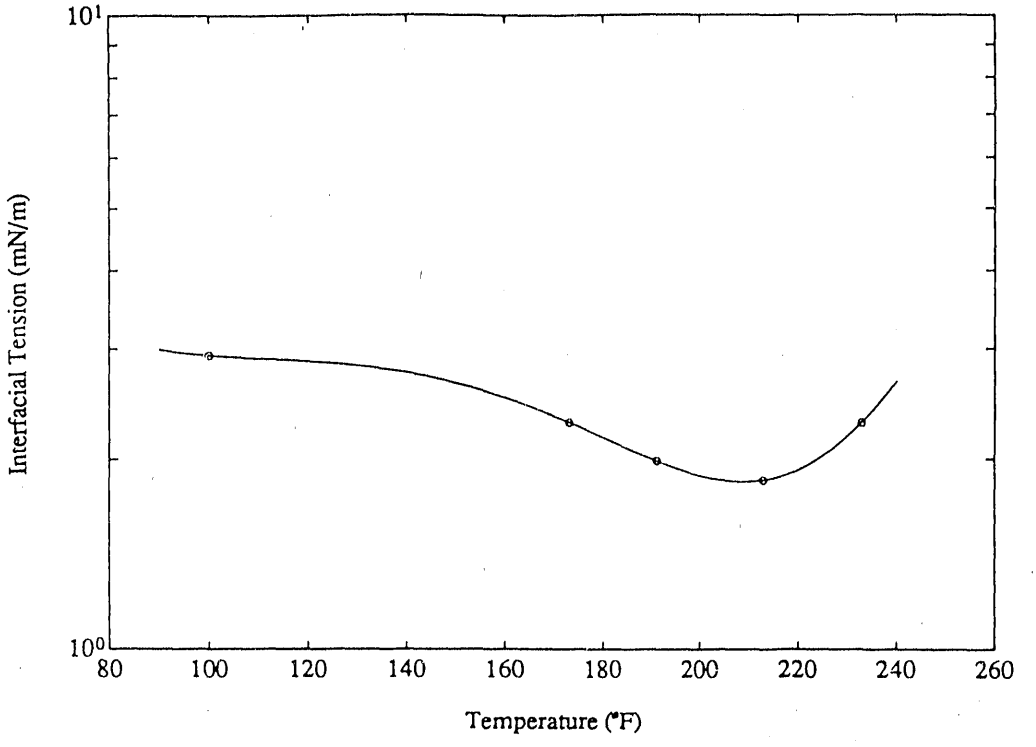

Figure 4.1: Interfacial tension of 1% Chaser SD1000 in 2% NaCl with dodecane vs. temperature.

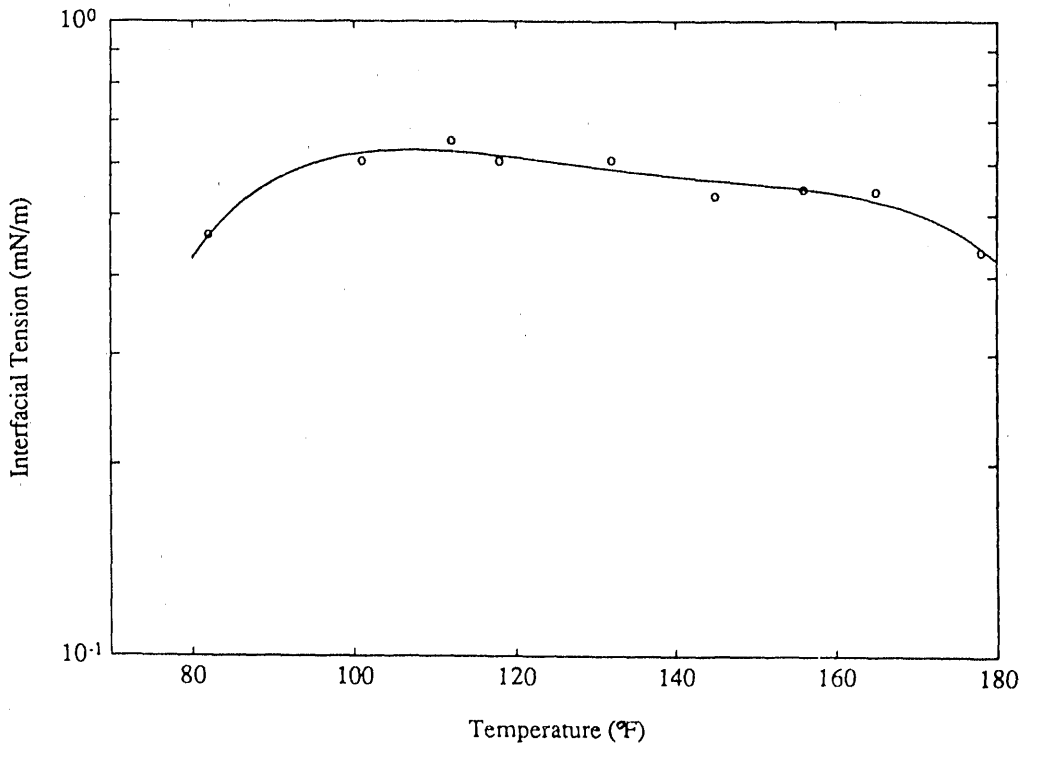

Figure 4.2: Interfacial tension of 0.5% LTS18 with dodecane vs. temperature.

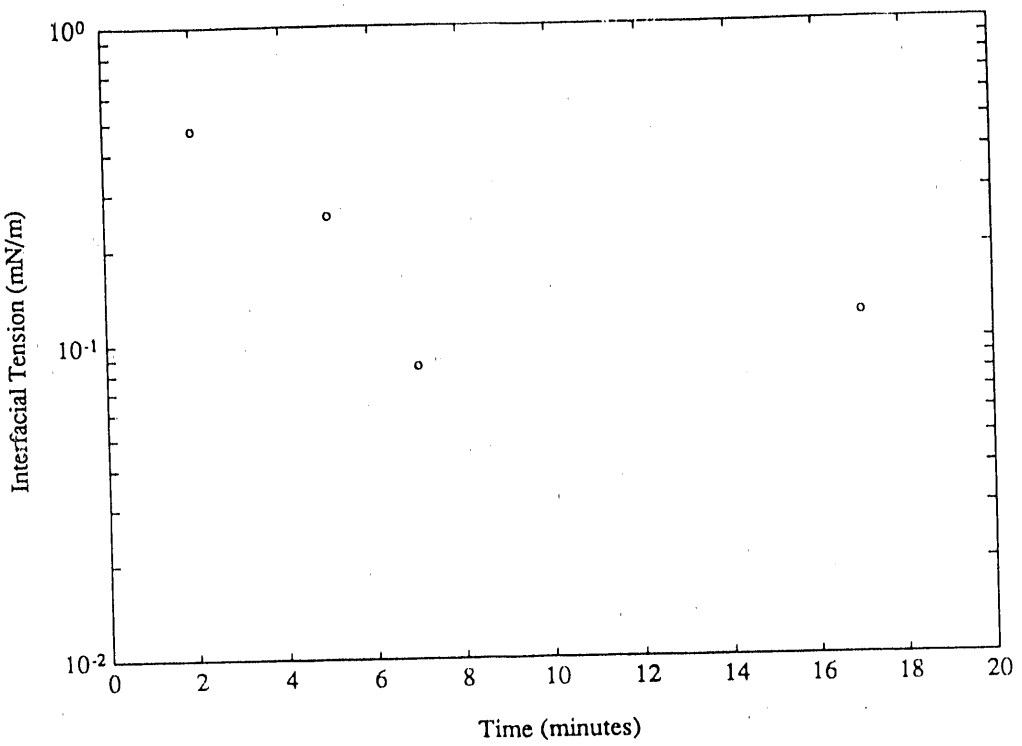

Figure 4.3: Effect of time on IFT with dodecane for 1% LTS18.

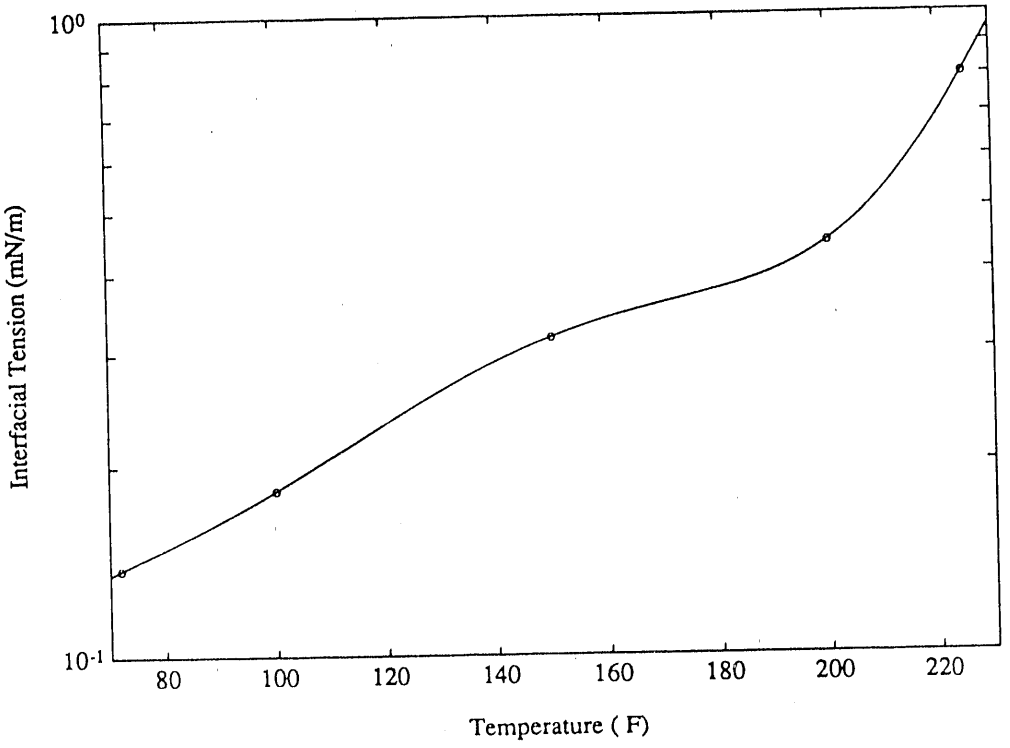

Figure 4.4: Effect of temperature on IFT of 1% LTS18 with crude oil.

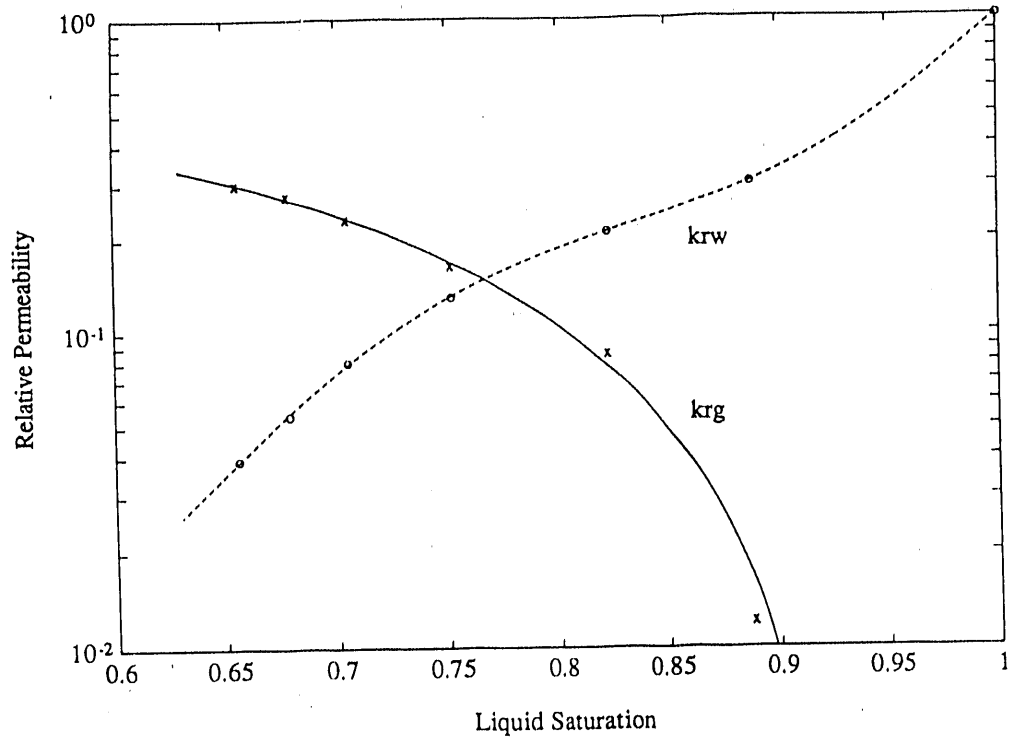

Figure 4.5: Steady state gas-brine relative permeability.

shown in Figure 4.5. The cross-over point of the relative permeability curves is at a somewhat high liquid saturation, but the overall shape of the curve as well as the values obtained are acceptable.

To compare the relative permeabilities of the gas and brine in the presence or absence of oil, kerosene was injected until a residual saturation to brine was reached (46.8%). The core was then waterflooded at 9.8 ft/day (1.01 ml/min) down to a residual oil saturation of 30.2%. Increasing the brine injection velocity to 30.6 ft/day (3.33 ml/min) lowered S_{or} to 28.6%. Simultaneous injection of gas and brine was initiated in order to evaluate the effect on oil displacement at the initial brine velocity of 9.8 ft/day. The oil saturation was reduced to about 24.2% with a gas velocity of 11.5 ft/day. Increasing the gas velocity to 202 ft/day displaced more oil and reduced the residual oil saturation to 16.1%. The pressure gradient under these conditions was similar to the pressure gradient obtained with only liquid flowing at 32 ft/day. However, injection of gas reduced S_{or} further. The results obtained at the different gas-brine ratios are shown in Table 4.1.

In order to investigate the effect of a surfactant solution on the relative permeability to the gas phase and on oil displacement, the core was resaturated and waterflooded again to a residual oil saturation (31.1%). Injection of surfactant solution (1% Chevron Chaser SD1000 in 0.5% NaCl) at 9.8 ft/day (1.02 ml/min) displaced an insignificant amount of oil (see Table 4.2). This also established equilibrium surfactant adsorption on the rock surface. Next, nitrogen gas was

Summary of Oil Displacement Results
by Gas and Brine Injection

V_p = 124 cc P_b = 225 psia
k_a = 540 md T = 22 °C

	$\Delta P/L$ (psi/ft)	v_g (ft/day)	v_l (ft/day)	PV (PV)	S_l (%)	S_g (%)	S_{or} (%)
Initial stage	---	---	---	---	46.8	0.0	53.2
Waterflooding	4.9	0.0	9.8	5.0	69.4	0.0	30.6
Waterflooding	15.8	0.0	32	5.0	71.4	0.0	28.6
Brine + Gas	11.2	11.5	9.8	1.76	64.2	11.6	24.2
Brine + Gas	15.6	202	9.8	22.5	68.8	15.0	16.1

Table 4.1: Summary of Oil Displacement Results by Gas and Brine Injection.

injected simultaneously with the surfactant solution. The results indicate that a significantly lower relative permeability to gas can be achieved in the presence of the foaming agent. It is noted that foam was not observed at the effluent end of the core until a high gas velocity of 1001 ft/day was reached.

Initially, the surfactant solution was not foaming due to the presence of a high oil saturation. When the residual oil saturation was reduced to a fairly low value (below 20%), the pressure gradient in the core increased due to the formation of foam. The residual oil saturation was determined to be 23.1% by material balance, but estimated to be less than 20% because some oil had been produced as an oil-in-water emulsion. The residual oil saturation was later determined to be 18.6% by extraction using toluene. It is worth noting that a similar S_{or} was obtained in the absence of surfactant where only gas and brine were flowing even though the gas-water ratio and the pressure gradient in the core were much lower than in the case of surfactant and gas injection.

Figure 4.6 shows the residual oil saturation in the core for the two experiments performed, that is, for gas-brine and gas-surfactant versus N_{ca}. The final oil saturations are almost identical. However, the capillary number in the two experiments differ by a factor of about 100. The final oil saturation for the gas-surfactant experiment (18.6%) was obtained by extracting oil from the core.

Summary of Oil Displacement Results
by Gas and Surfactant Injection

V_p = 124 cc P_b = 225 psia
k_a = 540 md T = 22 °C

	$\Delta P/L$ (psi/ft)	v_g (ft/day)	v_l (ft/day)	PV (PV)	S_l (%)	S_g (%)	S_{or} (%)
Waterflooding	4.9	0.0	9.8	5.0	68.9	0.0	31.1
Surfactant flooding	5.0	0.0	9.8	8.0	69.7	0.0	30.3
Surfactant + gas	14.2	32.3	9.8	7.1	39.2	34.5	26.3
Surfactant + gas	38.9	263	9.8	48.2	27.4	48.8	23.9
Surfactant + gas	59.2	557	9.8	107	26.1	50.9	23.1
Surfactant + gas	112	1001	9.8	218	25.8	51.1	23.1
Surfactant + gas	171	1273	9.8	271	25.0	51.9	23.1

Final oil saturation determined by extraction = 18.6

Table 4.2: Summary of Oil Displacement Results by Gas and Surfactant Solution Injection.

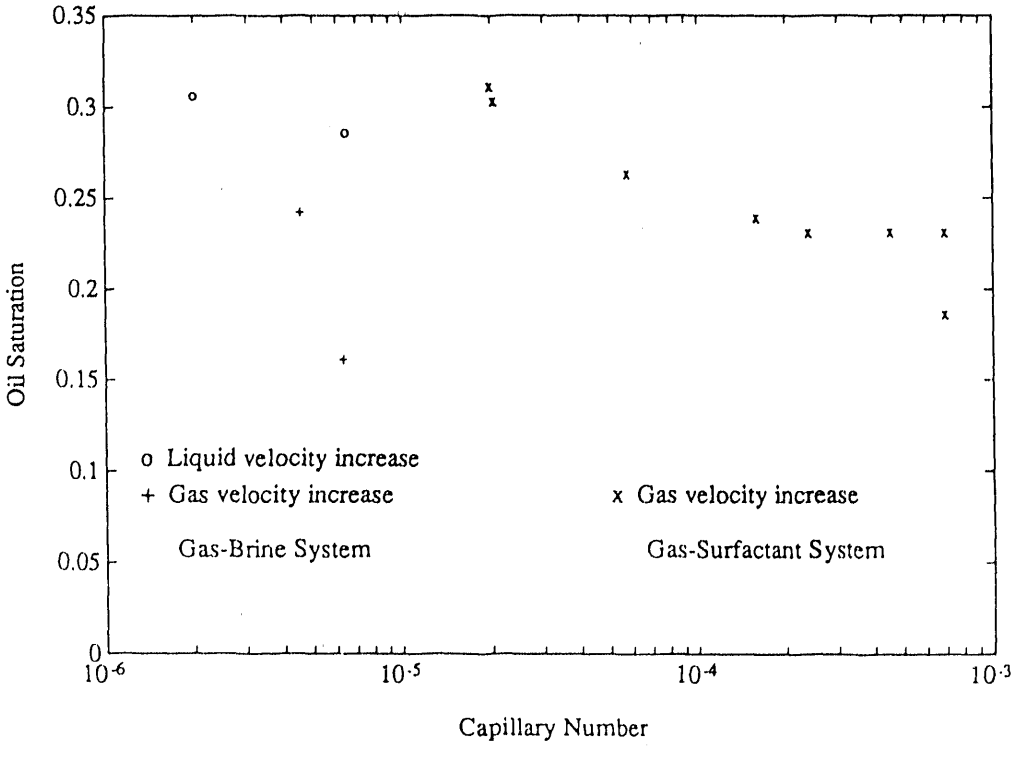

Figure 4.6: Oil saturation as a function of capillary number in oil displacement experiments.

4.3 Foam Generation and Propagation in Short Cores

4.3.1 Foam Incubation Period

The study of foam flow mechanisms, with special emphasis on the conditions under which foam generation is initiated in a porous medium, was undertaken using Chevron SD1000. A number of foam flow experiments was conducted in the 4 inch long Berea core (1 inch in diameter). The absolute permeability of the core was 700 md. Results show that it is possible to generate foam in a porous medium at relatively low flow velocities after prolonged periods of time, referred to as "incubation periods," indicating a stage when no significant change in the pressure gradient is taking place. However, it takes several hundred pore volumes of fluid injection.

The system was set at a back pressure of about 100 psig for all experiments. Gas flow velocities were calculated based on the flow rates measured at the effluent end of the core. These velocities, $\frac{q}{\phi A}$, were calculated at the upstream conditions in the core. The gas flow controller kept a constant volumetric flow rate allowing a constant foam quality to be injected.

After equilibrium surfactant adsorption was established by injecting SD1000 surfactant solution (0.5% Chevron Chaser SD1000 in 1% NaCl), gas injection was started along with continuous surfactant injection. Immediately after foam started forming, the pressure increased so rapidly that the experiment had to be stopped. The same experiment was performed with lower injection velocities. It took a while before the pressure upstream of the core increased. However, the pressure gradient in the core increased to a value above the demodulator calibration setting. Therefore, the experiment was repeated at lower velocities. Before starting the next experiment, the liquid saturation in the core was determined by removing the core and weighing it. The liquid saturation was evaluated at about 25%. This low value is due to some liquid being displaced from the core when the system was depressurized to atmospheric pressure. Taking into account this displaced liquid yields a liquid saturation of about 35%, which is within the range reported in the literature.

A third experiment was started with even lower velocities. The surfactant flow velocity was 5.74 ft/day (0.175 ml/min) and the gas flow velocity was 45.9 ft/day (1.4 ml/min). The liquid volume fraction was 0.11, based on the above mentioned velocities. It took about six days or 900 pore volumes of foam injection before the pressure kicked off, as shown in Figure 4.7. The system appears to have two states and the passage from the unstable state to the stable one is relatively rapid. It is worth noting that the pressure surge, that is, sudden increase of resistance to flow, occurred when the pressure gradient exceeded about 45 psi/ft (15 psi across the core).

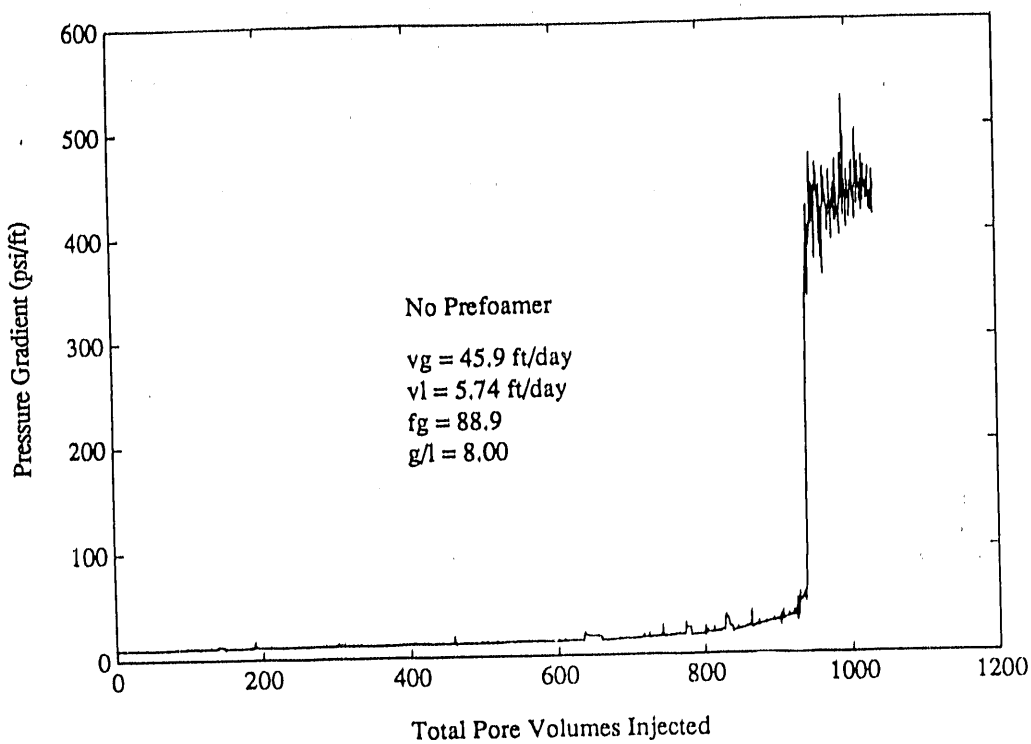

Figure 4.7: Pressure gradient history with simultaneous flow of gas and surfactant solution without prefoamer.

Further experiments were performed to define better the conditions under which foam formation is initiated. Experiments run under different conditions of flow velocities show similar patterns. The pressure gradient history of another run that behaved in a similar manner is plotted versus injected foam pore volumes and is shown in Figure 4.8. The pressure gradient started to increase rapidly when it reached a gradient of about 60 psi/ft across the core (v_g = 24.6 ft/day and v_l = 3.33 ft/day). This experiment was initiated with the prefoamer in line. Therefore some small bubbles generated by the prefoamer may have entered the core and propagated some distance. Even though both the liquid and gas velocities were lower than in the previous experiment, the steady state pressure gradient reached was higher. Also, the pressure increase occurred with a much smaller number of pore volumes of fluid injection.

This last experiment was repeated with the same liquid velocity (3.33 ft/day) but with higher gas velocities (48.2 and 53.1 ft/day). Figure 4.9 shows the effect of higher gas velocities. The incubation period for the system to reach the steady state pressure gradient is shorter than that shown in the previous figure, but the steady state value of the pressure gradient is about 520 psi/ft in all three cases. It took only a few tens of pore volumes to generate foam rather than several hundreds of pore volumes.

Another experiment conducted using a prefoamer and a liquid velocity higher than the previous experiments (10.7 ft/day) responded within a few pore volumes. Also, the steady

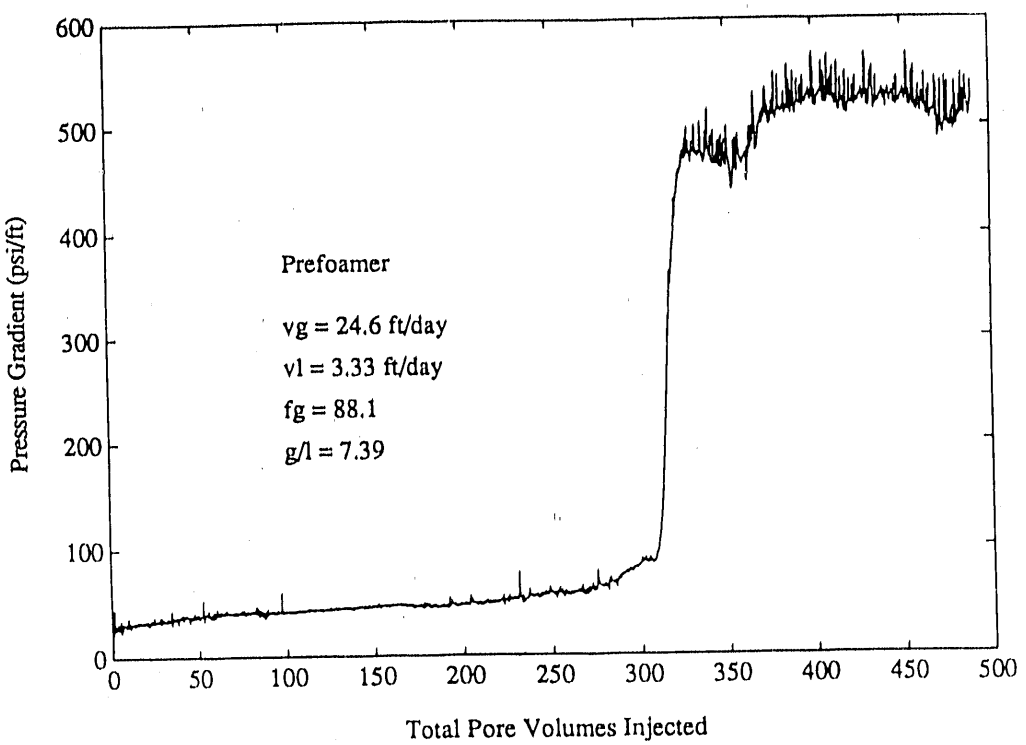

Figure 4.8: Pressure gradient history with simultaneous flow of gas and surfactant solution with prefoamer at low gas velocity.

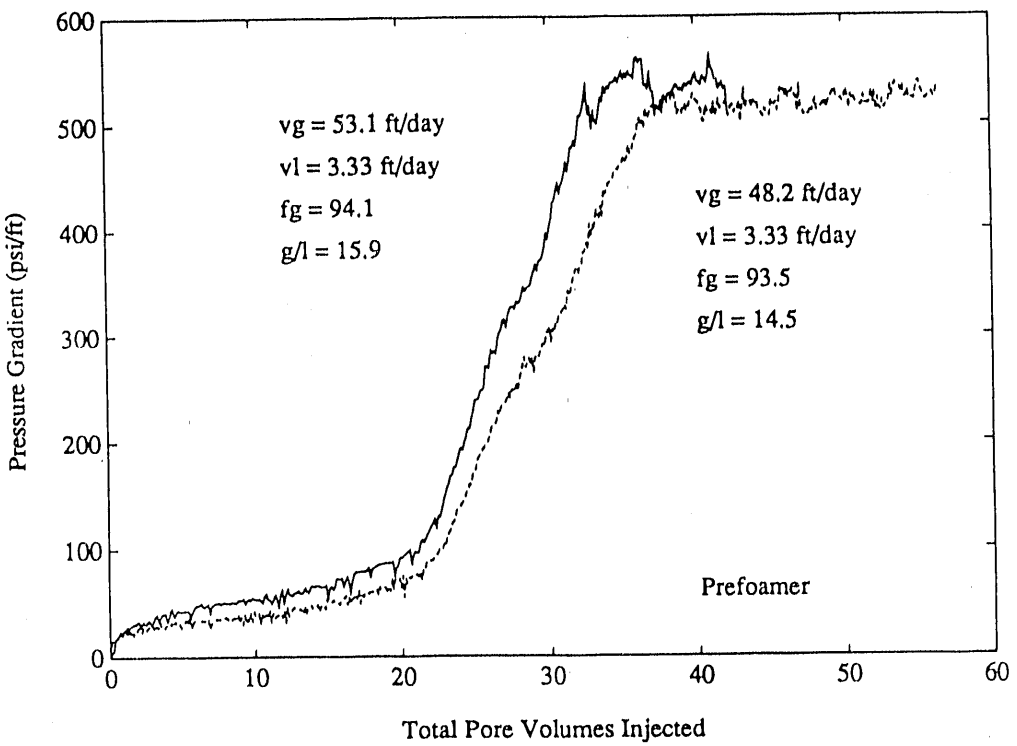

Figure 4.9: Pressure gradient histories with simultaneous flow of gas and surfactant solution with prefoamer at high gas velocities.

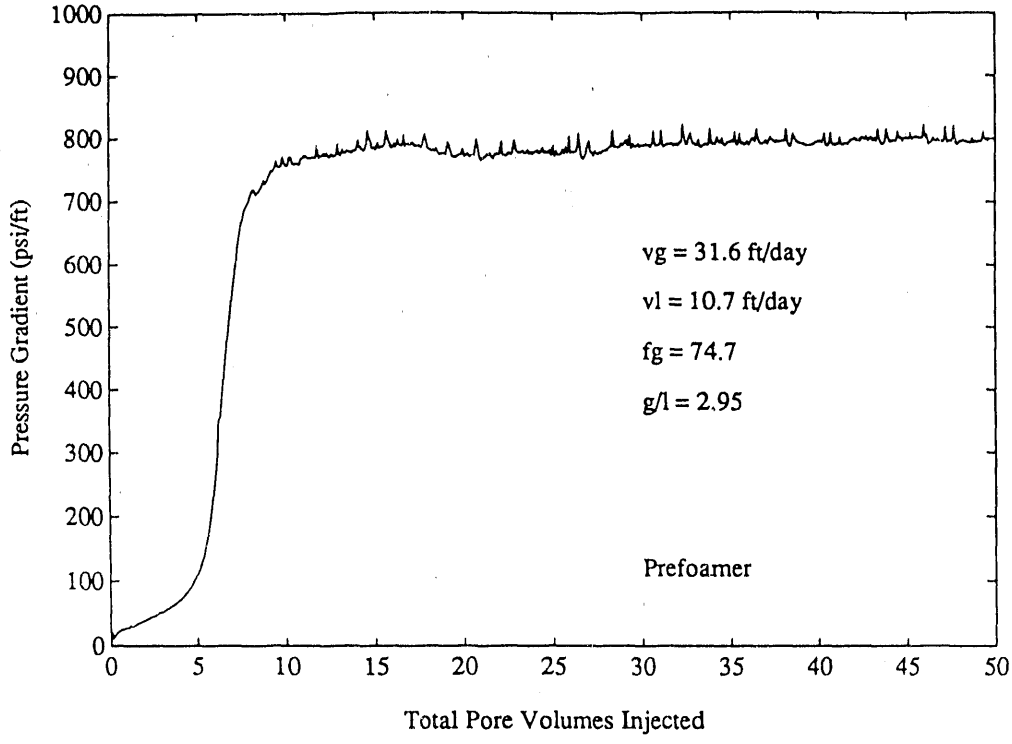

Figure 4.10: Pressure gradient history with simultaneous flow of gas and surfactant solution with prefoamer at high liquid velocity.

state pressure gradient was much higher than with lower liquid velocities. These results are shown in Figure 4.10.

4.3.2 Effect of Gas Velocity

Results show that higher gas and liquid velocities cause foam to be generated with a smaller number of pore volumes of fluid injected and cause higher steady state pressure gradients. In order to investigate the effect of each variable, experiments were conducted in which the gas or liquid velocities were varied and steady state pressure gradients were recorded for each step.

After reaching a steady state pressure gradient, the gas velocity was reduced and the pressure gradient recorded for the new steady state. This procedure was repeated for different steps and in different directions with increasing and decreasing gas velocities. The effect of gas velocity on pressure gradient was determined and results are shown in Figure 4.11. The pressure gradients appear to be nearly independent of gas velocity over a wide range of velocities for these experiments with a prefoamer. All of these experiments were performed with a back pressure of 100 psig using a prefoamer. Also, these points represent conditions where foam was generated in the core at high velocities, steady state foam flow was achieved, and then velocities

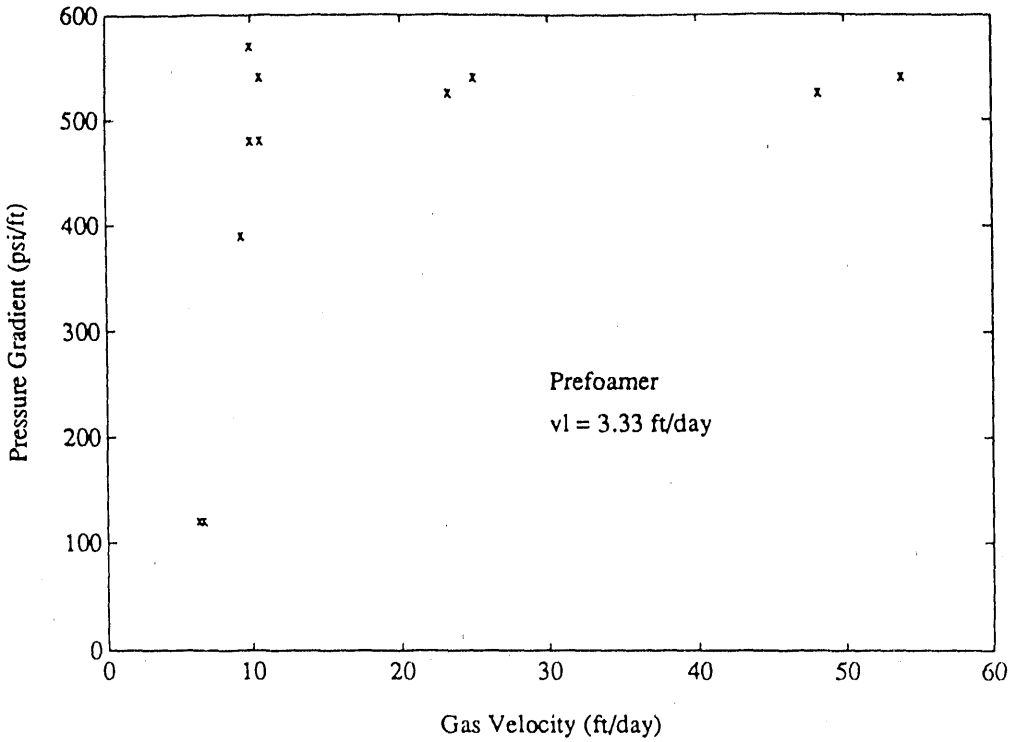

Figure 4.11: Pressure gradient versus gas velocity at constant surfactant velocity with prefoamer.

were reduced. This procedure ensured that any unstable flow conditions, such as those observed during incubation periods, were avoided.

4.3.3 Effect of Liquid Velocity

Figure 4.12 shows the effect of surfactant injection velocity on pressure gradient, for constant gas velocity with no back pressure. The surfactant velocity was reduced stepwise and the pressure gradient was recorded at each steady state. Increasing the surfactant velocity from 3.3 ft/day (0.1 ml/min) to 6.7 ft/day (0.2 ml/min) and reducing it to 3.3 ft/day (0.1 ml/min) caused the pressure gradient to increase and then decrease to the initial value, indicating no hysteresis effect. When the liquid velocity was reduced by 0.33 ft/day (0.01 ml/min), a fairly rapid collapse of the foam in the porous medium occurred suggesting a critical liquid velocity for foam generation in these experiments. It should be noted, however, that in the absence of a back pressure considerable gas expansion occurs in the core and that the effluent gas velocity is about fifteen times the injected gas velocity. The effluent foam quality is very high.

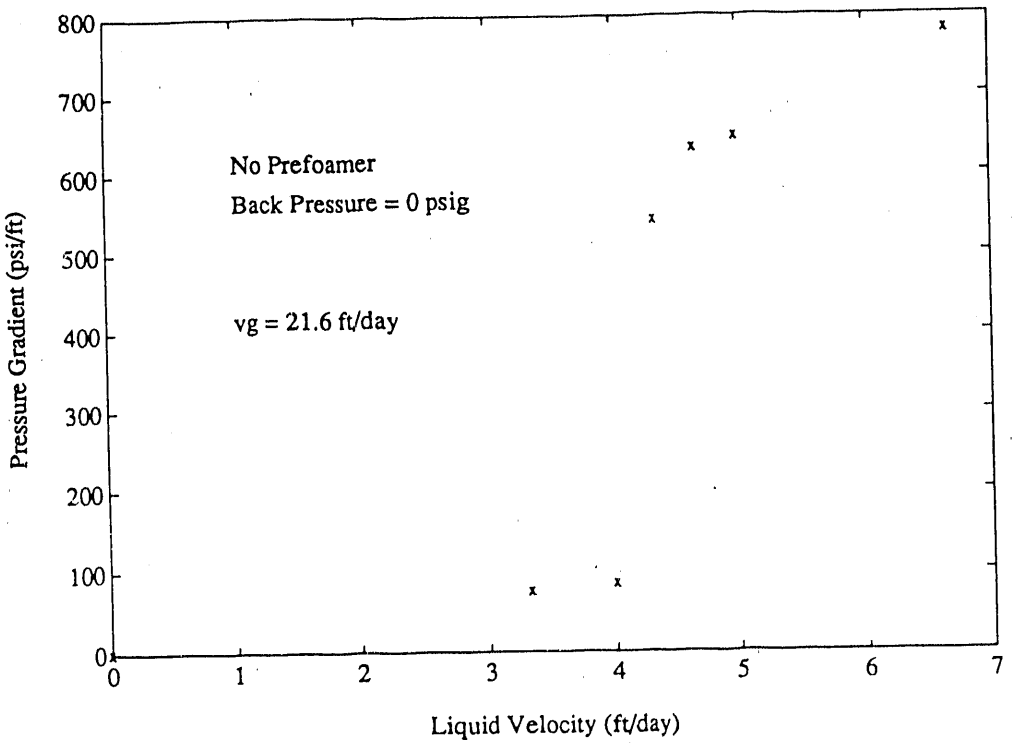

Figure 4.12: Pressure gradient versus surfactant velocity at constant gas velocity without prefoamer or back pressure.

4.3.4 Hysteresis Effect

There is apparently no hysteresis effect. Increasing velocities up to conditions of foam generation then decreasing velocities back to the original value causes the pressure gradient to increase, then to drop back to the original value. Also after foam was generated in the core, decreasing velocities down to low values then increasing velocites back to the initial high value causes the pressure gradient to drop, then to increase back to the original value. This verifies that no significant pressure gradient hysteresis occurs with foam flow in porous media with changing flow velocities. Persoff et al. [97] had noticed that changing the liquid flow velocitiy does not change the saturations significantly, although foam flow resistance increases. This may explain why there is no hysteresis in pressure response during foam flow in porous media.

When the flow experiment was stopped, the liquid saturation in the core had an average value of about 35%. After steady state foam flow conditions were attained, injecting 24 pore volumes of surfactant solution alone at 6.7 ft/day increased the liquid saturation to about 45%. Injecting 11 pore volumes of gas alone at 25 ft/day reduced the liquid saturation to about 17%. The presence of the surfactant in the liquid phase prevents a wide range of saturation from occurring.

4.3.5 Effect of Foam Generator

The effects of using a foam generator for simultaneous injection of gas and surfactant solution was evaluated. The use of a foam generator increased the steady state pressure gradient attained in the experiment. Under all flow conditions, the use of a foam generator gives a finer texture foam. This, in turn, contributes to higher pressure gradients. When injecting foaming solutions, the use of a foam generator produces small bubbles that may enter the porous medium and propagate, whereas the lack of a foam generator causes the fluids to enter the core in slugs. Results, however, do not indicate the distance or the length of core affected by the prefoamer. Use of pressure taps along the length of the core would show the differences in the pressure gradients with or without prefoamer. Therefore, experiments were conducted in longer systems where pressure taps were installed and pressure profiles monitored.

4.4 Foam Generation and Propagation in Long Cores

The study of foam flow mechanisms was next conducted in longer cores where three taps connected to pressure transducers provided pressure distributions in the core. Therefore, foam propagation was monitored along with the study of the depth of penetration of pregenerated foam. Pressure profiles in the core as a function of length would show how far the effect of a prefoamer extends and whether foam propagates as a front. These experiments were initiated at high velocities to cut down on the incubation times.

Experiments were conducted using 0.5% Chevron Chaser SD1000 surfactant solution in 1% brine. All sectional pressure profiles were normalized based on the absolute brine permeability of the section. This minimizes the effect of the differences in permeability for the four sections on the pressure gradients obtained with foam. The core used had an average absolute permeability of 500 md.

Several experiments were conducted using the same procedure. First the core was saturated with brine. Injection of about 40 pore volumes of surfactant solution equilibrated the sandstone with surfactant. Next, keeping the surfactant solution flowing at a fixed velocity, gas injection was started. The two fluids were mixed in the tubing before entering the foam generator or the core. With the prefoamer in line, foam was generated immediately. The produced foam was injected into the core and pressure profiles were monitored continuously.

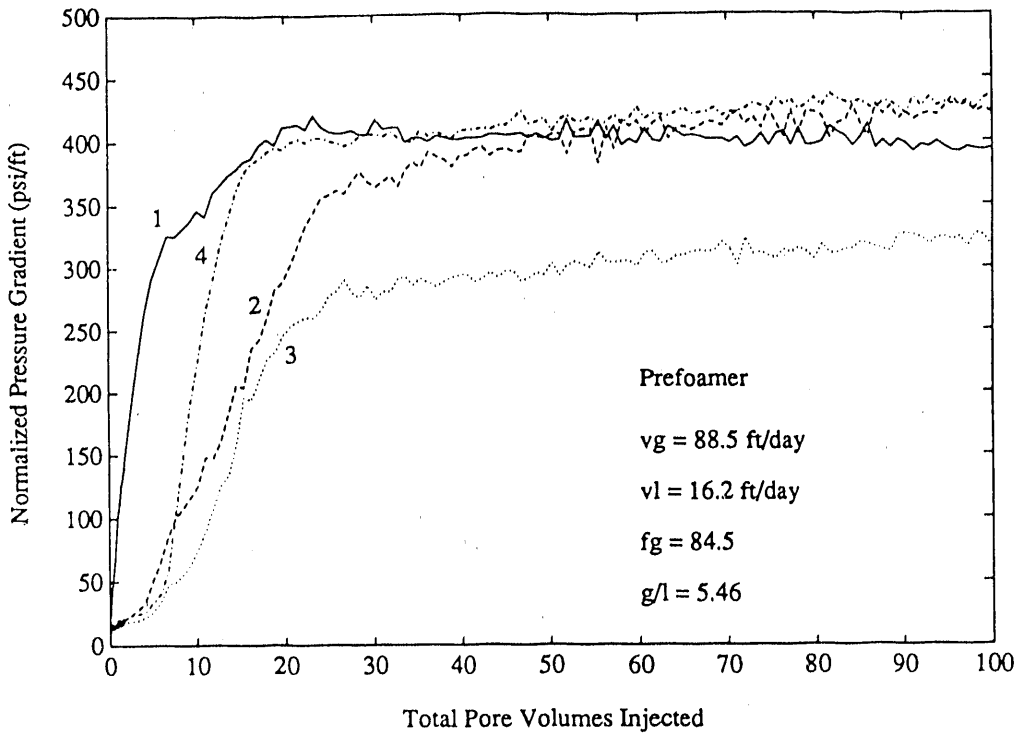

Figure 4.13: Pressure gradient history in Berea core using a prefoamer with v_l = 16.2 ft/day and v_g = 88.5 ft/day.

4.4.1 Experiments Initiated with a Prefoamer

The following experiments were all started with the core saturated with surfactant solution. Foam generation was initiated with the prefoamer in line.

An experiment was conducted with a surfactant injection velocity of 16.2 ft/day and gas injection velocity of 88.5 ft/day, measured at the inlet end of the core. The pressure gradient history is shown in Figure 4.13. The curve labels 1 through 4 correspond to the the core sections, inlet through outlet.

The pressure in the first section of the core increased immediately after gas injection was initiated, then increased shortly thereafter in the rest of the core. It is clear that foam propagation did take place. A sharp foam front has developed where foam mobilization has caused high pressure gradients. Some foam started generating in the core downstream of the foam front as well. This is indicated by the increase in pressure gradient in the downstream sections of the core before the foam front reached there. The effluent end of the core responded faster than the two middle sections, presumably, because of the discontinuity at the end of the core. Steady state pressure gradients were obtained within about 25 pore volumes of fluid injection.

An attempt was made to duplicate the results of the previous experiment. The core was resaturated with brine and flushed with about 40 pore volumes of surfactant solution. Foam

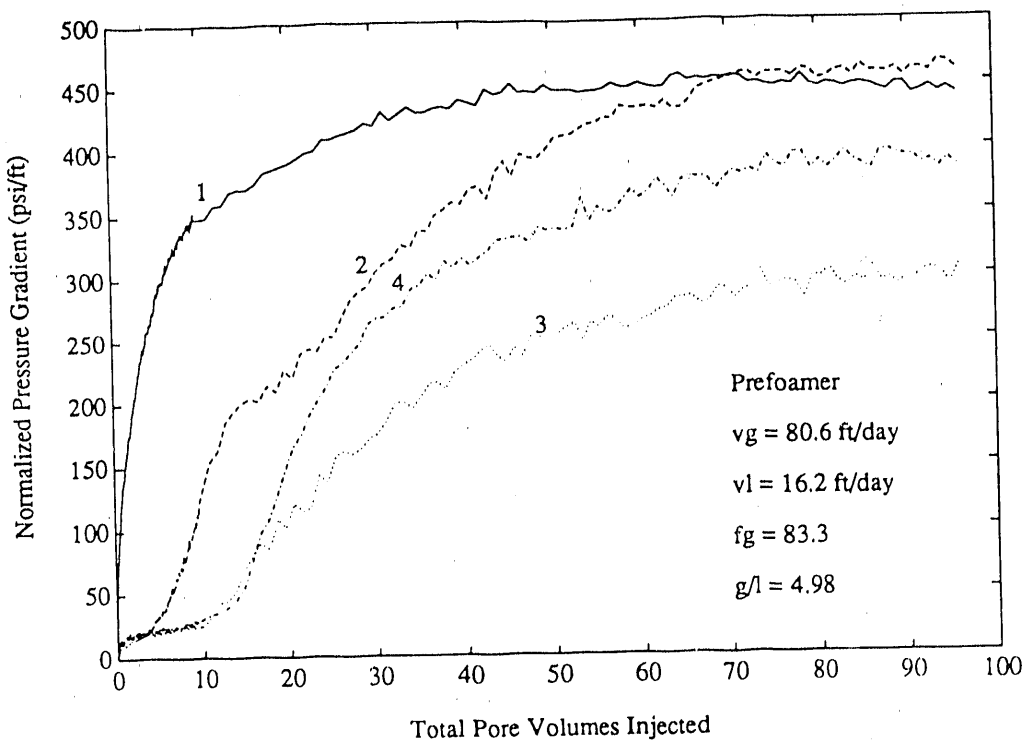

Figure 4.14: Pressure gradient history in Berea core using a prefoamer with v_l = 16.2 ft/day and v_g = 80.6 ft/day.

flow was initiated in the core but the gas velocity was slightly lower than in the previous case. The pressure gradient history of this experiment is shown in Figure 4.14. About 50 pore volumes of foam injection were necessary to reach steady state. The frontal foam generation and propagation was similar to the previous one with the exception that the overall response was slower. The pressure gradient in the third section of the core is the lowest in both of these experiments. The two upstream sections of the core exhibit high pressure gradients due to the effect of the prefoamer. The effluent end of the core shows a high pressure gradient which may be due to end effects.

An experiment was then conducted with higher quality foam. After restoring the core to the starting conditions with evacuation, saturation with brine and surfactant flooding, pregenerated foam was injected in the core with a higher gas velocity (112 ft/day), but with a lower liquid velocity of 9.90 ft/day. In this case, more than 180 pore volumes of fluid injection were necessary to reach steady state pressure gradients (Figure 4.15). Foam propagated as a front from the upstream end to the downstream end of the core. Note that, compared to the previous experiments, the difference between pressure gradients in the first two sections of the core and the last two sections is greater. High gas velocities in the prefoamer give finer texture foams [44]. In this experiment, gas velocities and gas/liquid ratios are higher than in the previous

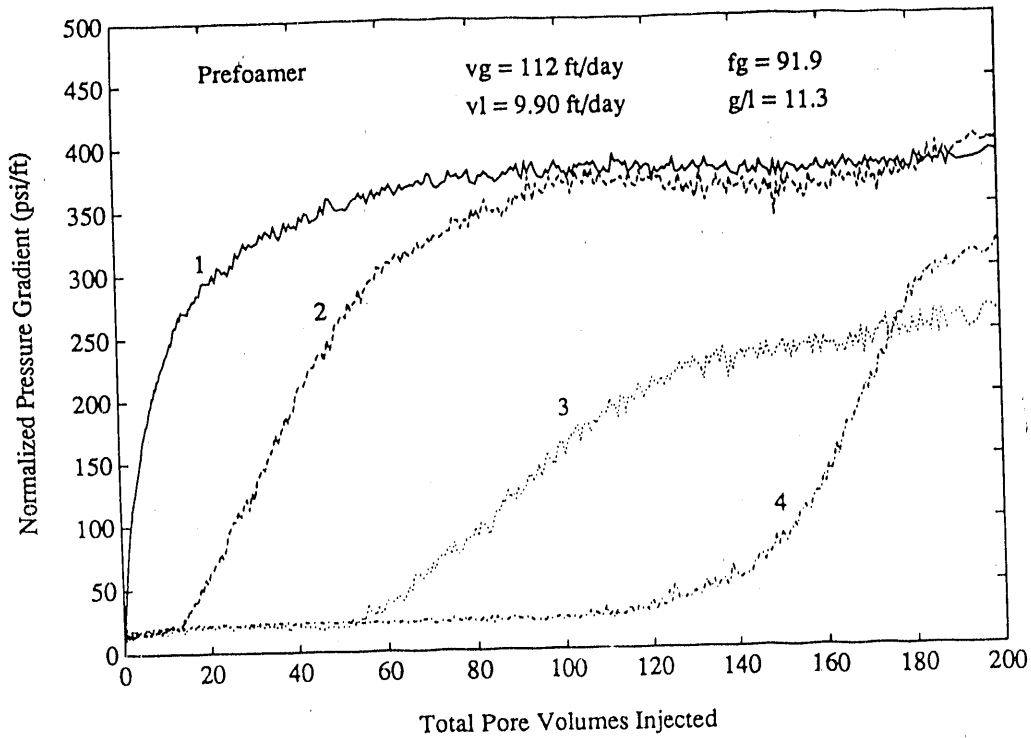

Figure 4.15: Pressure gradient history in Berea core using a prefoamer with v_l = 9.90 ft/day and v_g = 112 ft/day.

experiments. The final effect is limited gas mobility reduction in the two downstream sections of the core.

In another experiment, foam was injected into the core initially saturated with surfactant solution. After the sectional pressure gradients stabilized, the prefoamer was bypassed and the fluids were mixed in the tubing before entering the core. The pressure gradient history is shown in Figure 4.16. This caused a rapid decline in the pressure gradients in the two upstream sections of the core. The pressure gradient in all four sections stabilized at about the same level. A detailed graph for early time in the experiment is shown in Figure 4.17. The previous observations of an immediate pressure response in the inlet section of the core, the propagation of foam as a front, and the confining of the effect of the prefoamer mostly to the two upstream sections of the core are verified.

4.4.2 Experiments Initiated without a Prefoamer

All of the previous experiments were initiated with a prefoamer. Foam generation in situ was also studied. Experiments were conducted under conditions similar to the previous ones except that foam was not pregenerated. Nitrogen gas and surfactant solution were mixed in the tubing before being injected in the core.

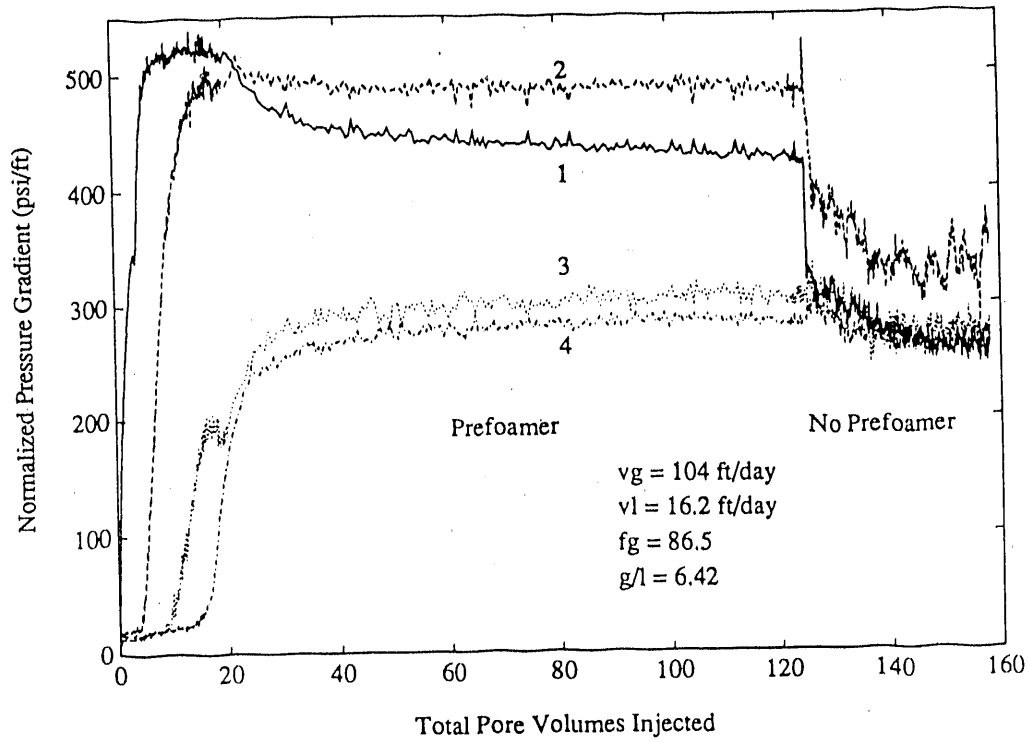

Figure 4.16: Pressure gradient history in Berea core using a prefoamer with v_l = 16.2 ft/day and v_g = 104 ft/day.

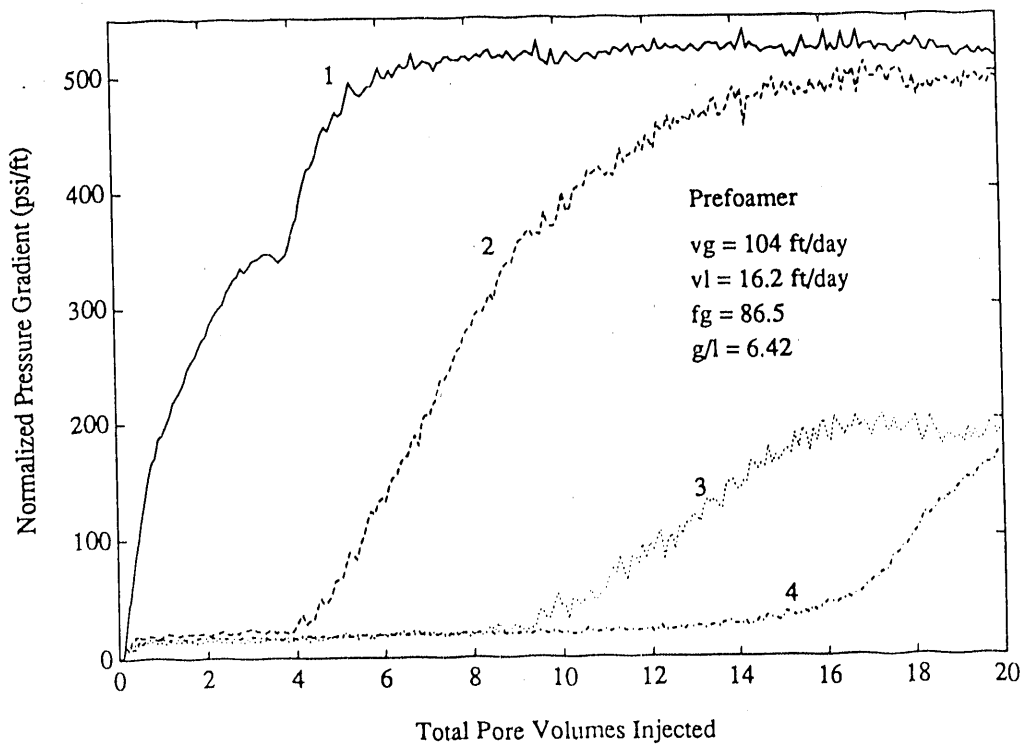

Figure 4.17: Pressure gradient history in Berea core using a prefoamer with v_l = 16.2 ft/day and v_g = 104 ft/day (early time).

With an initial liquid velocity of 16.2 ft/day and a gas velocity of 97 ft/day, foam generation in the core was delayed, as the pressure gradient history in Figure 4.18 indicates. The influent section did not respond immediately upon the start of gas injection as in the previous experiments where pregenerated foam was injected. In fact, the first section was the last to respond. A detailed graph of the early time shown in Figure 4.19 indicates that, after an incubation period of about ten pore volumes, foam did start generating in section 2 of the core and then propagated dowstream. In addition to foam front propagation, in situ foam generation throughout the core is significant. Pressure gradients increase almost simultaneously throughout the three downstream sections of the core.

Foam generation in the inlet section was delayed the most. After steady state was reached with about 140 pore volumes of fluid injection, the prefoamer was turned on for a brief time period and then bypassed again. When steady state was reached, the surfactant velocity was reduced to half of its initial value, causing a proportional reduction in the pressure gradients. Upon attaining a new steady state, the prefoamer was turned on again and then off. Figure 4.20 shows the pressure gradient response while the prefoamer was in line. As soon as the prefoamer was turned on, the inlet section experienced a sudden pressure increase. The inlet section is the most affected by the prefoamer. Section 2 shows a lesser response whereas the two downstream sections are almost unaffected. The effect of injecting pregenerated foam is immediate and rapid. After bypassing the prefoamer, the foam returns slowly to its initial texture.

Bypassing the prefoamer caused a drop in the pressure in all the sections, most significantly in the inlet end. Also note that the pressure decline was slightly slower than the pressure build up, indicating that it takes a longer time for the effect of a finely textured foam from the prefoamer to disappear through coalescence than the time necessary to propagate a high lamellae density foam. The reason the last two sections of the core show a slightly higher pressure gradient could be due to higher gas velocities. Higher pressures in the upstream end of the core cause higher mass flow rates, and consequently higher volumetric flow rates downstream.

The previous experiment was repeated to confirm the results. Figure 4.21 shows the pressure gradient history throughout the experiment. After injection of about 150 pore volumes of gas and surfactant solution, the gas and surfactant velocities were reduced. The surfactant velocity was dropped by a factor of two and the gas velocity by a factor of 1.5. The pressure gradient decreased by a factor of slightly more than two, indicating that the liquid flow follows Darcy's law and that the pressure gradients are independent of gas flow velocities.

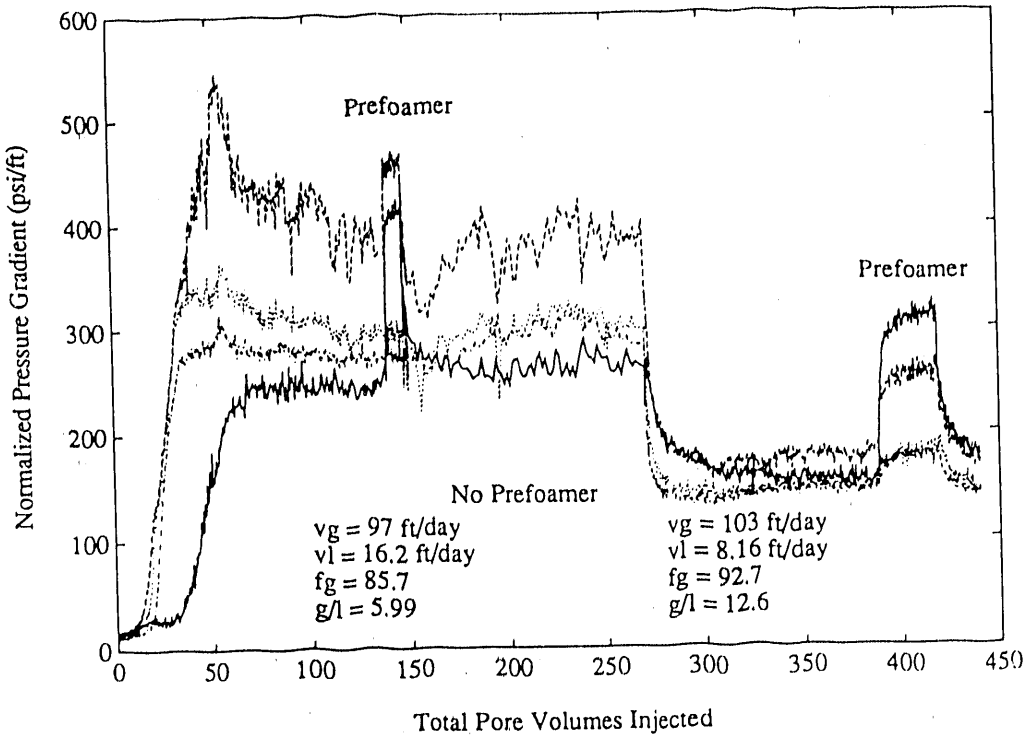

Figure 4.18: Pressure gradient history in Berea core without a prefoamer with $v_l = 16.2$ ft/day and $v_g = 97$ ft/day.

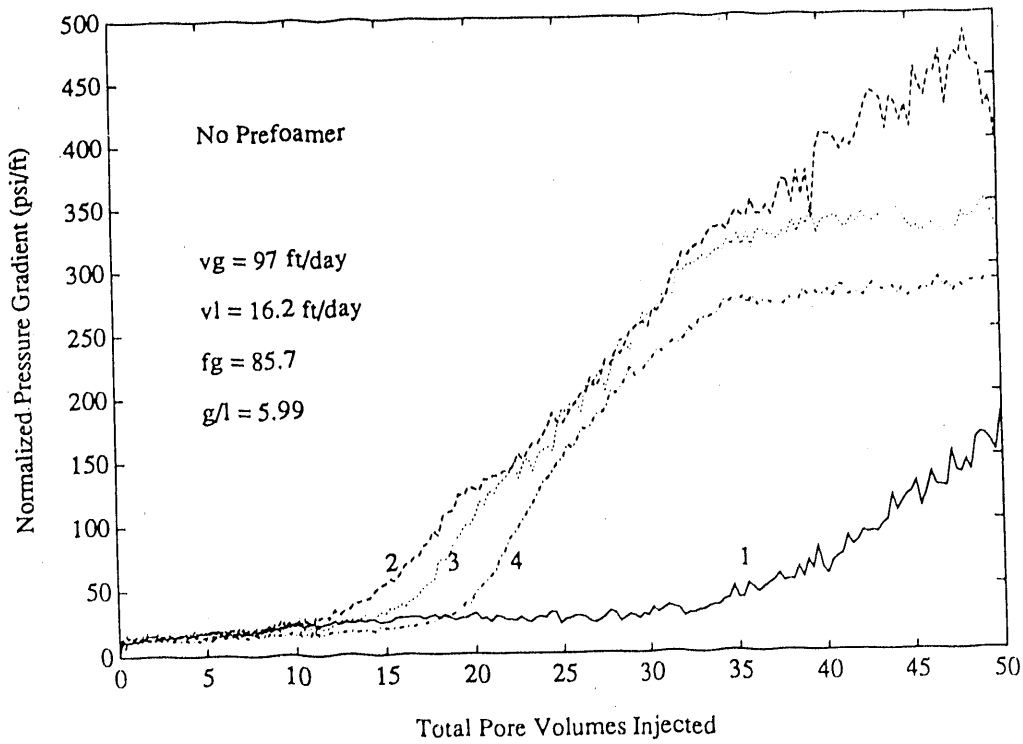

Figure 4.19: Pressure gradient history in Berea core without a prefoamer with $v_l = 16.2$ ft/day and $v_g = 97$ ft/day (early time).

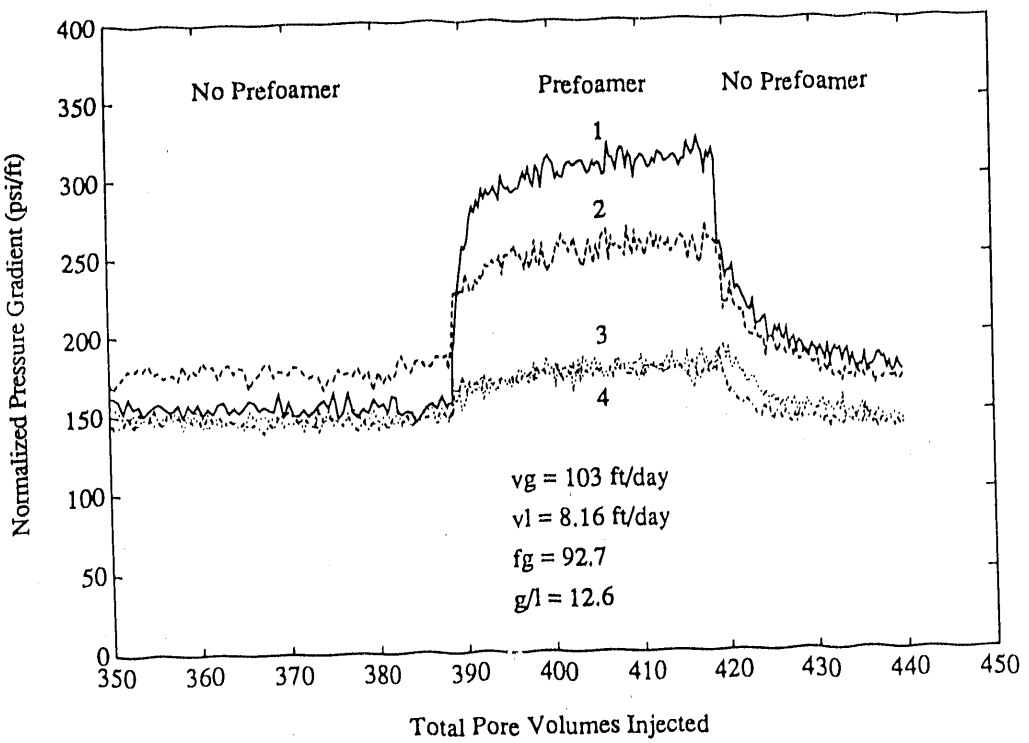

Figure 4.20: Pressure gradient history in Berea core with $v_l = 8.16$ ft/day and $v_g = 103$ ft/day (effect of prefoamer).

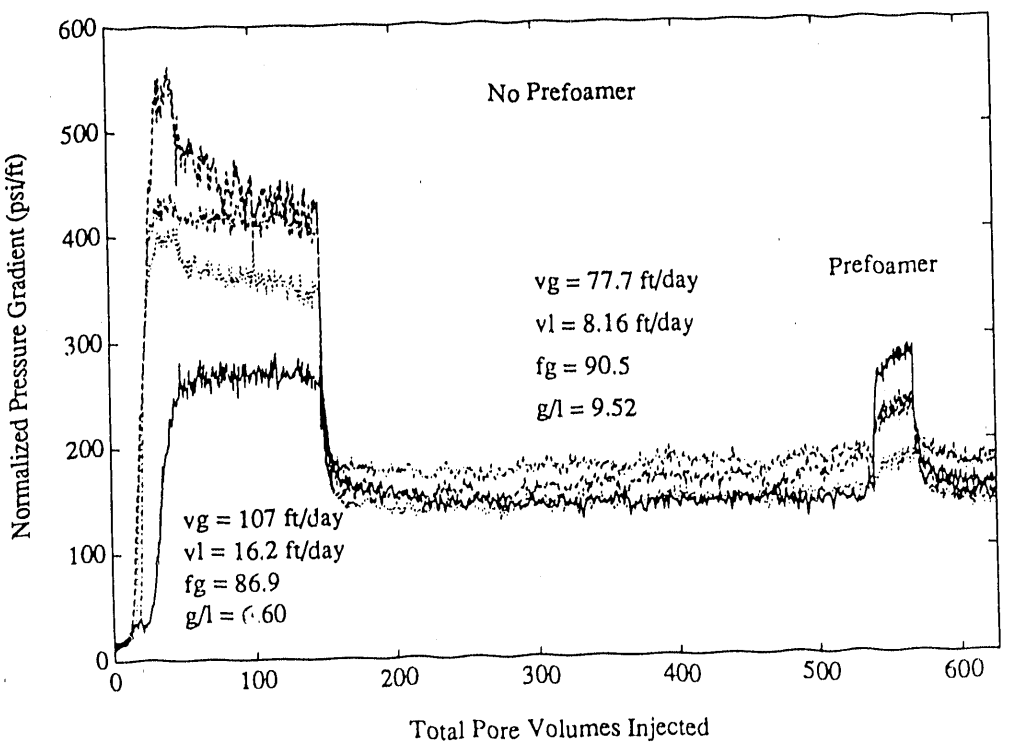

Figure 4.21: Pressure gradient history in Berea core without a prefoamer with $v_l = 16.2$ ft/day and $v_g = 107$ ft/day.

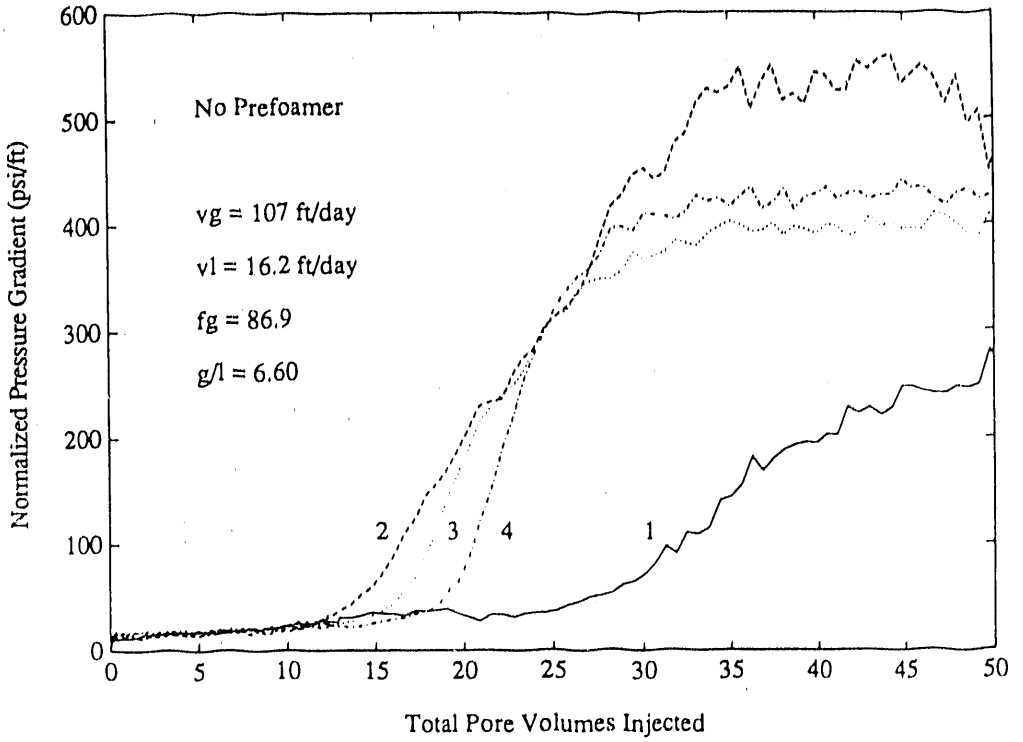

Figure 4.22: Pressure gradient history in Berea core without a prefoamer with v_l = 16.2 ft/day and v_g = 107 ft/day (early time).

The similarities between the two experiments can be identified by a detailed analysis of the early time as well as during the time period when the prefoamer was in line. Figure 4.22 shows the early time response of the in situ foam generation experiment. After an incubation period of about ten pore volumes, foam started generating in section 2 and propagated downstream through sections 3 and 4. Simultaneously, in situ foam generation occurred throughout the core, but the inlet section was last to respond. Analysis of the effect of the prefoamer, Figure 4.23, reveals conclusions similar to the ones previously stated. The effect of the prefoamer is most significant in the inlet section followed by section 2. In this case, the pressure gradient in the effluent section is more pronounced than in the previous experiment.

Other experiments were conducted to study the effect of gas and surfactant velocities on the in situ foam generation and propagation mechanism. An experiment was conducted without a prefoamer with a liquid velocity of 11.8 ft/day and gas velocity of 117 ft/day (Figure 4.24). After an incubation period of about fifteen pore volumes, the previously observed sequence of foam front propagation was observed with foam starting to generate in section 2 and then propagating downstream, but at a slower rate than previously observed. The frontal propagation was sharp and no significant in situ foam generation took place while the front was propagating due to the low liquid velocity and high quality of the foam.

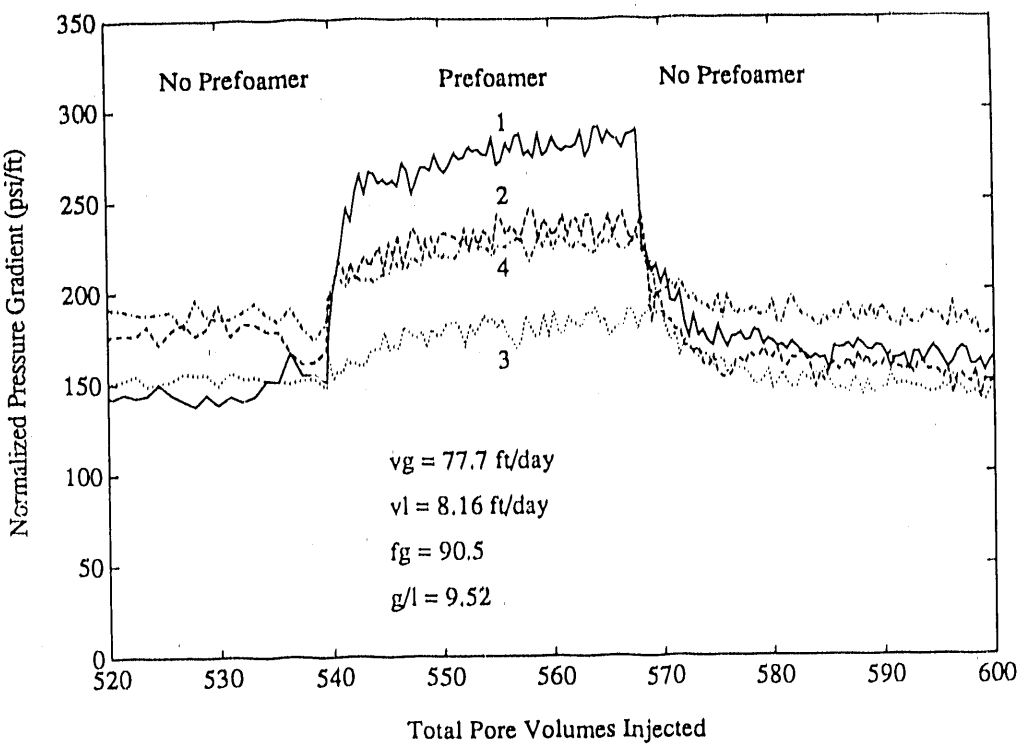

Figure 4.23: Pressure gradient history in Berea core with $v_l = 8.16$ ft/day and $v_g = 77.7$ ft/day (effect of prefoamer).

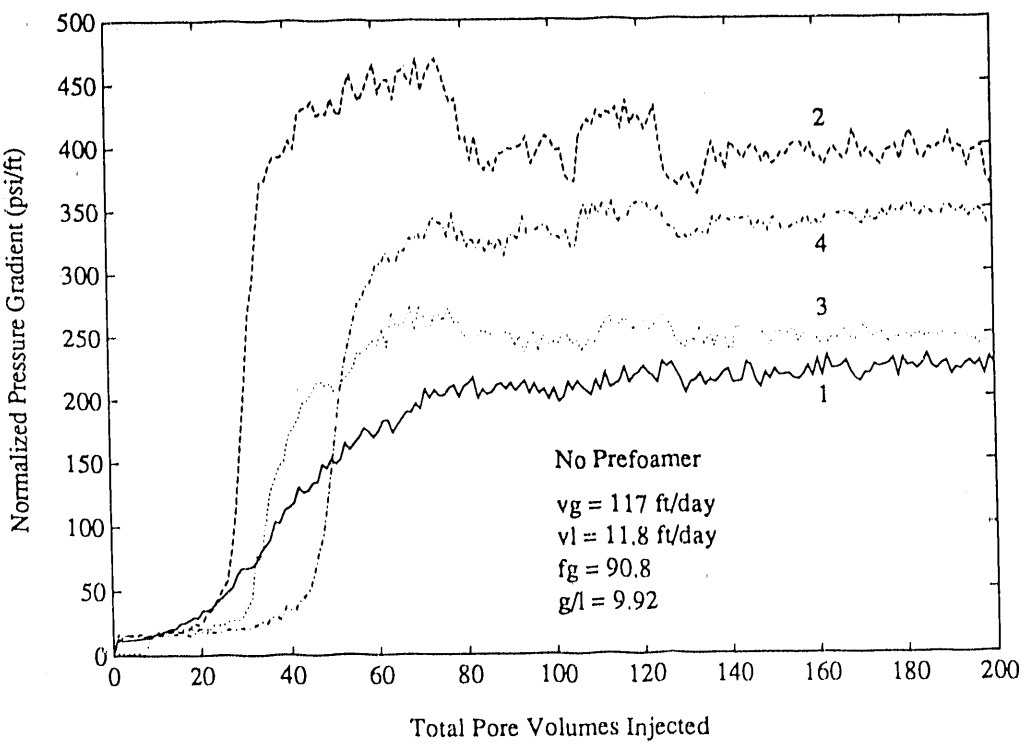

Figure 4.24: Pressure gradient history in Berea core without a prefoamer with $v_l = 11.8$ ft/day and $v_g = 117$ ft/day.

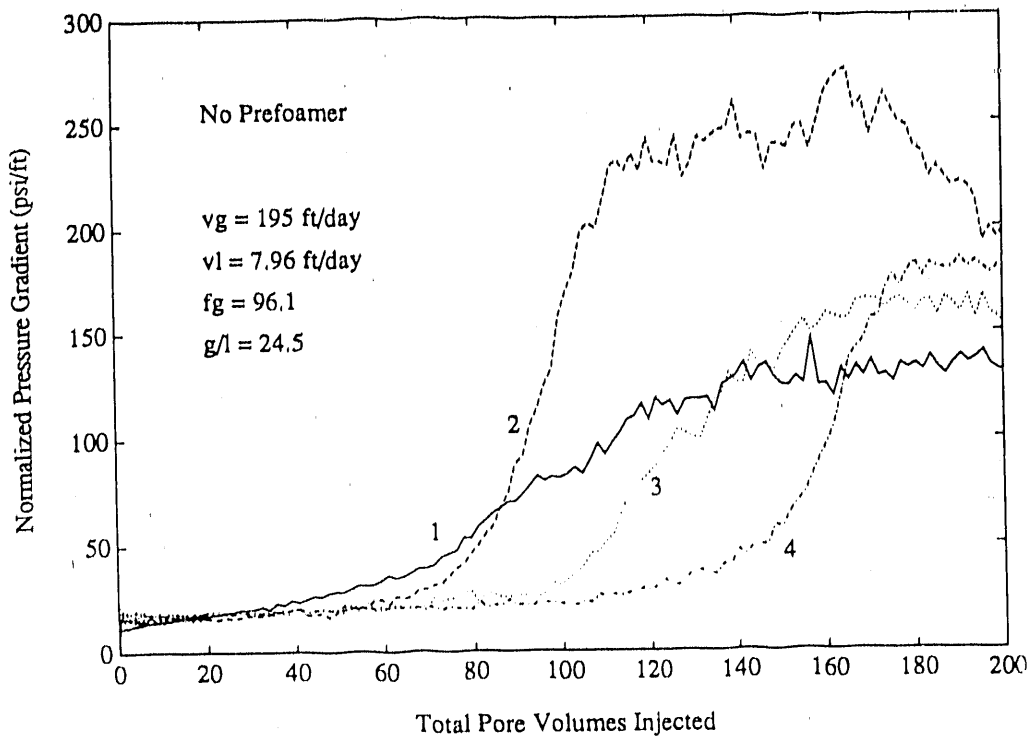

Figure 4.25: Pressure gradient history in Berea core without a prefoamer with v_l = 7.96 ft/day and v_g = 195 ft/day.

Another experiment was performed with even a higher foam quality (96.1%), a lower liquid velocity but higher gas velocity, as shown in Figure 4.25. The response was similar except that the incubation period lasted for about fifty pore volumes and the foam propagation rate was even slower than in the previous runs. However, the upstream section of the core responded faster than before. The effect of liquid velocity seems to be an important one. Also, in situ foam generation did not take place while the foam front was propagating.

The next experiment was conducted with a liquid velocity of 7.96 ft/day, same as the previous experiment, but with at a much lower foam quality (84.7%). The pressure gradient history is shown in Figure 4.26. Foam generation occurred under conditions very similar to those previously observed. Almost the same number of pore volumes were necessary to start foam generation (fifty pore volumes). Steady state pressure gradients were reached in even fewer pore volumes than the previous experiment. However, the inlet section responded more slowly than before.

In view of the above results, it is apparent that foam can be generated in situ at low velocities, given enough incubation time. The effect of even lower velocities was also investigated. An experiment was started with a liquid velocity of 3.98 ft/day, about half the liquid velocity of the previous experiment, and a gas velocity of 7.3 ft/day. After the core was restored to the conditions of 100% liquid saturated, gas flow was started along with the surfactant solution.

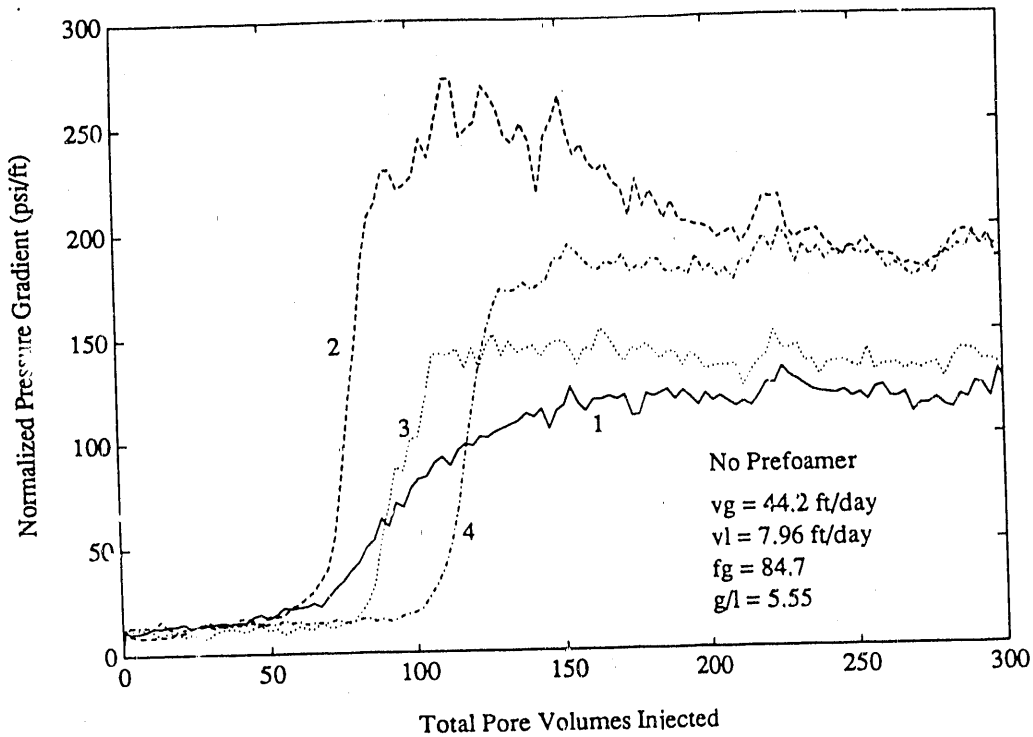

Figure 4.26: Pressure gradient history in Berea core without a prefoamer with $v_l = 7.96$ ft/day and $v_g = 44.2$ ft/day.

The pressure gradients did not show any increasing trend after injection of about thirteen pore volumes of fluid, as indicated in Figure 4.27. The gas velocity was, therefore, increased to a value similar to the previous experiment, 41.2 ft/day, to reduce the incubation time. The increase in the gas velocity was abrupt and a spike in the pressure gradients occurred as the regulating check valve was jammed. At this foam quality of 91%, the pressure gradient in the influent end of the core started increasing.

After injecting about 500 pore volumes of gas and liquid, the pressure gradient stabilized in the upstream section of the core as shown in Figure 4.28 while the pressure gradient in the second section started increasing. The foam propagated downstream through sections 3 and 4 until the front reached the effluent end. This propagation required about 3500 pore volumes of fluid injection. It took about 65 days of constant injection at the specified velocities.

Steady state pressure gradients for these particular flow velocities were previously measured starting with higher velocities and then lowering them. A comparison of these data with data from an experiment started with a core 100% surfactant saturated would verify the validity of the hypothesis that foam flow in porous media is dependent only upon the flow velocities irrespective of the direction of change in the velocities, given enough time. The steady state was reached after the simultaneous injection of the gas and surfactant solution for a period of 65 days.

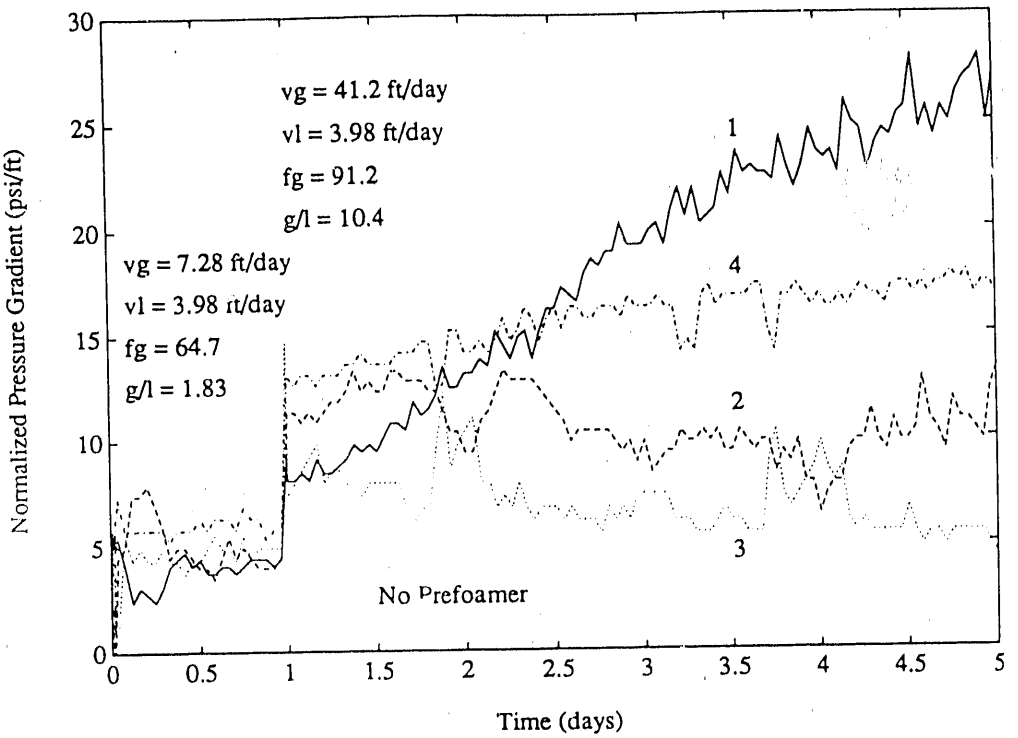

Figure 4.27: Pressure gradient history in Berea core at low velocities without prefoamer (early time).

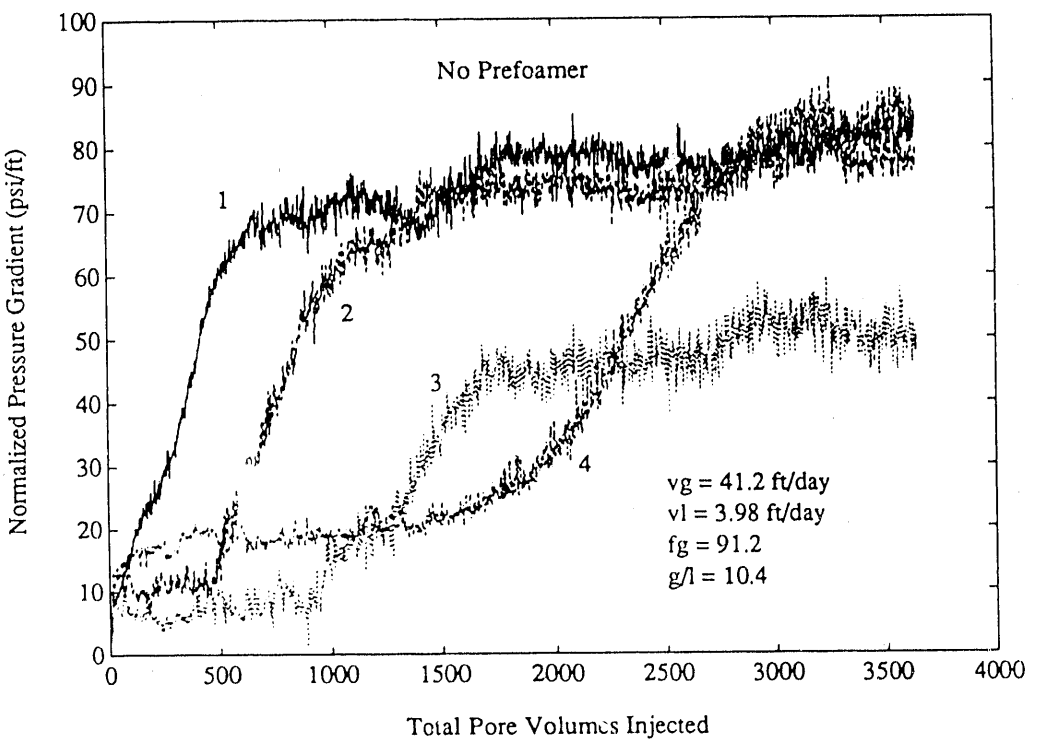

Figure 4.28: Pressure gradient history in Berea core without a prefoamer with $v_l = 3.98$ ft/day and $v_g = 41.2$ ft/day.

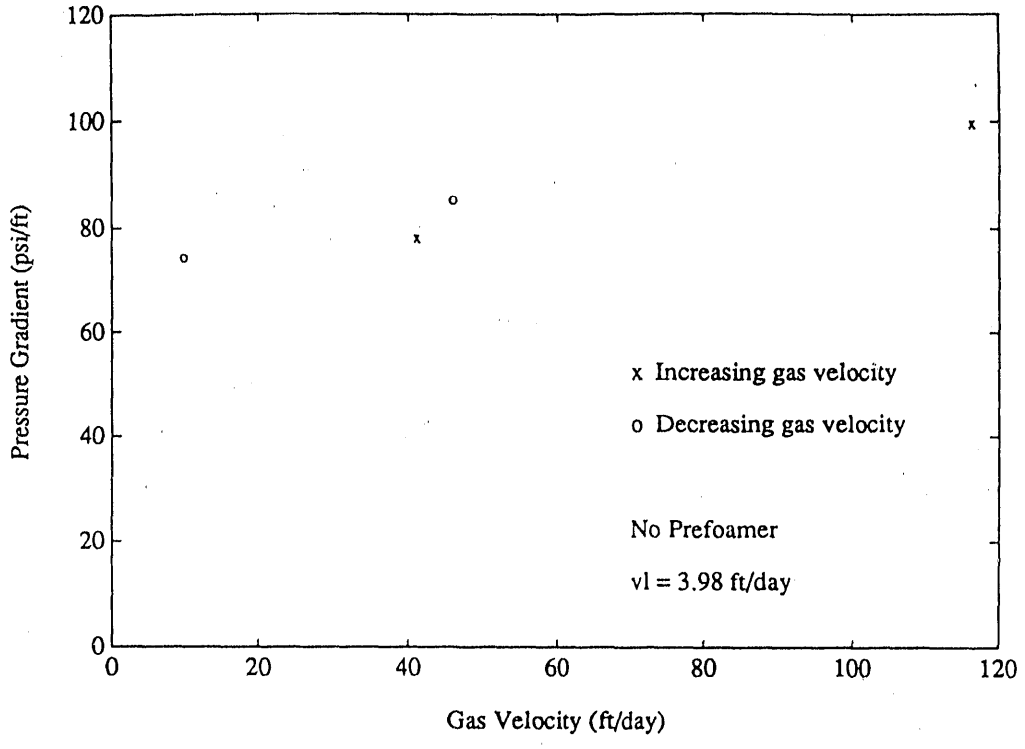

Figure 4.29: Pressure gradient versus gas velocity with $v_l = 3.98$ ft/day.

The steady state reached after lowering velocities from foam flow at high velocities and the steady state reached from the 100% surfactant saturated core at low velocities are practically identical, as indicated in Figure 4.29. The difference in the pressure gradients reached by the two paths is negligible. The hypothesis appears to be valid, then, that the steady state pressure gradient is independent of the direction from which it is reached, and that the final pressure gradient depends on the magnitude but not on the history of the flow velocities.

The pressure distribution inside the core as a function of the number of pore volumes of fluid injection is plotted in Figure 4.30. The pressure gradient increases at the inlet end of the core and propagates downstream. The steady state pressure gradient is nearly linear.

Based on the above results, one can conclude that the use of a prefoamer enhances foam flow by generating a foam front that propagates in the porous medium. Also, the effect of pregenerating a foam before injection into a porous medium does not extend too far from the inlet end. Foam can be generated in situ, but the process is slower and requires a large number of pore volumes. A high pressure spike may trigger foam generation.

4.4.3 Effect of Gas and Surfactant Velocities

Results of experiments conducted so far indicate the importance of fluid velocity on foam flow. Foam generation is dependent on both gas and surfactant velocities. Experiments were

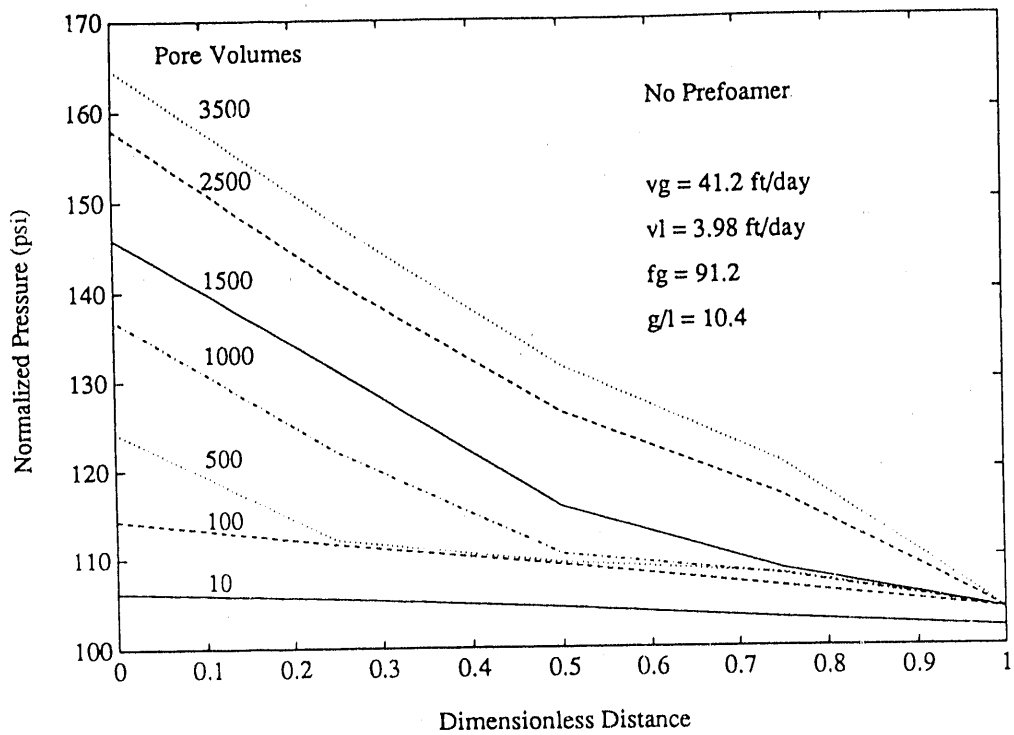

Figure 4.30: Pressure ditribution inside the core as a function of pore volumes of fluid injected with $v_l = 3.98$ ft/day and $v_g = 41.2$ ft/day.

conducted to evaluate further the effect of gas and surfactant velocities on foam flow in porous media. After reaching a steady state pressure gradient for specific gas and liquid velocities, the gas velocity was changed and a new steady state pressure gradient and pressure profile were recorded. The system was then shifted to a new steady state by varying the gas velocity but maintaining the same liquid velocity. One such experiment is shown in Figure 4.31. After generating a set of data at a particular liquid velocity, this procedure was then repeated for other liquid velocities.

Such results were obtained with and without surfactant in solution. The importance of the presence of foaming agent on gas-liquid flow pressure gradients is seen in Figure 4.32. A substantial increase in pressure gradient is observed in the presence of surfactant in solution.

Data sets generated for the steady states at different gas velocities with several liquid velocities have been gathered into Figure 4.33. The plotted data points have been obtained through the successive steady states at each particular pair of of gas and surfactant velocities. For each set of data at a fixed liquid velocity, the data points have been fitted into a polynomial function, as displayed by the curves. All the lines displayed in the figure are curving downward. If gas mobilities were to remain unchanged with increasing gas velocities, the pressure gradients should be increasing linearly. Therefore, since the lines of pressure gradients versus gas velocities curve downward, as gas velocities are increased at fixed liquid velocities, gas mobilities

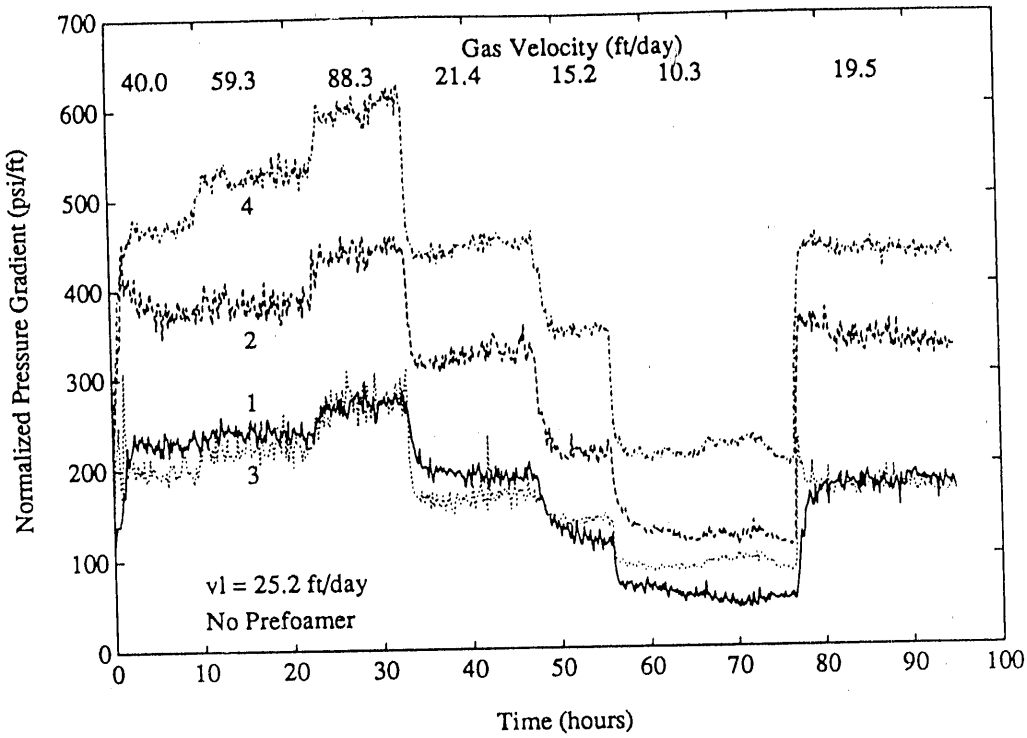

Figure 4.31: Normalized pressure gradients obtained at steady state for different gas velocities with $v_l = 25.2$ ft/day.

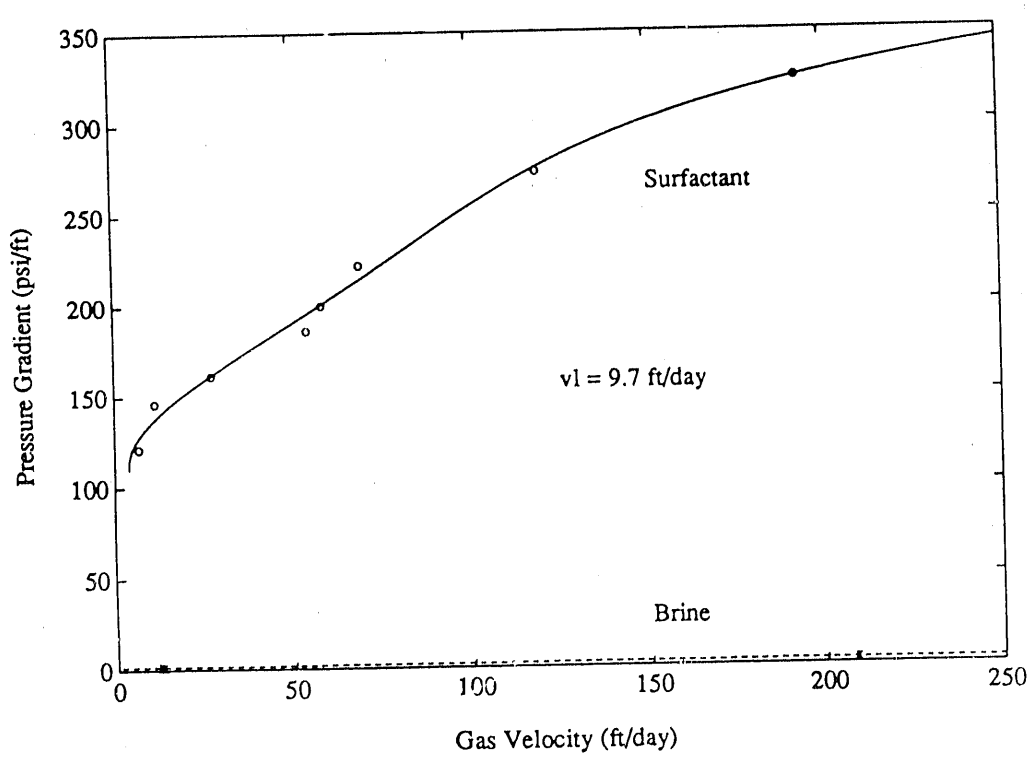

Figure 4.32: Pressure gradient versus gas flow velocity in Berea core with and without surfactant for a liquid velocity of 9.7 ft/day.

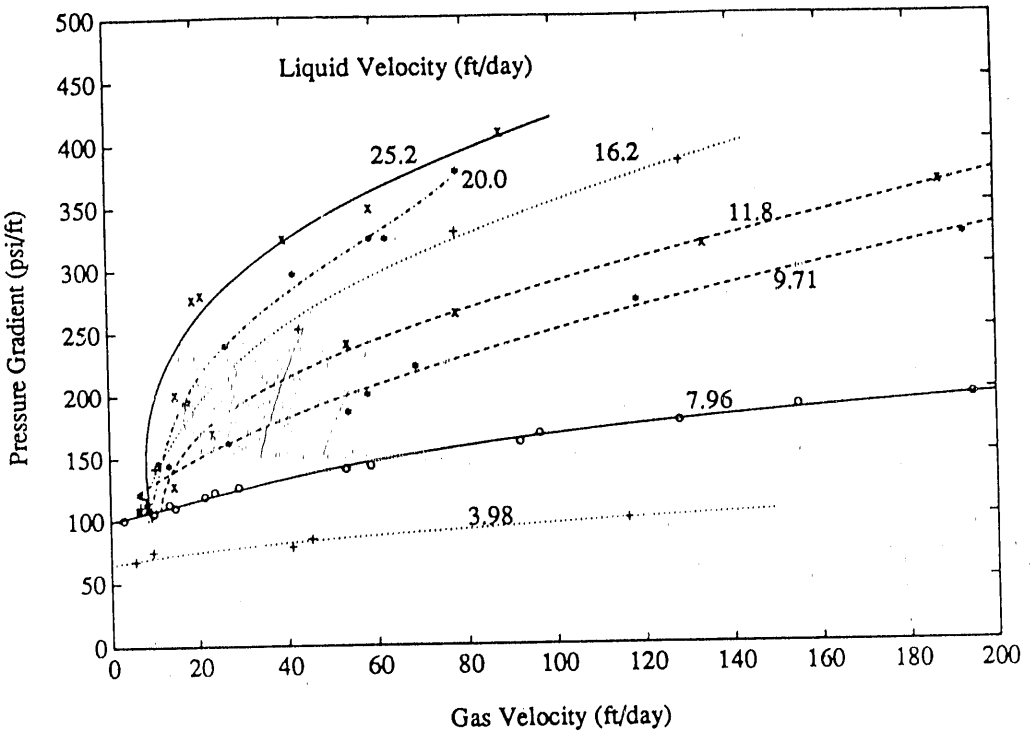

Figure 4.33: Cumulative plot of pressure gradient versus gas velocity for different surfactant velocites without prefoamer.

increase as well. The figure also indicates that pressure gradients are weak functions of gas velocities.

At fixed gas velocities, data were obtained from the fitted curves and a cross plot made. Figure 4.34 shows the effect of liquid velocity on pressure gradient at constant gas velocity. At low gas velocities, the pressure gradient is a linear function of liquid velocity indicating unchanged liquid mobilities. This also indicates that the liquid flow follows Darcy's law over a wide range of velocities. However, at higher gas velocities, the lines of constant gas velocities curve slightly downward, indicating increasing liquid mobility with increasing liquid velocity. Nevertheless, pressure gradients are a strong function of liquid velocities.

4.4.4 Pressure Distributions with Foam Flow

As the cross plot data were generated, the pressure gradient profile was recorded for each set of gas and liquid velocities. A plot of the pressure profile in the core as a function of gas velocity is possible. Figures 4.35 through 4.40 show the pressure distributions in the core at a particular liquid velocity for different gas velocities. The pressure distributions are almost linear but have a slight curvature downward, with lower pressure gradients at the influent end of the core and higher pressure gradients at the effluent end.

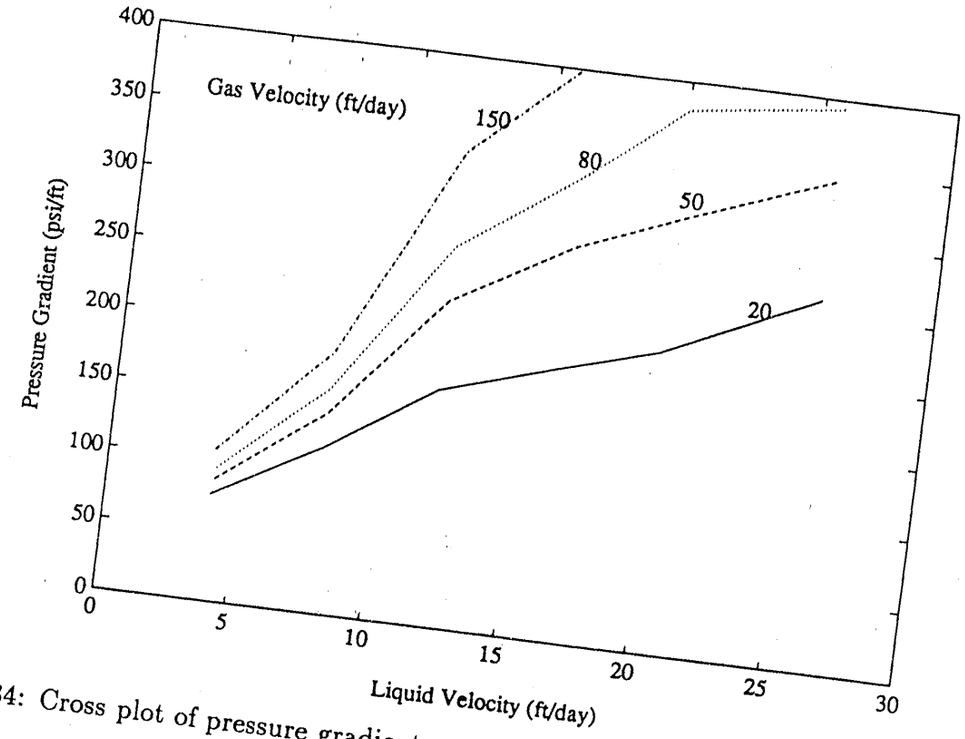

Figure 4.34: Cross plot of pressure gradient versus liquid velocity at different gas velocitites.

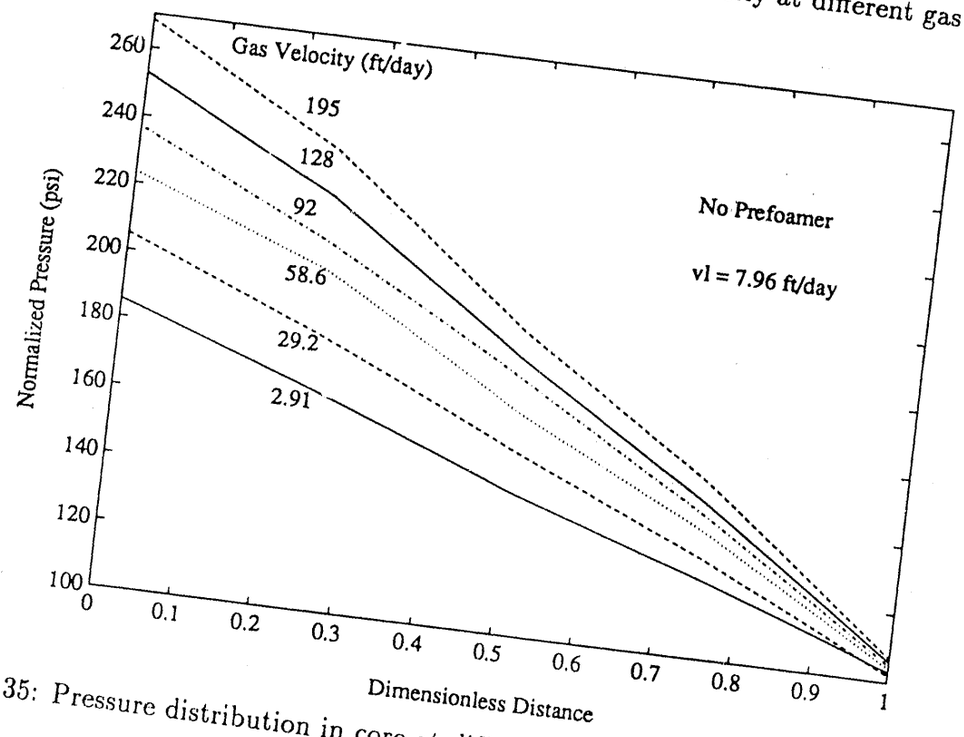

Figure 4.35: Pressure distribution in core at different gas velocities for $v_l = 7.96$ ft/day.

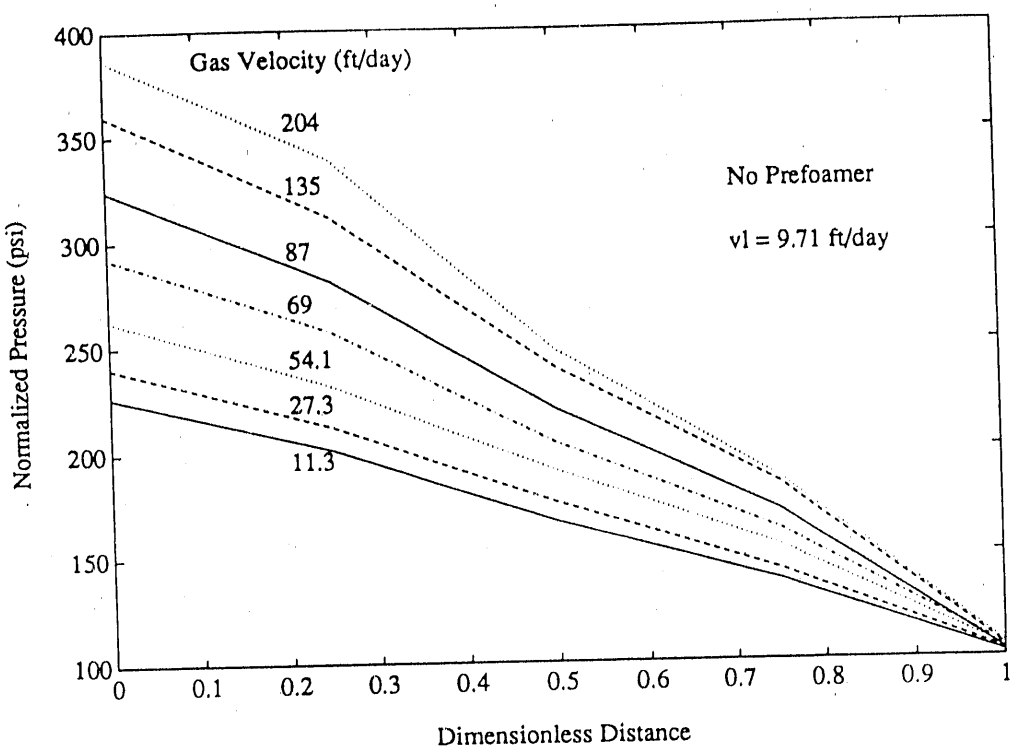

Figure 4.36: Pressure distribution in core at different gas velocities for $v_l = 9.71$ ft/day.

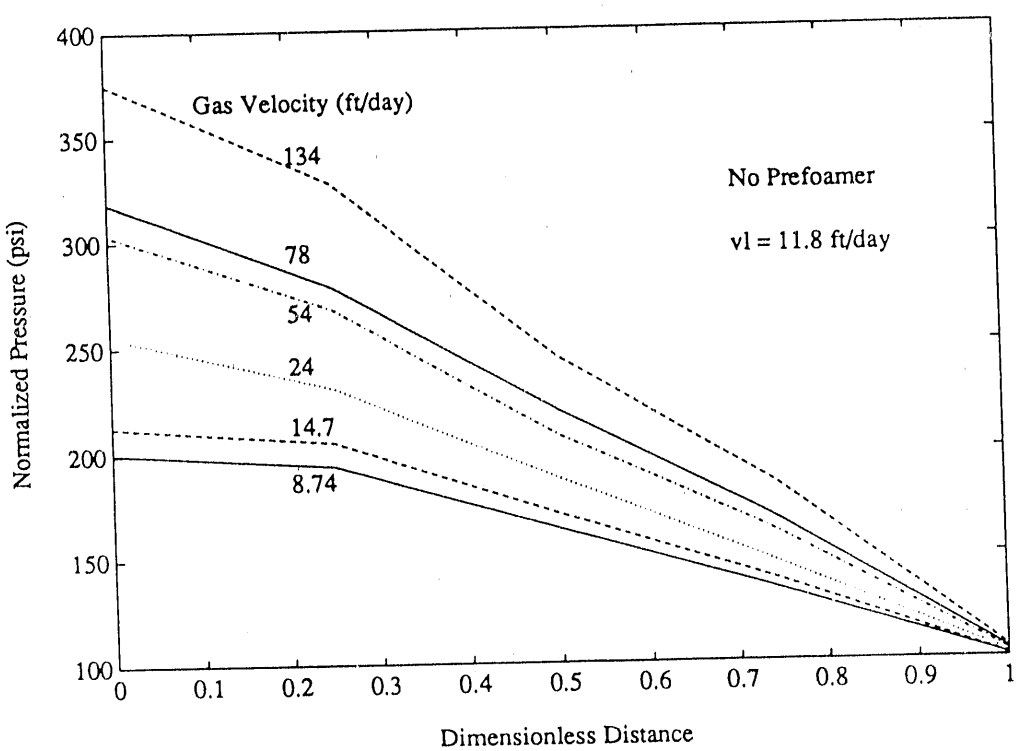

Figure 4.37: Pressure distribution in core at different gas velocities for $v_l = 11.8$ ft/day.

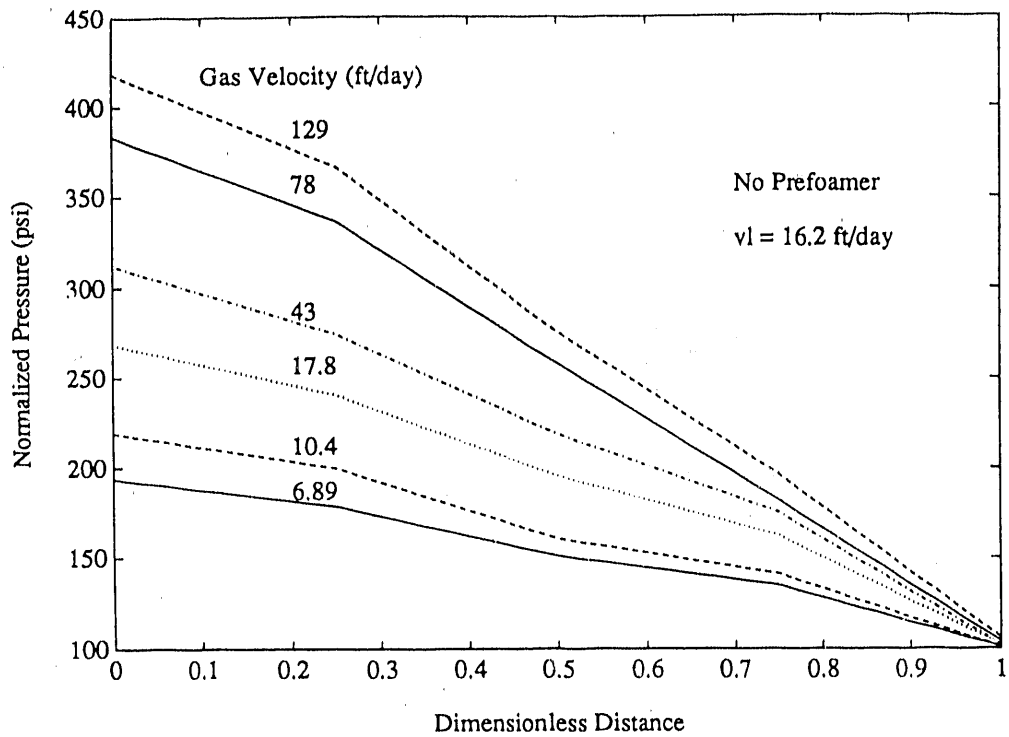

Figure 4.38: Pressure distribution in core at different gas velocities for v_l = 16.2 ft/day.

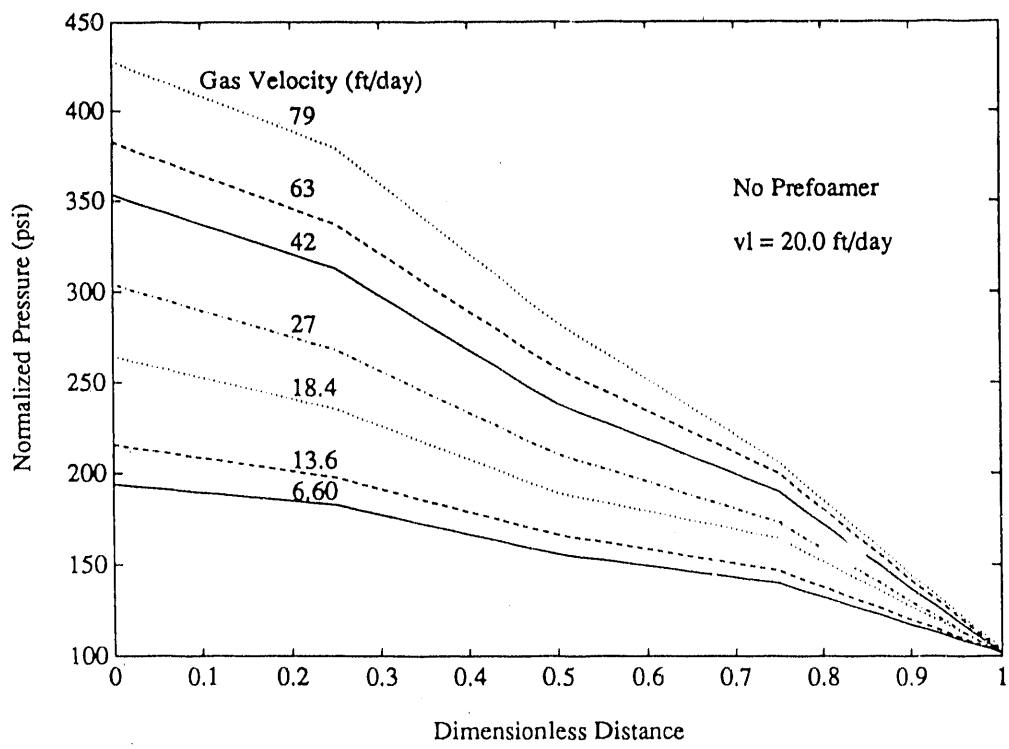

Figure 4.39: Pressure distribution in core at different gas velocities for v_l = 20.0 ft/day.

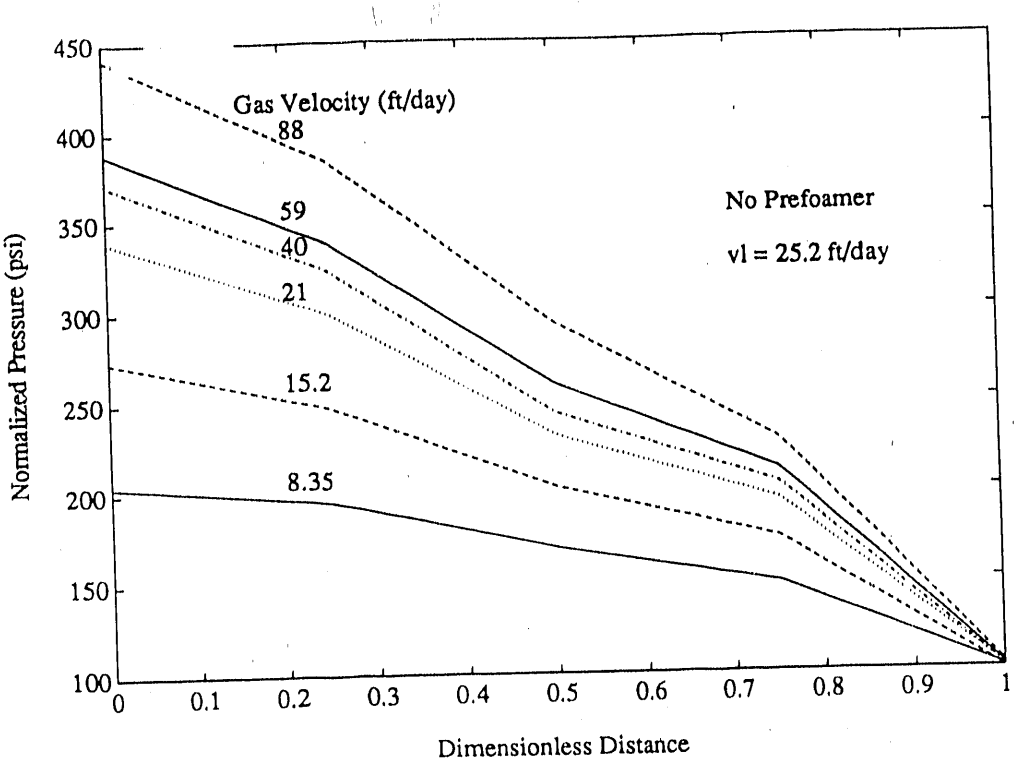

Figure 4.40: Pressure distribution in core at different gas velocities for v_l = 25.2 ft/day.

An experiment was conducted at relatively low gas velocities ranging from 6.7 to 9.2 ft/day. The pressure gradient across the core varied insignificantly as the liquid velocity was varied from 7.96 to 20.0 ft/day. The pressure distributions in the core for each of those surfactant velocities are shown in Figure 4.41. Higher liquid velocities exhibit higher pressure gradients in the effluent section of the core. These steady states were reached by injecting very low quality foams (33 to 56%).

The pressure distributions in the core with injection of pregenerated foam for a liquid velocity of 7.96 ft/day, at different gas velocities, are shown in Figure 4.42. Since these results were obtained with the prefoamer in line, higher pressure gradients are observed in the two upstream sections of the core. The downstream sections are also affected by the prefoamer since higher pressures in the inlet end of the core translate to higher gas flow velocities downstream because of gas expansion as gas flows towards lower pressure levels.

4.4.5 Effect of Foam Generator

While generating data for the cross plot, the effect of gas velocity on pressure gradient with and without prefoamer was also studied over a wide range of gas velocities at a constant liquid velocity. Results indicate that pressure gradients are greater and increase more rapidly with gas velocity with the prefoamer than without. At low gas velocities, as shown in Figure 4.43,

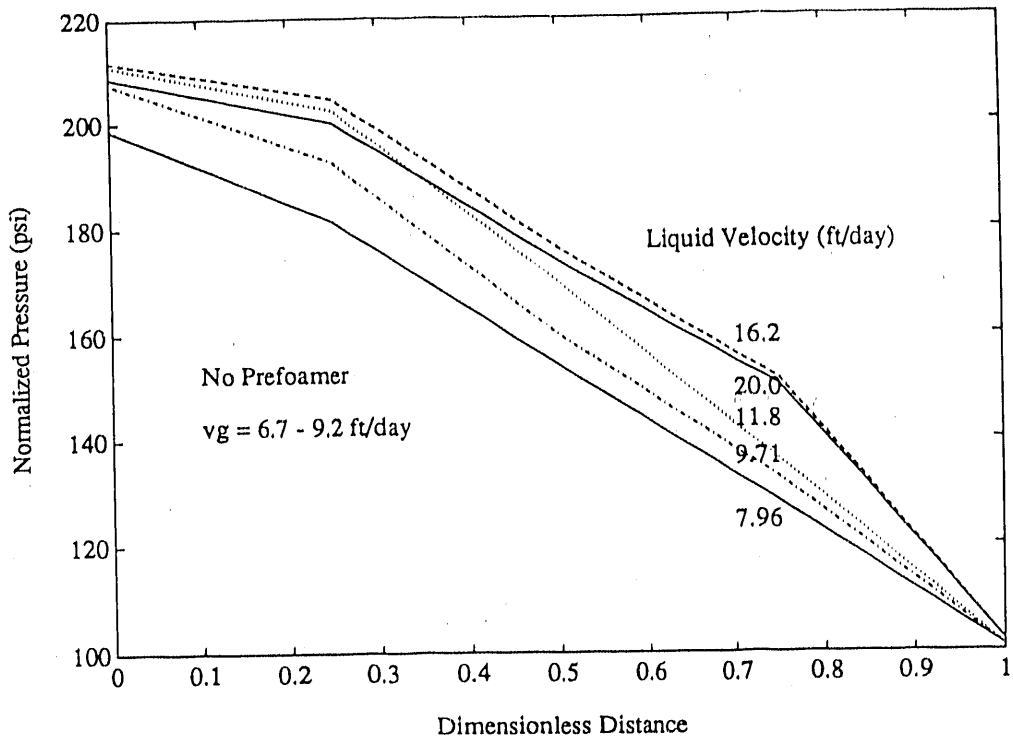

Figure 4.41: Pressure distribution in core at different surfactant velocities for v_g = 6.7 - 9.2 ft/day.

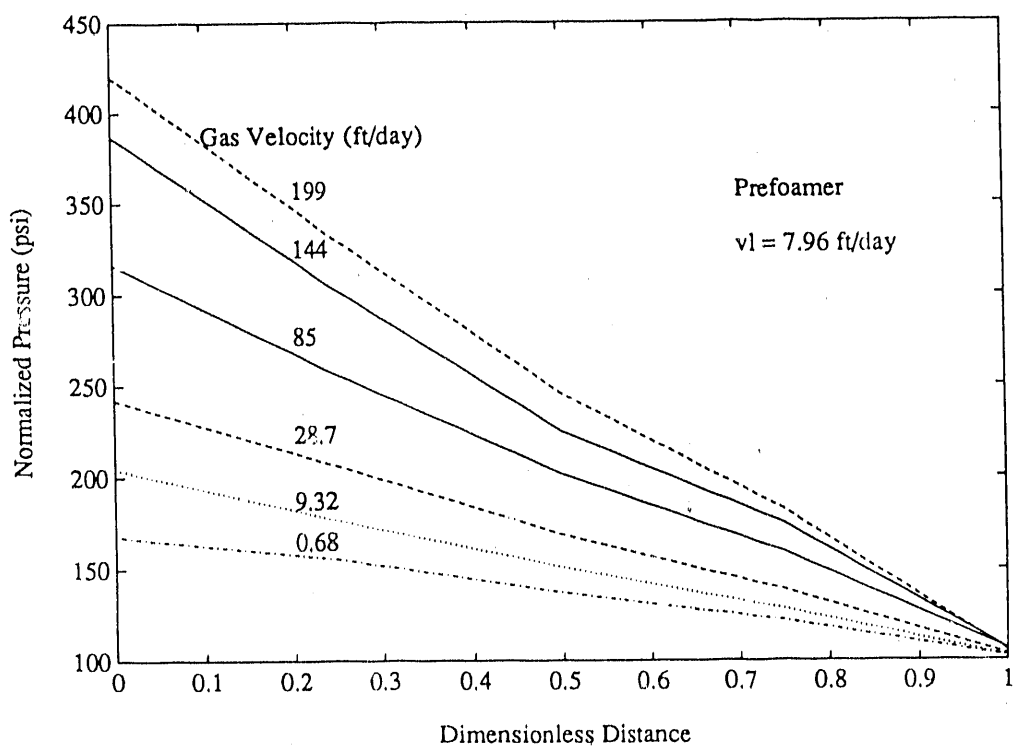

Figure 4.42: Pressure distribution in core at different gas velocities for v_l = 7.96 ft/day with a prefoamer.

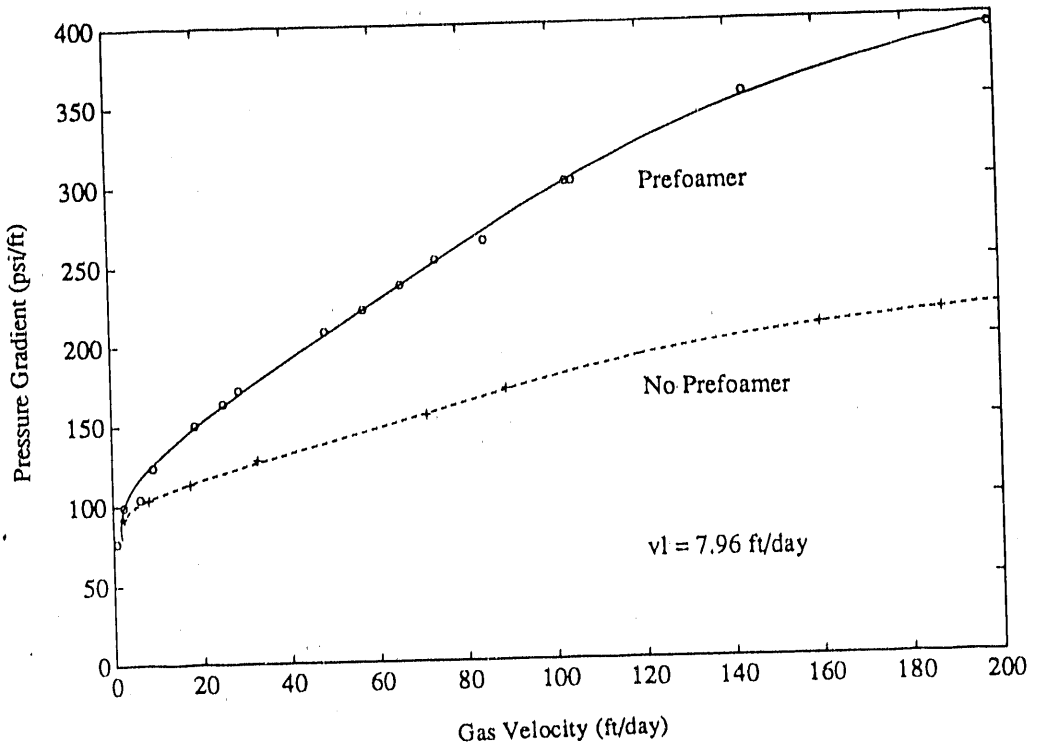

Figure 4.43: Pressure gradient in Berea core at different gas velocites obtained with and without prefoamer for v_l = 7.96 ft/day.

pressure gradients obtained with or without prefoamer seem to converge. Therefore, the effect of the prefoamer is more pronounced at higher gas velocities.

Pressure gradients at constant liquid velocity for different gas velocities were obtained from an experiment without the prefoamer being used as well as from an experiment where the prefoamer was used and then bypassed. Results show that there is a residual effect of the prefoamer at high gas velocities (Figure 4.44).

4.4.6 Hysteresis Effect

Another set of data was generated after attaining steady state pressure gradients with the prefoamer at a liquid velocity of 7.96 ft/day and a gas velocity of 104 ft/day. The gas velocities were decreased stepwise and a new steady state pressure gradient and pressure distribution recorded at each gas velocity. After reaching a low gas velocity of 2.9 ft/day, the gas velocity was increased stepwise and the above procedure repeated. Plotting these two variations of increasing and decreasing gas velocities in Figure 4.45 shows no hysteresis effect on steady state pressure gradients over the range of velocities investigated.

Similar results were also obtained from an experiment without the prefoamer in use (Figure 4.46). Starting with a steady state pressure gradient attained at a gas velocity of 195 ft/day,

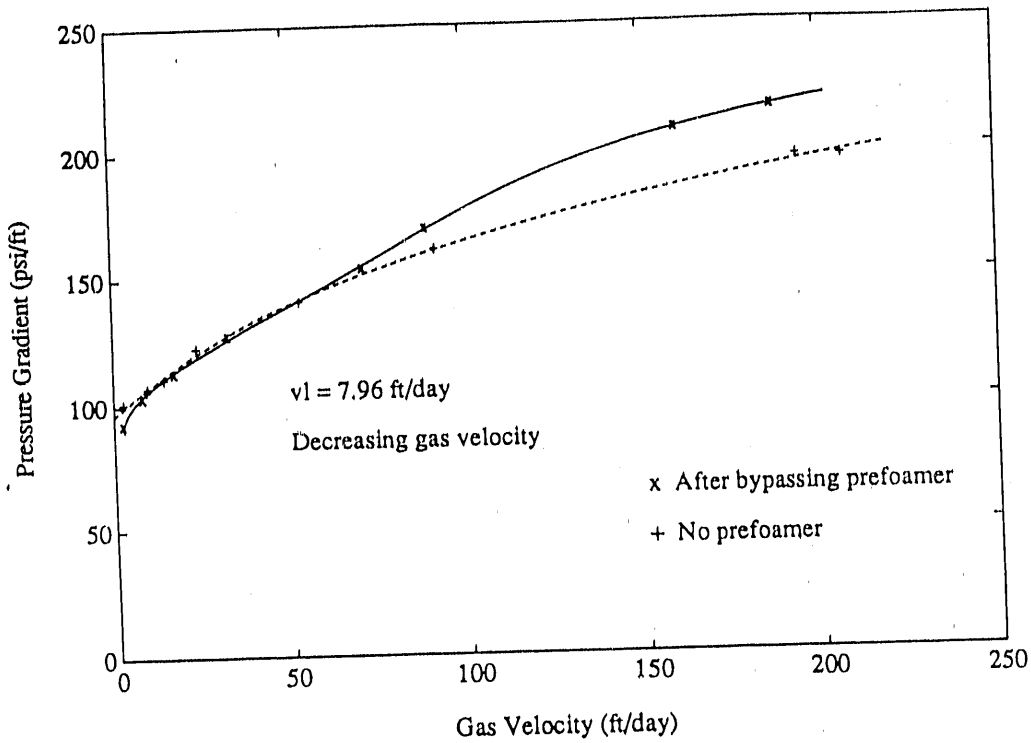

Figure 4.44: Residual effect of prefoamer on pressure gradient versus gas velocity in Berea core for $v_l = 7.96$ ft/day.

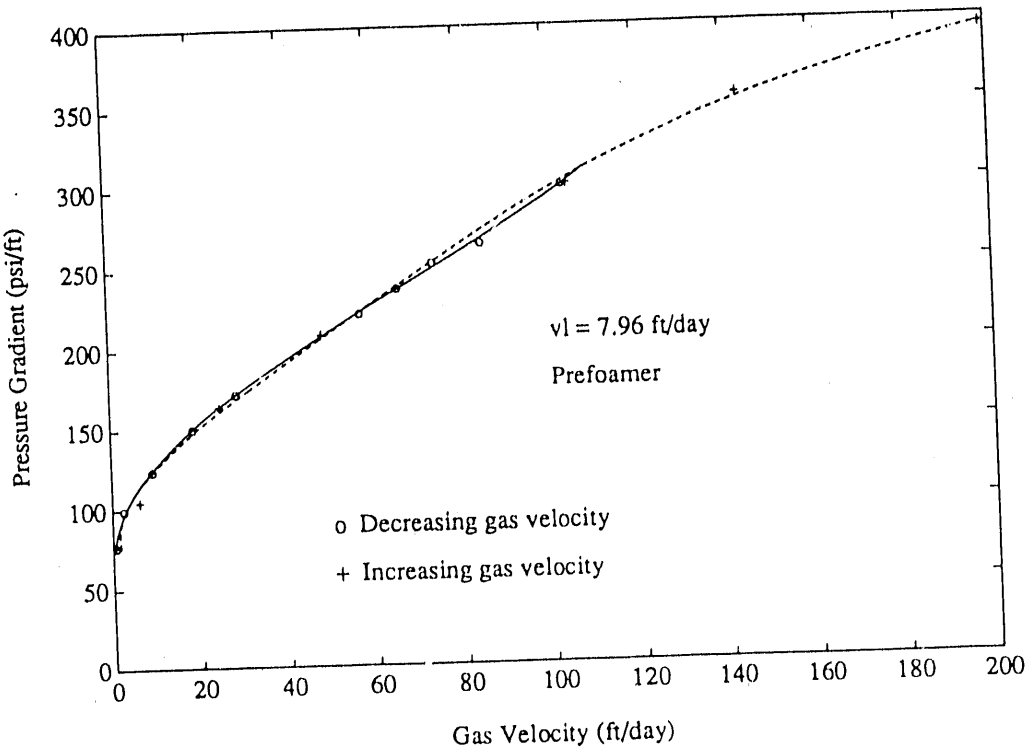

Figure 4.45: Pressure gradient versus gas velocity with increasing and decreasing gas velocities at $v_l = 7.96$ ft/day with a prefoamer.

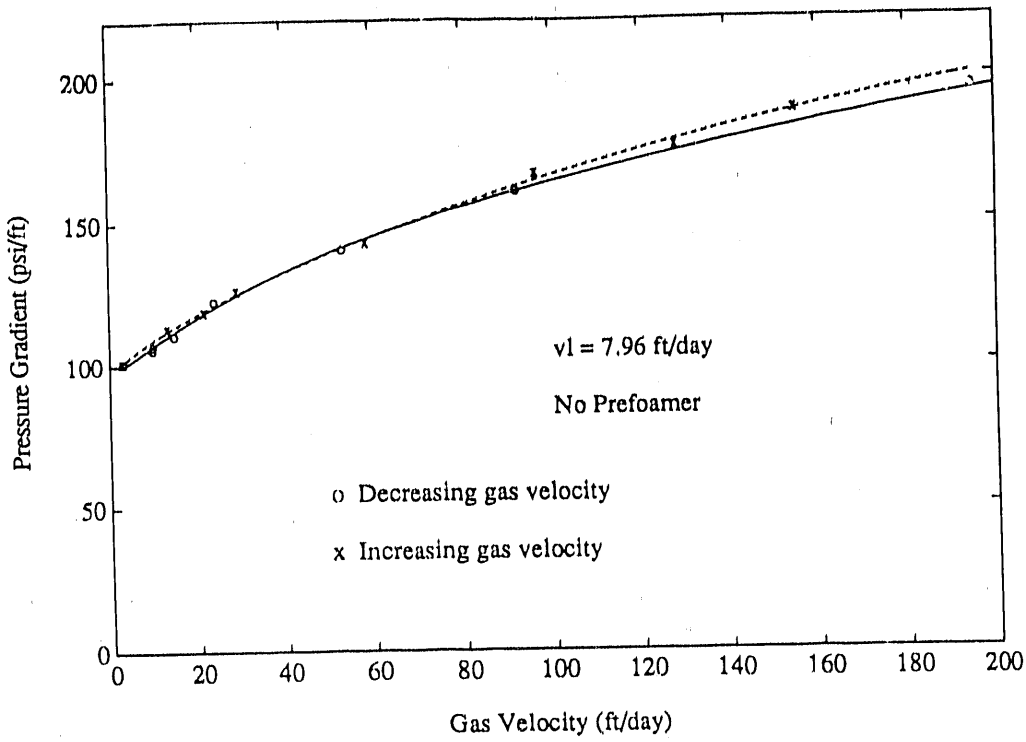

Figure 4.46: Pressure gradient versus gas velocity with increasing and decreasing gas velocities at $v_l = 7.96$ ft/day without a prefoamer.

reducing the gas velocity in steps down to 2.9 ft/day and then increasing it in steps to the initial value does not affect the steady state pressure gradient for a particular set of flow velocities. Therefore, no hysteresis was observed with varying gas velocities, with or without prefoamer.

Chapter 5

DISCUSSION

Foam in porous media may be divided into two classes: weak foam and strong foam. Weak foam consists mainly of trapped gas. The gas flows mostly through a few channels with lamellae forming and breaking. The presence of lamellae generated through the leave-behind mechanism at low gas velocities contributes to gas trapping. The immobile gas does not contribute to flow but decreases gas mobility by reducing the cross-sectional area of the pore network available for flow. Limited gas mobility reduction is obtained with weak foam. Strong foam is generated by mobilizing lamellae. A large number of channels contribute to gas flow. Lamellae generated through snap-off and leave-behind are mobilized, thereby changing the foam texture by increasing the lamella density. This fine textured foam causes significant gas mobility reduction.

Results available in the literature support these definitions and conclusions [37, 43, 60, 62, 92, 97, 101, 104, 115, 118]. Weak foams exist when gas and surfactant solution are flowing simultaneously in porous media. However, the conditions that trigger strong foam generation are still not well understood. In order to study the conditions that promote a fine textured foam formation, pressure histories of several flow experiments were monitored as a function of a range of different parameter settings.

To investigate foam generation in porous media, flow experiments were conducted over a wide range of velocities with Chevron Chaser SD1000. This surfactant was selected for its high solubility in brine and its high foamability at room temperature. It has been extensively used in several experimental investigations as well as field trials [25, 43, 44, 45, 46, 64, 78, 81, 100, 103, 104, 115]. However, other surfactants may show different foam responses due to surfactant properties.

In the literature, there is a lack of agreement on the criteria that distinguish the transition between the weak foam and strong foam regimes [43, 104, 115]. Weak foams and strong foams can be differentiated by the mechanisms by which gas mobility is reduced and they can be

separated quantitatively on the basis of pressure gradients and gas mobility reduction. Results obtained in this study show that the transition from weak foam to strong foam is quite abrupt, especially at higher velocities.

The experimental results to be discussed in this study show that steady state pressure gradients with foam can be attained at low flow velocities if continued for a prolonged period of time. During this period, defined here as "incubation time," the pressure gradients increase at a very slow rate. The changes are not obvious over a short time period. The initial weak foam flow regime may have been mistaken in the literature as steady state. Given enough time, however, strong foam can be generated if the fluid velocities which cause foaming are capable of increasing the pressure gradient enough to initiate foam mobilization. After reaching steady state, results indicate no hysteresis in the pressure gradient response with changing flow velocities.

The use of a prefoamer was found to cause higher pressure gradients and this has been attributed to the forming of small bubbles in the prefoamer which enter and propagate through the porous medium. However, this effect does not extend far from the injected sandface. The effect of a prefoamer is more significant at higher gas velocities. It was also found that there is no hysteresis effect of pressure gradient versus gas velocity with or without a prefoamer. From this it is concluded that there are only limited saturation changes in the core. It was apparent that a minimum pressure gradient is necessary in order to form a fine textured foam by mobilizing lamellae.

In the discussion that follows, oil displacement experiments will be explained first. Next, results for the transient behavior of foam flow in porous media will be reported. Unsteady state experiments provide an insight into foam generation mechanisms. A discussion of steady state results which clarify the effects of gas and liquid velocities on foam flow will follow. The effect of pregenerating foam before injection into the core was investigated for different flow velocities. The effect of the prefoamer on steady and unsteady state foam flow will also be discussed. The mechanisms of foam flow in porous media will then be considered based on the experimental results of weak foam and strong foam. Finally, the feasibility of applying foam in field tests is evaluated.

5.1 Oil Recovery with Foaming Solution.

The effect of foaming agents on oil recovery was studied. When foam is used for mobility control, it works as the driving fluid as well. Ideally, a single surfactant could function both as a foaming agent and as an oil-water interfacial tension reducer. Residual oil displacement can

be accomplished by increasing the capillary number which is defined by the ratio of viscous to capillary forces, $\frac{k\Delta P}{L\sigma}$. To reduce residual oil saturations using foaming solutions, the capillary number would be increased by decreasing the mobility of the gas phase and by reducing the interfacial tension between the aqueous and the oil phases.

In this study, IFT measurements for the oil-water interface were made using the spinning drop apparatus. The IFT reduction is dependent on the extent and the rates of adsorption and desorption of surfactant molecules at the oil/water interface [65, 102, 116]. Results show that IFT measured by the spinning drop method increases with time after an initial reduction, as shown in Figure 4.3. This phenomenon has been related to the oil/water ratio in the spinning tube [65, 116].

IFT values between oil and aqueous surfactant phases exhibit various trends as a function of temperature. Results of IFT studies showing minima with temperature [12, 54], a minor dependence on temperature [12, 54, 65], a significant decrease with temperature [51], and an increase with temperature [65, 133] have all been reported in the literature. The IFT-temperature behavior is a function of salinity and is highly unpredictable [65].

Oil-surfactant solution interaction was studied with two surfactants, Chevron CHASER SD1000 and Shell ENORDET LTS18. The Shell LTS18 surfactant is not completely in solution as supplied and shows low solubility in water at room temperature. Therefore, it is not a good foamer at 72^oF, the temperature for the experiments reported in this study. However, heating it continuously at 95°F for more than 24 hours puts most of the undissolved solids into solution. At higher temperatures, its solubility and foamability increase but its interfacial tension increases as well. Results of IFT measurements with LTS18 indicate little dependence on temperature with refined oils, but the crude oil-LTS18 system showed a marked increase in IFT with temperature. The main purpose of these IFT measurements, however, was to evaluate the extent of IFT reduction with foaming solutions. Chaser SD1000 reduced the IFT between oil and water by a factor of about ten, as shown in Figure 4.1. LTS18 decreased the IFT by another order of magnitude compared to the values obtained with Chaser SD1000 as shown in Figures 4.2 and 4.4. The IFT values for Chaser SD1000 are of the same order of magnitude as those obtained by Jensen and Friedmann [67] and Isaacs et al. [64]. Even though LTS18 is a better IFT reducing agent, SD1000 was used in the oil displacement experiments because of its higher solubility and, therefore, better foamability at room temperature.

Oil displacement experiments were conducted in Berea cores pre-equilibrated with surfactant solution containing 1% by weight surfactant. Adsorption data of SD1000 on Berea cores [43] indicate that it takes about 20 pore volumes of foam injection to reach equilibrium. These results

were obtained with foam for which the liquid volume fraction was 0.05. This is equivalent to about one pore volume of surfactant solution.

To determine the potential benefits of displacing oil by foam, a comparison needed to be made with oil recoveries obtained by alternative displacement processes. A series of experiments had to be performed to evaluate the effect of injecting water, gas or surfactant solution. When injected individually, it is expected that water, gas or surfactant solution would not provide a high enough pressure gradient or a low enough interfacial tension to increase the capillary number to a value such that the residual oil saturation would be reduced significantly. Simultaneous injection of gas and brine has been observed to be an effective displacement process, but the presence of surfactant solution along with gas may be even more effective in displacing oil as a result of reduction in IFT and the formation of foam which increases the pressure gradient in the system. Both of these phenomena contribute to an increase in the capillary number.

The most important experimental comparison to be made was that between gas-water injection versus gas-surfactant solution. It was observed in this study that the relative permeability to gas is much lower in the presence of a residual oil saturation for a given gas saturation than in the absence of oil. This is attributed to the presence of oil in large pores making the flow path for gas more tortuous. Gas, being a non-wetting phase like oil, displaces the latter from the large pores. The volumetric sweep efficiency is improved because of water mobility reduction when gas and water are injected simultaneously [69]. This mechanistic process is responsible for the high oil recovery obtained with gas and brine injection.

Oil occupies the larger pores in the form of isolated blobs. With three phases present, water is always the wetting fluid and gas the non-wetting fluid. However, with oil present in the system, oil is wetting with respect to gas and non-wetting with respect to water. Therefore, oil spreads in between gas and water and forms a thin film. This process may be responsible for oil recovery at high gas/oil ratios. With oil present at connate water saturations, residual oil saturations below 5% have been achieved by gravity drainage alone [31, 50, 71].

In oil displacement experiments, Chevron Chaser SD1000 was used. Injection of surfactant solution alone did not reduce S_{or} significantly due to the limited reduction in IFT. Further residual oil displacement can be achieved, however, by increasing the capillary number [14, 124]. Foam was formed in the core by simultaneously injecting gas and surfactant solution. Pressure gradients higher than those observed for gas-brine displacement of oil indicate foam generation. The surfactant also contributed to higher trapped gas saturation which caused higher pressure gradients. However, the pressure gradients obtained with these excessively high gas velocities are much lower than those obtained in the absence of oil. Therefore, oil has a detrimental effect

on foaming with Chaser SD1000. This may be due to the sensitivity of this surfactant to oil [67]. Isaacs et al. [64] observed higher pressure gradients for foam displacement experiments at low oil saturations as compared to those at higher oil saturations, which also indicates more foaming with less oil.

In the foam floods, the oil saturation was not reduced significantly even though ΔP was increased by a factor of ten and σ was also reduced by a factor of about ten which gave an increase in the N_{ca} by two orders of magnitude, as indicated in Figure 4.6. Nevertheless, the oil saturation was not reduced significantly.

The oil was produced mainly at the beginning of the foam flood. What oil was produced later was in the form of an emulsion which could not be broken. The oil that was recovered was produced at very high water-oil and gas-oil ratios, as summarized in Tables 4.1 and 4.2. Oil recovery results indicate that, if any additional oil is recovered with foaming solutions, it would be recovered at uneconomically high gas and water to oil ratios. Although Jensen and Friedmann [67] report S_{or} values of less than 10% with foam pregenerated at high velocities, this was obtained only after injection of 1000 pore volumes of foam.

These results suggest it would take two surfactants to increase the capillary number enough to affect residual oil saturations: one to produce foam and another to reduce the interfacial tension. Alternatively, a new surfactant could be formulated which provides both mobility control and reduced capillary forces.

5.2 Unsteady State Results

Extensive foam generation and propagation experiments were conducted in two different size cores: 10 inch long cores, 2 inches in diameter, and 4 inch long cores, 1 inch in diameter. Foam incubation was observed in both systems. Interpretation of the experiments conducted in the short cores was limited, however, by the lack of pressure taps as well as by core length. Only pressure drops across the whole core were measured and these data were not adequate to explain the experimental results. Pressure taps on the long core permitted measurements of pressure profiles. These data were used to determine the conditions necessary for foam generation and propagation as well as to evaluate the effect of a prefoamer on foam mobilization. Results of experiments initiated without prefoamer will be discussed first, followed by unsteady state experiments with prefoamer. Finally, data obtained in the short cores will be interpreted.

5.2.1 Foam Mobilization without Prefoamer

Results obtained from the long systems without the prefoamer provide an insight into foam generation and mobilization mechanisms. In experiments initiated without foam pregeneration, the inlet section of the core was the last to show a pressure response, except in one case as explained later. This may be due to gas fingering in the inlet section caused by the adverse mobility ratio of the injected gas to the displaced liquid. A limited number of channels contribute to gas flow in the inlet section. Lamellae that are generated at high gas velocities break quickly and, therefore, do not contribute to pressure increase. The pressure gradients increased throughout the core due to gas trapping and gradual increase in the lamella density. An incubation time was observed during which weak foam flow causes a limited gas mobility reduction. The flow of gas toward lower pressures in the downstream sections results in gas expansion and, consequently, higher gas velocities. As the pressure gradient increased throughout the core, the second section showed a pressure response first. This may be attributed to higher liquid-gas velocity ratios than those in the downstream sections due to gas expansion from decreasing pressures with distance in the core. This indicates that lamella migration was triggered at a certain distance away from the inlet end of the core. However, as this foam front started propagating, the downstream sections also began to respond even before the front reached the downstream sections. Therefore, the flow conditions were favorable for foam mobilization in the experiments shown in Figures 4.19 and 4.22. Later, the inlet section began to respond indicating a slow backward propagation of foam as the three downstream sections reached steady state.

Foam mobilization was observed after a critical pressure gradient was attained. Lamellae propagation contributed to increasing the pressure gradients in the downstream sections. Lamellae were mobilized throughout the three downstream sections almost simultaneously. Therefore, strong foam generation occurred throughout the three downstream sections in addition to a frontal propagation effect.

Responses of other experiments with lower liquid velocities indicate foam frontal propagation rather than in situ foam mobilization, as shown in Figures 4.24, 4.25, and 4.26. A high pressure gradient front was generated in section 2 of the core through lamellae mobilization. Lamellae propagation caused foam mobilization ahead of the front. The flow velocities in the downstream sections did not promote lamellae mobilization. Foam mobilization occurred only after the high pressure gradient foam front reached the downstream sections. At the same time, a slow pressure response in section 1 was observed. This response may indicate a backward propagation of foam or gradual foam mobilization.

At lower liquid velocities, the pressure gradients do not reach the foam mobilization pressure gradient simultaneously throughout the core. The inlet section was always affected by the adverse mobility ratio between the injected and displaced fluids. The second section of the core has the highest liquid-gas velocity ratio of the three dowstream sections due to gas expansion. This causes increased pressure gradients and hence foam mobilization. Once foam mobilization is initiated, the foam texture changes and this translates downstream causing an increase in the pressure gradients through a sharp frontal propagation.

5.2.2 Foam Mobilization with Prefoamer

Results obtained from the long systems with a prefoamer show a much different pressure response. These experiments show an immediate increase in pressure gradient in the inlet section of the core upon the start of gas flow, as indicated in Figures 4.13, 4.14, 4.15, and 4.16. As gas flow is initiated, the foam generator creates bubbles that are of the order of the pore sizes and are, therefore, small enough to enter the core. Bubble generation in the prefoamer is dependent on the gas velocities, with higher velocities promoting smaller size bubble generation [44]. With the low velocity experiments, bubbles generated by the prefoamer would be larger and, therefore, would not propagate as quickly and easily as a foam with smaller bubbles. This may be the reason for the lag in the frontal propagation of foam at the lower gas velocities observed in Figures 4.13 and 4.14. The smaller bubbles generated by higher gas velocities in the prefoamer provoke an immediate pressure response in the inlet section of the core which propagates downstream as a front, as observed in Figures 4.15 and 4.16. The high pressure gradients propagate downstream accompanied by foam mobilization. The mobilization frontal advance is noticeably sharp, as displayed by the pressure responses in the downstream sections. This high pressure gradient front propagates downstream so fast that in situ foam mobilization does not have time to take place in the downstream sections before arrival of the front.

A comparison of Figures 4.13 and 4.14 with 4.16 shows that at lower gas velocities but with the same liquid velocity, foam mobilization occurs simultaneously with the advance of the foam front. At the same time as the foam front is propagating, foam mobilization occurs in the downstream sections due to high liquid flow velocities. Lamellae that were generated by snap-off and left stranded due to low pressure gradients become mobilized. This causes more lamellae to be generated at the vacated pore constrictions. Also, the mobilized lamellae are now capable of dividing, thereby increasing bubble density.

At lower liquid velocities but at similar gas velocities, higher quality foams would be produced. Figure 4.15 shows that the response obtained is still a sharp frontal advance even though

a large number of pore volumes of fluid injection (about 200) were necessary to reach steady state. The flow conditions did not trigger in situ foam mobilization because liquid velocities were too low. Foam mobilization occurred as the high pressure gradients in the inlet section, generated because of the prefoamer, advanced through the core.

5.2.3 Foam Mobilization in Short Cores

Experiments in the short cores can be explained better now after getting some understanding of the foam generation and propagation mechanisms in the long cores. Figure 4.7 shows that, without a prefoamer, strong foam generation occurs only after an extremely large number of pore volumes of fluid injection. The foam generation mechanism is triggered by attaining the foam mobilization pressure gradient.

For experiments with prefoamer in the 4 inch cores, the mechanism of foam generation is very similar to that without a prefoamer. The effect of prefoamer is not as significant in the experiments shown in Figures 4.8, 4.9, and 4.10 as in the case of the longer cores because the velocities used in these experiments were lower. With lower velocities, the bubbles generated by the prefoamer are larger and, therefore, may not enter and propagate in the core as easily as the small bubbles. Bubbles that enter the core may trigger foam mobilization causing more lamellae to be generated, but with the velocities used in the short cores, the prefoamer does not generate bubbles that are small enough to enter the core and propagate downstream. Consequently, the pressure gradients do not rise as sharply as those for the inlet section of the longer systems with prefoamer. If foam mobilization occurred near the effluent end of the core, the pressure gradient may not increase spontaneously as the foam has to propagate backward. The reverse propagation of foam seems to be a slow process and is very much dependent on the gas flow velocities.

5.3 Steady State Results

The pressure gradient responses at various steady states for strong, stable foams are shown in Figures 4.33 and 4.34. From these gradients, one can deduce that the relative permeability to gas increases and the relative permeability to liquid decreases as the gas velocity increases. The pressure gradients obtained are a strong function of liquid flow velocity but a weaker function of gas flow velocity over the range of velocities studied. The dependence of pressure gradients on liquid velocities is close to that predicted from the Darcy equation [62, 97].

With higher gas velocities, foam texture coarsens but changes in saturations have been reported to be minor [36, 37, 72, 97]. These saturation changes are so small that trends in saturations may not be detectable. Nevertheless, small changes in liquid saturations could affect liquid relative permeabilities significantly as the liquid saturations in the presence of foam flow are only slightly higher than residual water saturations. Liquid relative permeabilities are strong functions of saturation, near residual liquid saturations. Results also show that as liquid velocity increases, liquid relative permeability does increase slightly, probably indicating a small increase in liquid saturations. For high quality foams, Khatib et al. [72] postulate a constant liquid mobility and a constant liquid saturation determined by the limiting capillary pressure of the system. They speculate that for low permeability porous media (less than 1 Darcy), the limiting capillary pressure is less than the capillary entry pressure making flowing lamellae unstable. However, their speculation is based on extrapolating data obtained in porous media with permeabilities of several tens of Darcies. Persoff et al. [97] had noticed that changing the liquid flow velocity does not change the saturations significantly, although foam flow resistance increases with increasing liquid velocities.

With foam flow in porous media, often it is not possible to duplicate unsteady state results. The lack of reproducibility may be due to gas flowing through different paths in different experiments [97]. However, steady state results are reproducible. Within the precision that was possible to achieve, no significant pressure gradient hysteresis was noticed for decreasing or increasing gas flow velocities after a strong foam flow regime had been attained. These results are shown in Figures 4.45 and 4.46. Results of Persoff et al. [97] confirm the lack of hysteresis on steady state foam mobilities. Therefore, foam can be generated at high flow velocities and then sustained at lower flow velocities.

Sanchez et al.[118] reported that it takes less time to reach steady state in an imbibition cycle than in a drainage cycle with trace quantities of foaming surfactants in solution. During incubation times, the flow of foam is in the weak foam flow regime. A high gas saturation has been achieved when compared to gas-brine experiments with similar velocities. A large fraction of the gas is trapped by lamellae. Continuous changes in saturations caused by increases in pressure gradients may be taking place during the incubation period. This incubation phenomenon rather than the lifetime effects of transient lamellae may explain the hysteresis effect described by Sanchez et al. [118]. In their system, the extremely low surfactant concentrations may not give rise to foam mobilization. The lamellae are not stable enough to become mobilized and, therefore, break. Consequently, increasing gas velocities would increase gas saturations by invasion of additional liquid filled pores.

With the prefoamer, the steady state pressure profiles show constant pressure gradients throughout the core, although slightly higher pressure gradients were observed in the upstream sections. The prefoamer generates bubbles that are small enough to enter the core and propagate. However, the porous medium adjusts the foam texture within a short distance [36]. De Vries et al. [129] did not notice any influence on their results upon varying the injected foam texture by changing the properties of the foam generator. In their experiments, the pressure drop was monitored in a very short section in the middle of the core. Consequently, the foam texture had been changed by the porous medium by the time it propagated to the middle section of the core.

Linear pressure gradients were observed for an effectively incompressible foam [97] as well as for a compressible foam [36]. Without the prefoamer, the findings in this study indicate that the pressure gradients increase with distance in the core. Gas expansion causes higher gas fractional flows and higher pressure gradients at the downstream end [62]. Gas expansion is more significant with the prefoamer as inlet pressures are much higher. Therefore, the effect of the prefoamer is more pronounced than the pressure distributions indicate.

5.4 Mechanisms of Foam Flow

The experiments reported in this study provide an insight into the mechanisms of foam generation, gas trapping and lamella mobilization. The mechanisms of lamellae generation and coalescence directly affect the foam flow process in porous media. Gas and liquid velocities and saturations and, consequently, capillary pressures play important roles on the stability of moving lamellae. The behavior of foam in porous media is a function of lamella density. Two foam flow mechanisms have been identified: one for weak foams and one for strong foams.

5.4.1 Weak Foam Flow Regime

When gas injection is initiated, gas flows into pores previously filled with liquid. Gas invades these pore bodies and displaces the liquid provided the pressure gradient is high enough to overcome the capillary entry pressure of the liquid filled pores. Lenses (thick lamellae) are formed by the leave-behind mechanism through liquid displacement by gas in two adjacent pores [115]. These lenses exist in the constrictions between two pore bodies.

The thicknesses of liquid films wetting the pore walls depend on the gas velocities, as established by Bretherton [10]:

$$h = 1.337 R_c N_{ca}^{2/3} \tag{5.1}$$

where h = film thickness, R_c = radius of capillary, and N_{ca} = capillary number. The curvature of the gas-liquid interface between the wetting liquid and the non-wetting gas can be explained through the equation of capillarity given by the Young-Laplace equation [1]:

$$P_c = P_g - P_l = \sigma \left(\frac{1}{R_1} + \frac{1}{R_2} \right) \tag{5.2}$$

where P_c = capillary pressure, P_g = pressure in gas phase, P_l = pressure in liquid phase, σ = interfacial tension, and R_1 and R_2 are the principal radii of curvature of the interface. Therefore, the capillary pressure is higher for a capillary with smaller radii of curvatures. Consequently, the capillary pressure in the pore neck is higher than that in the pore body due to differences in the interface curvatures.

For an inviscid fluid such as gas, the gas pressure is the same in the pore neck and in the pore body. Therefore, the liquid pressure in the pore body has to be higher than that in the pore neck causing liquid transport from the region of low capillary pressure to the region of high capillary pressure. For an interface of spherical shape, this net pressure driving force is defined as:

$$\Delta P = 2\sigma \left(\frac{1}{R_b} - \frac{1}{R_t} \right) \tag{5.3}$$

where σ = interfacial tension, R_b = pore body radius, and R_t = pore throat radius. Accumulation of liquid in the pore throat accelerates the process. When gas flows into adjacent pores, the displaced liquid contributes to liquid accumulation in neighboring pores. Such local effects cause instabilities in the nearby pores and channels. The liquid collar in the pore throat continues to grow provided a low capillary pressure exists. When enough liquid has flowed into the pore neck, snap-off occurs. This snap-off mechanism occurs if the right geometry and flow conditions are met [43, 103, 104, 115].

Surfactant is not necessary for snap-off to occur. In gas-water flow in porous media, lenses (thick lamellae) may be generated. In the absence of surfactant, however, these lenses may easily break due to minor fluctuations in the flow conditions, such as in the fluid velocities or in the capillary pressures. The presence of surfactant would stabilize the generated lenses. As the capillary pressure increases, liquid drains out of the lenses forming lamellae [115]. The disjoining pressure - capillary pressure balance dictates the life of a lamella. If a balance of pressures exists, the lamella will be stable [20].

Generation of a large number of stabilized lamellae creates channels that are separated from the main flow paths for gas. These lamellae block the gas channels thereby reducing the cross sectional area available for flow. This mechanism isolates a large fraction of the gas into what is called trapped gas [5, 15, 39, 43, 92, 101]. If the conditions are such that the stranded lamellae cannot be mobilized, the weak foam flow regime is in effect. Most of the gas is trapped and a few channels contribute to gas flow. Gas velocities are high in the channels contributing to gas flow. Therefore, lamellae generated in these flow paths would be short-lived as they would break easily. Consequently, the gas moves through the flow channels by breaking and reforming bubbles [60].

Results of Radke and Gillis [101] indicate that 70-99% of the gas is trapped. These measurements were obtained with tracer studies in the weak foam flow regime. Results of Friedmann et al. [43] show that the fraction of trapped gas is between 75 and 90%. These measurements were made for gas velocities ranging from 25 to about 130 m/day and for a liquid volume fraction of 0.05. According to the critical gas velocity for foam generation determined by Friedmann et al. [43] as shown in Figure 2.3, the critical velocity for foam formation would be 153 m/day. This is higher than the velocities used and, therefore, these measurements were made in the weak foam flow regime. Based on the observations of the present study, the velocities used by Friedmann et al. were capable of generating a strong foam given enough incubation time. Experiments should be conducted to determine trapped gas saturations under strong foam flow regimes. It is expected that, since a larger number of channels contribute to flow in the strong foam regime, a smaller fraction of the gas would be trapped.

Weak foam is generated when surfactant solution and gas are flowing simultaneously in a porous medium. With weak foams, high trapped gas saturations exist. Most of the gas is stagnant and only a few channels contribute to gas flow. The liquid flows mainly through a network of the small pores since it is the wetting phase. The gas flows through a few channels at high velocities where lamellae form and break continuously. The high trapped gas saturation along with the lamellae forming and breaking cause limited gas mobility reduction, as observed during the incubation periods of the experiments reported in this study.

5.4.2 Strong Foam Flow Regime

At low flow velocities, the generated foam is a weak foam. According to Rossen and Gauglitz [115], foam mobilization occurs when the flow velocities generate a high enough pressure gradient to mobilize stationary lamellae. The maximum pressure drop across a lamella as it is displaced from a pore throat is given by the following equation:

$$\Delta P_{max} = 4\sigma / r_{min} \tag{5.4}$$

where σ = surface tension, and r_{min} = minimum mean value of the principal radii of curvature of the gas-liquid interface. Therefore, the minimum pressure gradient to mobilize a lamella is given by:

$$\nabla P_{min} = \Delta P_{max} / L \tag{5.5}$$

where L = length between two points separated by a single lamella, otherwise connected through another gas channel.

Stranded lamellae become displaced from pore constrictions when the pressure gradient is high enough to mobilize them. As they travel into pore bodies, they may stretch enough to break [13, 68]. Given the right conditions for lamellae stability such as a low capillary pressure and a slow stretching rate, these lamellae are capable of flowing towards lower pressures [13, 36, 37, 72]. When they encounter channels that divide into two or more channels, these lamellae may divide [43, 104]. Also, when lamellae are dispaced out of pore constrictions, new lamellae would be generated by snap-off at these vacated pore necks.

The snap-off mechanism requires enough liquid to flow back from the pore body into the constriction to form the lamella. In addition, the capillary pressure difference between the pore body and the pore neck must be high enough to cause the liquid to flow into the constriction. The foam generation rate by snap-off increases with increasing gas velocities, above a critical gas velocity [36, 43]. Ettinger and Radke [36] proposed the following foam generation rate equation, at constant liquid velocity and saturation:

$$r_g = k_1 v_g^{1/3} \tag{5.6}$$

where r_g = rate of lamella generation, k_1 = lamella generation rate constant, and v_g = gas velocity.

As a stationary lamella is displaced from a pore constriction, a new lamella may be generated at the vacated pore neck by snap-off. A flowing lamella may also divide into two or more lamellae at dividing channels by the lamella division mechanism. After foam mobilization is initiated, repeated lamella generation by snap-off and lamellae division alter the foam texture. The increase in lamellae density causes a further increase in the pressure gradient, which in turn causes more lamellae to be mobilized. This mechanism is self propagating and would occur indefinitely if foam coalescence did not slow it down.

As lamellae become dislodged from pore constrictions due to increased press gradients, they stretch as they travel into large pore bodies. If the lamella velocity is high enough such that liquid does not have enough time to flow into the stretching lamella to stabilize it, it would break [13]. Therefore, low liquid saturations and, consequently, high capillary pressures promote bubble coalescence [72]. The mechanism of lamella collapse occurs repeatedly at high gas velocities in large pore bodies called termination sites [36, 68]. As the number of flowing lamellae increases, the rate of lamellae coalescence increases due to the larger number of lamellae being forced into the termination sites. For a specific surfactant at a constant concentration and fixed liquid velocity and saturation, the coalescence rate is given by Ettinger and Radke [36] as:

$$r_c = k_{-1} v_g n_F \tag{5.7}$$

where r_c = lamella coalescence rate, k_{-1} = lamella coalescence rate constant, v_g = gas velocity, and n_F = local bubble density.

Steady state is reached when the rate of lamellae generation and collapse are equal. Under these conditions, the net change in bubble density would be zero. Lamella mobilization causes some of the gas that was trapped during the weak foam flow regime to rejoin the flowing gas phase. With increasing pressure gradients, an increasing fraction of the trapped gas becomes mobilized. At steady state, any changes in the amount of trapped gas have to be in balance. If some gas becomes isolated due to a local decrease in pressure gradient, the lamellae collapse rate also decreases causing a net bubble generation rate. As the lamella generation rate increases, an increase in lamella density occurs. This causes an increase in pressure gradient forcing stationary lamellae to become mobilized. There is constant change at the pore level even though a dynamic equilibrium has been reached across the core as a whole. Stabilization occurs at the macroscopic level such that a net bubble density or balance is maintained.

The model proposed by Ettinger and Radke [36] accounts for the foam flow parameters of generation, coalescence, and trapping:

$$\frac{d(n_F v_g)}{dx} = r_g - r_c - r_t \tag{5.8}$$

where n_F = local bubble density, v_g = gas velocity, x = distance in the core, and r_t = bubble trapping rate. Foam texture alteration is a function of the rates of lamella generation and collapse through changes in gas velocities. An effective foam viscosity has been calculated by Ettinger and Radke [36] using the following equation:

$$\mu_e = \mu_g + B\mu_l n_F D_b^3 \left(\frac{\sigma}{\mu_l v_g}\right)^{1/3} \tag{5.9}$$

where μ_g = gas viscosity, μ_l = liquid viscosity, B = constant, n_F = bubble density, D_b = pore body diameter, σ = surface tension, and v_g = gas velocity.

Darcy's equation was applied by Ettinger and Radke [36] for foam flow in porous media such that the relative permeability to gas was obtained for a gas saturation corresponding to the gas flowing fraction. Darcy's equation, coupled with the population balance equation, was solved and the pressure profile in the core was predicted.

An attempt was made to adapt this population balance model to calculate the pressure profiles obtained in this study. However, the model can be made to predict the experimental results through only minor variations in D_b, the assumed characteristic pore body diameter, since it is elevated to an exponent of three. The model is much less sensitive to actual measured physical parameters and is, therefore, not suitable for predictive purposes. Results of Ettinger and Radke [36] indicate linear pressure profiles. The results obtained in this study show increasing pressure gradients with increasing distance along the core without prefoamer. However, almost linear profiles were obtained with the prefoamer.

A refinement to the population balance model, such as the one proposed by Ettinger and Radke [36], is necessary to accurately predict foam behavior in porous media. The model discussed above does not account for foam generation by lamella division. The importance of this mechanism should be emphasized as it causes significant texture alteration. As lamellae become mobilized, lamella density increases due to repeated snap-off at pore throats. These moving lamellae are capable of dividing when they encounter a branching flow path as they travel in the pore network. This mechanism increases the flowing lamella density by a number proportional to the number of lamellae entering the lamella division sites.

5.4.3 Foam Mobilization Mechanisms

A weak foam flow regime is observed for low fluid velocities for which a large fraction of the gas is trapped. With low fluid velocities, the pressure gradients are not high enough to mobilize the immobile lamellae. With higher flow velocities, higher pressure gradients cause lamella mobilization. During the incubation periods observed in this study, lamella mobilization is taking place. However, this process is very slow and requires long times. As lamellae become mobilized, the local gas flow velocity drops due to additional channels contributing to gas flow. The velocities are still high enough to destroy the mobilized lamellae. However, local

pressure gradients increase momentarily as new lamellae are generated at pore necks causing other lamellae to become mobilized. This phenomenon continues and accelerates as it is a self-propagating process. When the mobilization pressure gradient is exceeded, lamellae mobilization causes significant foam texture refinement. The participation of a large number of channels in gas flow reduces the gas velocities such that the lamellae coalescence rate decreases. However, as lamellae become mobilized and their number density increases, the coalescence rate increases due to the larger number of lamellae being forced into termination sites. Also, the rate of lamella generation by lamella division increases as more lamellae are mobilized. A steady state is reached when the net rate of lamella generation due to generation, coalescence, and trapping is zero.

Rossen and Gauglitz [115] show a strong dependence of the minimum pressure gradient for foam mobilization on the liquid volume fraction, as shown in Figure 2.3. Observations in this study verify their findings. Foam mobilization occurred in the second section of the core, the section that has the highest liquid volume fraction of the three downstream sections. Increases in the gas velocity in the downstream sections due to gas expansion is not sufficient to increase the pressure gradient to the level required for foam mobilization. Since $LVF = \frac{v_l}{v_l+v_g}$, a plot of $log\, LVF$ versus $log\, v_g$ will be essentially linear with a slope of -1 for values of v_l small compared to v_g. Superimposing this curve on Figure 2.3 would cross the critical gas velocity curve which has a slope of -0.65. This indicates that gas expansion reduces the liquid volume fraction and increases the gas velocity such that the net effect is detrimental for foam mobilization.

Even though the inlet section has the highest LVF in the core, it is affected by gas fingering. If fewer channels contribute to gas flow, higher gas velocities promote lamella collapse. According to Rossen and Gauglitz's analysis, foam mobilization pressure gradients decrease with increasing LVF. In experiments with high liquid volume fraction and high velocities reported in the present study, foam mobilization occurs simultaneously throughout the core. With lower velocities, foam mobilization occurs in the second section and propagates downstream. At the onset of foam mobilization, local gas velocities are reduced. Foam texture is refined and pressure gradients increase. Propagation of a high lamella density foam causes foam mobilization downstream and hence, increased pressure gradients. This frontal propagation is rapid at higher velocities.

The rise in pressure gradient caused by lamella mobilization and regeneration in channels in which flow is occurring induces pressure fluctuations in the neighboring channels. These pressure fluctuations can trigger lamella mobilization upstream of the high pressure gradient region. This may be the reason for the slow pressure response in the inlet section of the

core. Therefore, high pressure gradients are capable of propagating in any direction. However, propagation in the direction of flow is faster.

In experiments for which pregenerated foam was injected into the long system, the immediate pressure response in the inlet verifies the hypothesis that small bubbles are capable of entering the porous medium and propagating. The high pressure gradients representative of strong foams propagate downstream as a front, provided the gas velocities are high, thereby generating small bubbles in the prefoamer. With high liquid velocities and lower gas velocities, the high liquid volume fraction in the core promotes foam mobilization throughout the core. The pressure response is a combination of high pressure gradient frontal propagation as well as lamella mobilization ahead of the front.

5.5 Field Application of Foam

Many field projects of foam injection have been undertaken in recent years with several different surfactants [11, 25, 29, 26, 45, 60, 73, 74, 78, 89, 90, 95, 100]. Most of theses tests were conducted in the San Joaquin Valley in California. Applications involved continuous as well as slug injections. Surfactant penetration deep into the reservoir was observed. However, in all cases, no direct evidence of foam propagation deep into the reservoir was obtained. Increases in wellhead pressure at injection wells has been attributed to foaming in the near wellbore region. Incremental oil production was observed in most tests due to better sweep efficiency.

Ploeg and Duerksen [100] reported steam/foam tests in Midway Sunset Field using Chevron Chaser SD1000. For every barrel of incremental oil produced, 0.25 pounds of surfactant were required in one test whereas that number was 1lb/bbl for another test. The surfactant solution was injected in a semi-continuous method: 48 hours of foam injection followed by 120 hours of steam only. Nitrogen gas was also injected along with the large slugs of surfactant solution. The concentration of the surfactant was 0.5% by weight active sulfonate in the steam's liquid phase. Injection pressures increased by more than 100 psi in both tests.

Results of a Shell test in Midway Sunset Field show a significant increase in oil production with alpha olefin sulfonate foam injection [90]. The findings indicate the propagation of a primary foam front of liquid desaturation followed by a secondary front of finer texture foam that causes an increase in the resistance to steam.

A successful steam foam test was undertaken by Mobil in the South Belridge Field. Injection of a linear toluene sulfonate surfactant with steam and nitrogen gas resulted in significant

incremental oil production. Foam injection resulted in a barrel of incremental oil for every pound of surfactant.

Recent results by Friedmann et al. [45] indicate that foam mobilization pressure gradients for Chaser SD1020, a linear alkyl toluene sulfonate very similar to Shell LTS18, are about 1 psi/ft. This mobilization pressure gradient is about one thirtieth that of Chaser SD1000. These mobilization pressure gradient were determined from contant pressure drop experiments in cores. They arbitrarily selected a mobility reduction factor of ten as indicating the onset of strong foam generation. Field results with SD1020 indicate increased pressures in injection wells due to foam formation in the vicinity of the well. The pressure gradient in the reservoir was about the same as the critical pressure gradient for foam mobilization for this surfactant. Therefore, the authors claim foam generation deep in the reservoir.

In this study, a sharp and brief pulse in the gas velocity triggered foam generation in the inlet section of the core for an experiment in the long system without a prefoamer at low fluid velocities, as shown in Figure 4.27. Once foam generation was initiated, the foam front propagated downstream but at an extremely low velocity, as indicated in Figure 4.28. Strong foam generation can also be attained at high velocities and foam propagation maintained with lower velocities. However, results show that strong foam propagation is possible at low flow velocities only at the expense of a large number of injected pore volumes over a long time.

Under the best performing conditions observed in this study, injection of pregenerated foam caused an immediate pressure response in the inlet section. Therefore, foam pregeneration may be beneficial to initiate foam propagation. Nevertheless, several pore volumes of foam are necessary to propagate strong foam to the effluent end. Foam mobilization is required to generate the strong foams that cause significant gas mobility reduction. Otherwise, most of the gas mobility reduction would be attributed to reduction in the cross sectional area available for gas flow through gas trapping caused by stationary lamellae. These lamellae generated by the snap-off and leave-behind mechanisms contribute to only limited gas mobility reduction [115]. Minimum pressure gradients are necessary for foam mobilization to cause repeated snap-offs and lamellae division to obtain a fine texture foam and provide a significant gas mobility reduction.

Since the conditions for strong foam generation cannot be attained away from the wellbore in field applications, strong foam propagation deep into the reservoir does not appear feasible with Chevron Chaser SD1000. Strong foam formation may be limited to the near wellbore region where high pressure gradients are present. In view of the findings of this study, this surfactant

may be more beneficial in cyclic well stimulation applications where the near wellbore region is affected.

Selective plugging of high permeability layers in the near wellbore region may be accomplished by cyclic stimulation of injection wells with foam. Application of foams in production wells may divert the heat injected with steam towards regions in the reservoir where there is oil. However, such cyclic stimulation treatments of production wells should be undertaken at low surfactant concentrations to minimize emulsion problems. Results of this study show emulsion formation of 1% active sulfonate solutions with refined oil.

In oil reservoirs, local heterogeneities can cause foam generation. Ransohoff and Radke [104] and Falls et al. [37] observed lamellae generation at permeability discontinuities going from low to high permeabilities. Also, coalescence of bubbles take place at high to low permeability discontinuities. Such permeability heterogeneities may contibute to foam generation or collapse at large distances away from the injection well.

Chapter 6

CONCLUSIONS

Mechanisms of foam generation and propagation were investigated in Berea sandstone using Chevron Chaser SD1000. In addition, oil displacement experiments were conducted. From the extensive experimental research, the following conclusions can be drawn:

- Results of foam generation experiments suggest that after long incubation times, foam can be generated in situ with flow velocities lower than those cited in the literature. The critical factor is pressure gradient and this is self-generating as foam is formed.

- Two classes of foam were observed: weak foam and strong foam. Weak foam is a foam with a high trapped gas saturation and a coarse texture causing limited gas mobility reduction. Strong foam, generated by lamellae mobilization, forms a finely textured foam that causes a substantial gas mobility reduction.

- Higher gas and surfactant velocities reduce the foam incubation time. Limited gas mobility reduction occurs during the incubation period. The transition of this weak foam regime to the strong foam regime is relatively abrupt.

- As foam is mobilized, its texture changes. Repeated snap-off and lamella division are responsible for the generation of a fine textured foam causing significant gas mobility reduction. When steady state is reached in the strong foam regime, the net lamellae generation rate due to lamellae generation, coalescence and trapping is zero.

- No hysteresis in the pressure response was observed with changing flow velocities after steady state had been achieved in the strong foam regime. The lack of hysteresis may be explained by postulating that liquid saturations vary only slightly regardless of flow conditions in the strong foam flow regime. This indicates that foam flows through the same channels irrespective of the direction of the change in flow rate.

- Varying the gas flow rate changes lamellae density through changes in the lamellae generation and collapse rates, causing a net effect on the pressure gradient. The changes in pressure gradient with velocity are reversible in the strong foam flow regime. Consequently, experiments can be initiated at high injection velocities which later can be reduced. Once foam mobilization has occurred, strong foam would persist even at low velocities.

- Strong velocity dependence was observed on pressure gradients at low flow velocities in short cores. As gas velocities are reduced from the strong foam flow regime, foam mobilization decreases and the foam texture coarsens.

- Gas mobilities increase and liquid mobilities decrease with increasing gas velocities at constant liquid velocities in the strong foam regime. Liquid mobilities increase and gas mobilities decrease with increasing liquid velocities at constant gas velocities in the strong foam regime. The steady state pressure gradients have a strong dependence on liquid flow velocities and a much lesser dependence on gas flow velocities.

- The use of a prefoamer accelerates foam propagation by generating bubbles that enter the porous medium and propagate. In general, the effect of pregenerating a foam before injection into a porous medium does not extend far from the inlet end. A residual effect of the prefoamer was observed at high gas velocities after bypassing the prefoamer.

- Pregenerated foam propagates as a front and lamellae are mobilized with the advancing foam front. Frontal propagation is delayed at low gas velocities. Foam mobilization occurs provided the fluid flow velocities are high enough to generate a high pressure gradient. Without prefoamer, high liquid volume fractions promote foam mobilization.

- Under steady state conditions, pressure gradients are almost linear with distance in the core. With a prefoamer, higher pressure gradients are encountered at the upstream end due to the finely textured foam whereas without a prefoamer, pressure gradients increase with distance from the inlet end of the core due to gas expansion.

- Even if foam propagation under field conditions were possible, an excessively large number of pore volumes of foam injection would be necessary to accomplish the desired objective of propagating foam deep into the reservoir. Excessively high pressure gradients are required for foam mobilization. Therefore, foam mobilization and propagation with Chevron Chaser SD1000 surfactant are feasible only in the near wellbore region. In-depth foam penetration can be accomplished only in the weak foam flow regime.

- Oil displacement is not feasible with this foaming agent because the foam is not stable in the presence of oil. Foaming agents do not provide a low enough IFT for oil displacement. However, a combination of reduced IFT and increased pressure gradient due to foaming may reduce residual oil saturation.

Chapter 7

RECOMMENDED FUTURE WORK

Results reported in this work provide better understanding of the foaming process in porous media. However, results would be strengthened by studying other related aspects.

- A basic postulate in this work is that weak foams are primarily trapped gas and that strong foams are mostly gas with moving lamellae. Tracer experiments should be conducted to evaluate this postulate.

- Experiments of foam flow, just like any experiment conducted in porous media, should be carried out in a system where accurate in situ fluid saturation measurements are possible.

- Surfactants should be selected which generate a strong foam with short incubation times. This would make better foaming surfactants by minimizing the time and amount of surfactant that it would take to generate a strong foam. Foaming surfactants should also be capable of reducing oil-water IFT values significantly. The combination of increasing pressure gradients and decreasing IFT values is desirable. Lamella-oil interaction should be investigated and surfactants that do not have a high affinity to oil and sandface should be formulated. Lamella stability investigations in the presence of oil should also be carried out.

- The effect of pregenerating a foam before injection into a porous medium should be studied further. The effect of generating foam at constant velocity in the prefoamer and injecting it at different velocities into the core should be studied. This would allow a study of foam velocity for a foam of constant texture. Pregeneration of foam is a function of velocity. In this study, it was not possible to keep the properties of the pregenerated foam constant.

- Constant pressure drop experiments should also be conducted for surfactant screening purposes and for comparison with constant rate. More precise experimental equipment

should be used to study foam flow in porous media at extremely low velocities. Liquid pumps and gas flow controllers should operate in a pulse free constant rate mode. A number of results obtained during the unsteady state flow regime indicate that the section that responds first goes through a maximum then declines. This is due to reaching near the upper limit on the gas flow controller at high gas velocities. This peak occurs as the pressure at the inlet end of the core becomes too high and the gas rate drops slightly.

- Modeling of foam flow in porous media is still in its infancy. Significant contribution is necessary to formulate foam generation, collapse, and propagation mechanisms. Experiments should be conducted to study specific parameters needed in the models. The kinetic rates of lamellae generation and collapse should be refined and better formulated. Studies should include foam texture and the parameters affecting it. Foam mobility as a function of population balance or bubble size distribution should be undertaken. The fraction of gas that is trapped as a function of velocities and pressure gradients should be modeled.

NOMENCLATURE

A = area, cm^2
A_H = Hamaker constant, J
B = constant
C = bulk surfactant concentration, $mole/cm^3$
d = lamella thickness, m
D_b = characteristic pore body diameter, m
E = modulus of surface elasticity, $dyne/cm$
f = force, $dyne$
f_g = gas fractional flow, fraction
g/l = gas-liquid ratio, dimensionless
h = film thickness, m
k = absolute permeability, md
k_c = foam collapse rate constant, s^{-1}
k_1 = generation rate constant, $(m/s)^{-1/3}m^{-3}s^{-1}$
k_{-1} = coalescence rate constant, $(m/s)^{-1/3}m^{-3}s^{-1}$
l = length of line element, cm
L = length, cm
LVF = liquid volume fraction, fraction
M = hydraulic radius defined as "flow volume/wetted surface," cm
n = number of moles of gas, $mole$
n_F = local bubble density, m^{-3}
N_{ca} = capillary number = $\frac{k\Delta P}{\sigma L}$, dimensionless
P = pressure, $psia$
P_b = back pressure, $psia$
P_c = capillary pressure, psi
PV = pore volumes injected, dimensionless
q = flow rate, cm^3/min
q_l = lamella surface charge density, C/m^2
r_{min} = minimum mean value of the principal radii of curvatue of gas-liquid interface, m
R = ideal gas constant, $dyne\ cm/mole\ ^oR$
R_b = pore body radius, m
R_c = radius of capillary, m
R_t = pore throat radius, m
R_1, R_2= radii of curvature of bubbles, cm

r = average radius of Plateau border, cm
r_c = rate of coalescence, $m^{-3}s^{-1}$
r_g = rate of generation, $m^{-3}s^{-1}$
r_t = rate of trapping, $m^{-3}s^{-1}$
$S_{o/w}$ = initial spreading coefficient, mN/m
S_l = liquid saturation, fraction
S_o = oil saturation, fraction
S_{or} = residual oil saturation, fraction
t = time, s
$t_{1/2}$ = half life of foam, s
T = temperature, ^oC, ^oR
v_{av} = average liquid flow velocity, cm/s
v_c = critical gas velocity, m/day
v_g = gas velocity, ft/day
v_l = liquid velocity, ft/day
V = volume, cm^3
V_0 = volume of foam at time zero, cm^3
V_p = pore volume of core, cm^3
y = one-half minor axis of drop, cm

Greek Symbols:

α = shape factor
Γ = excess of solute present in the surface layer, $mole/cm^2$
Δ = difference
ϵ = permittivity constant, F/m
η_s = surface shear viscosity, g/s
κ = inverse Debye length, m^{-1}
κ_s = surface dilational viscosity, g/s
μ = viscosity, cp
∇ = gradient
Π = disjoining pressure, psi
ρ = density, g/cm^3
σ = interfacial tension, mN/m
ϕ = porosity, %
ω = rotational speed rad/s

Subscripts:

g = gas
l = liquid (surfactant)
o = oil
w = water

REFERENCE LIST

[1] A.W. Adamson. *Physical Chemistry of Surfaces.* John Wiley & Sons, New York, 1982.

[2] A.H. Al-Khafaji, P.-T. F. Wang, L.M. Castanier, and W.E. Brigham. Steam Surfactant Systems at Reservoir Conditions. Paper SPE 10777 presented at the California Regional Meeting, San Francisco, CA, March 24-26, 1982.

[3] J. Ali, R.W. Burley, and C.W. Nutt. Foam Enhanced Oil Recovery from Sand Packs. *Chem. Eng. Res. Des.*, 63:101–111, 1985.

[4] P. Armitage and R.A. Dawe. What Is the Rheology of Foam in Porous Media? Paper SPE 18495 presented at the International Symposium on Oilfield Chemistry, Houston, TX, Feb. 8-10, 1989.

[5] G.G. Bernard and L.W. Holm. Effect of Foam on Permeability of Porous Media to Gas. *SPEJ*, 4:267–274, 1964.

[6] G.G. Bernard, L.W. Holm, and W.L. Jacobs. Effect of Foam on Trapped Gas Saturation and on Permeability of Porous Media to Water. *SPEJ*, 5:295–300, 1965.

[7] J.J. Bikerman. The Unit of Foaminess. *Trans. Faraday Soc.*, 34:634–638, 1938.

[8] J.J. Bikerman. *Foams.* Springer-Verlag, New York, 1973.

[9] J.K. Borchardt, D.B. Bright, M.K. Dickson, and S.L. Wellington. Surfactants for CO2 Foam. *ACS Symposium Series*, (373):163–180, 1987. Surfactant-Based Mobility Control.

[10] F.P. Bretherton. *J. Fluid Mech.*, 10:166, 1961.

[11] W.E. Brigham, J.A. Marcou, S.K. Sanyal, O.P. Malito, and L.M. Castanier. A Field Experiment of Improved Steam Drive with In-Situ Foaming. Paper SPE 12784 presented at the California Regional Meeting, Long Beach, CA, April 11-13, 1984.

[12] M. Burkowsky and C. Marx. Applications for the Spinning-Drop Technique for Determining Low Interfacial Tensions. *Tenside Detergents*, 15, 1978.

[13] K.T. Chambers and C.J. Radke. *Interfacial Phenomena in Petroleum Recovery.* Marcel Dekker, Inc., New York, 1990. N.R. Morrow, Editor.

[14] I. Chatzis and N.R. Morrow. Correlation of Capillary Number Relationships for Sandstone. *SPEJ*, 24:555–562, 1984.

[15] H-L. Chen, M-J. Ke, T-K. Chuang, and R.W. Flumerfelt. Experimental Studies of Capillary Pressure Effects of Foams in Porous Media. Paper SPE 20069 presented at the 60th California Regional Meeting, Ventura, CA, April 4-6, 1990.

[16] Y. Cheng-Zhi and H. Da-Kuang. Maitrise de l'adsorption de l'alkylbenezene sulfonate de sodium en solution sur l'argile par le polyelectrolyte. *EOR Meeting in Rome*, 1985.

[17] J.C. Chiang, S.K. Sawyal, L.M. Castanier, W.E. Brigham, and A. Sufi. Foam as a Mobility Control Agent in Steam Injection Processes. Paper SPE 8912 presented at the California Regional Meeting, Los Angeles, CA, April 1980.

[18] F.T.H. Chung and D.A. Hudgins. Development of an Engineering Methodology for Applying Foam Technology. *DOE Report*, (NIPER-374 (DE 89000740)), 1989.

[19] S.E. Dellinger, J.T. Patton, and S.T. Hollbrook. CO2 Mobility Control. *SPEJ*, 24:191–196, 1984.

[20] B.V. Derjaguin, Y.I. Rabinovich, and N.V. Churnaev. Direct Measurement of Molecular Forces. *Nature*, 272:313–318, 1978.

[21] C.H. Desch. *Rec. Trav. Chim.*, 42:822, 1923.

[22] D.N. Dietz, J. Bruining, and H.B. Heijna. Foamdrive Seldom Meaningful. *JPT*, 37:921–922, 1985.

[23] R.E. Dilgren, A.R. Deemer, and K.B. Owens. The Laboratory Development and Field Testing of Steam/Noncondensible Gas Foams for Mobility Control in Heavy Oil Recovery. Paper SPE 10774 presented at the California Regional Meeting, San Francisco, CA, March 24-26, 1982.

[24] R.E. Dilgren and K.B. Owens. Surfactant-Enhanced Steam Drives for Heavy Oil Recovery. *J. Amer. Oil Chem. Soc.*, 59:818A–822A, 1982.

[25] N.F. Djabbarah, S.L. Weber, D.C. Freeman, J.A. Muscatello, J.P. Ashbaugh, and T.E. Covington. Laboratory Design and Field Demonstration of Steam Diversion with Foam. Paper 20067 presented at the California Regional Meeting, Ventura, CA, April 4-6, 1990.

[26] T.M. Doscher and E.C. Hammershaimb. Field Demonstration of Steam Drive with Ancillary Materials. *JPT*, 34:1535–1542, 1982.

[27] T.M. Doscher, M.K. Hosseinmardi, and S.Y. Baghdikian. On the Equivalence of a Hot Water and Gas Drive to a Steamdrive. Paper SPE 13657 presented at the California Regional Meeting, Bakersfield, CA, March 27-29, 1985.

[28] T.M. Doscher and V.A. Kuuskraa. Reviving Heavy-Oil Reservoirs with Foam and Steam. *Oil and Gas J.*, 80:99–105, 1982.

[29] T.M. Doscher, V.A. Kuuskraa, and E.C. Hammershaimb. Analysis of Five Field Tests of Steamdrive Additives. Paper SPE 12057 presented at the 58th Annual Technical Conference and Exhibition, San Francisco, CA, Oct. 5-8 1983.

[30] J.H. Duerksen. Laboratory Study of Foaming Surfactants as Steam-Diverting Additives. *SPE Res. Eng.*, 1:44–52, 1986.

[31] J.M. Dumore and R.S. Schols. Drainage Capillary-Pressure Functions and the Influence of Connate Water. *SPEJ*, 14:437–444, 1974.

[32] G.K. D'yakonov. Application of the Theory of Similarity to the Study of the Process of Foam Formation. *Zh. Tekhn. Fiz.*, 12:302–314, 1942.

[33] M.M. El-Gassier. *The Effect of Temperature on Interfacial Tension of Surfactant-Oil Systems.* PhD thesis, University of Southern California, Los Angeles, 1980.

[34] R.L. Eson and R.W. Cooke. A Comprehensive Analysis of Steam Foam Diverters and Application Methods. Paper SPE 18785 presented at the California Regional Meeting, Bakersfield, CA, April 5-7, 1989.

[35] R.L. Eson and S.K. O'Nesky. The Application of In-Situ Steam Foams to Improve Recovery in Mature Steam Drives. Paper SPE 11704 presented at the California Regional Meeting, Ventura, CA, March 23-25,1983.

[36] R.A. Ettinger and C.J. Radke. The Influence of Texture on Steady State Foam Flow in Berea Sandstone. Paper SPE 19688 presented at the 64th Annual Technical Conference and Exhibition of SPE, San Antonio, TX, Oct. 8-11, 1989.

[37] A.H. Falls, G.J. Hirasaki, T.W. Patzek, P.A. Gauglitz, D.D. Miller, and J. Ratulowski. Development of a Mechanistic Foam Simulator: The Population Balance and Generation by Snap-Off. *SPE Res. Eng.*, 3:884–892, 1988.

[38] A.H. Falls, J.B. Lawson, and G.J. Hirasaki. The Role of Noncondensable Gas in Steam Foams. *JPT*, 40:95–104, 1988.

[39] A.H. Falls, J.J. Musters, and J. Ratulowski. The Apparent Viscosity of Foams in Homogeneous Beadpacks. *SPE Res. Eng.*, 4:155–164, 1989.

[40] R.W. Flumerfelt, H-L. Chen, W. Ruengphrathuengsuka, W-F. Hsu, and J. Prieditis. Network Analysis of Capillary and Trapping Behavior of Foams in Porous Media. Paper SPE 20066 presented at the California Regional Meeting, Ventura, CA, April 4-6, 1990.

[41] R.W. Flumerfelt and J. Prieditis. Mobility of Foam in Porous Media. *ACS Symposium Series*, (373), 1988. Surfactant-Based Mobility Control.

[42] A.N. Fried. Foam-Drive Process for Increasing the Recovery of Oil. *U.S. Bureau of Mines Report of Investigation*, 1961.

[43] F. Friedmann, W.H. Chen, and P.A. Gauglitz. Experimental and Simulation Study of High-Temperature Foam Displacement in Porous Media. Paper SPE 17357 presented at the SPE/DOE Enhanced Oil Recovery Symposium, Tulsa, OK, April 17-20, 1988.

[44] F. Friedmann and J.A. Jensen. Some Parameters Influencing the Formation and Propagation of Foam in Porous Media. Paper SPE 15087 presented at the California Regional Meeting, Oakland, CA, April 2-4, 1986.

[45] F. Friedmann, M.E. Smith, W.R. Guice, J.M. Gump, and D.G. Nelson. Steam Foam Mechanistic Field Trial in the Midway-Sunset Field. Paper SPE 21780 presented at the Western Regional Meeting, Long Beach, CA, March 20-22, 1991.

[46] P.A. Gauglitz, C.M. St. Laurent, and C.J. Radke. An Experimental investigation of gas-bubble breakup in constricted square capillaries. *JPT*, 39:1137–1146, 1987.

[47] P.A. Gauglitz, C.M. St. Laurent, and C.J. Radke. Experimental Determination of Gas-Bubble Breakup in a Constricted Cylindrical Capillary. *Ind. Eng. Chem. Res.*, 27(7):1282–1291, 1988.

[48] J.W. Gibbs. *The Collected Works of J.W. Gibbs*, volume 1. Longmans, New York, 1931.

[49] F.W. Gray, J.F. Gerecht, and I.J. Krems. The Preparation of Model Long Chain Alkylbenzenes and a Study of their Isomeric Sulfonation Products. *J. Org. Chem.*, 20(511-524), 1955.

[50] J. Hagoort. Oil Recovery by Gravity Drainage. *SPEJ*, 20:139–150, 1980.

[51] L.L. Handy. Behaviour of Surfactants in EOR Applications at High Temperatures. *Proceedings to the European Symposium on Enhanced Oil Recovery*, 1981. Bournemouth, England.

[52] L.L. Handy. Fluid Flow Through Porous Media. Personal Notes, 1984.

[53] L.L. Handy, J.O. Amaefule, V.M. Ziegler, and I. Ershaghi. Thermal Stability of Surfactants for Reservoir Application. Paper SPE 7867 presented at the International Symposium on Oilfield and Geothermal Chemistry, Houston, TX, Jan. 22-24, 1979.

[54] L.L. Handy, M. El-Gassier, and I. Ershaghi. A Modified Spinning Drop Method for High-Temperature Applications. *SPEJ*, 23:155–156, 1983.

[55] H.S. Hanna and P. Somasundaran. Equilibration of Kaolinite in Aqueous Inorganic and Surfactant Solutions. *J. of Col. & Int. Sci.*, 70(1):181–191, 1979.

[56] J.P. Heller and M.S. Kuntamukkula. Critical Review of the Foam Rheology Literature. *Ind. Eng. Chem. Res.*, 26(2):318–325, 1987.

[57] G.J. Hirasaki. Supplement to SPE 19505, The Steam Foam Process. Paper SPE 19518 available from SPE Book Order Dept., Richardson, TX, 1989.

[58] G.J. Hirasaki. The Steam-Foam Process. *JPT*, 41:449–456, 1989.

[59] G.J. Hirasaki and J.B. Lawson. Mechanisms of Foam Flow Through Porous Media - Apparent Viscosity in Smooth Capillaries. *SPEJ*, 25:176–190, 1985.

[60] L.W. Holm. The Mechanisms of Gas and Liquid Flow Through Porous Media in the Presence of Foam. *SPEJ*, 8:359–69, 1968.

[61] K.C. Hong and J.W. Ault. Effects of Noncondensable Gas Injection on Oil Recovery by Steamflooding. Paper SPE 11702 presented at the California Regional Meeting, Ventura, CA, March 23-25, 1983.

[62] D.G. Huh. *Flow of Gas and Foaming Solution Through Consolidated Porous Media.* PhD thesis, University of Southern California, Los Angeles, 1986.

[63] D.G. Huh, T.D. Cochrane, and F.S. Kovarik. The Effect of Microscopic Heterogeneity on CO2/Foam Mobility: Part 1 - a Mechanistic Study. Paper SPE 17359 presented at the SPE/DOE Enhanced Oil Recovery Symposium, Tulsa, OK, April 17-20, 1988.

[64] E.E. Isaacs, L. Jian, K. Green, C. McCarthy, and D. Maunder. Use of Foam-Forming Surfactants to Enhance the Recovery of Heavy Oils. *AOSTRA J. of Res.*, 4:267–276, 1988.

[65] E.E. Isaacs and K.F. Smolek. Interfacial Tension Behavior of Athabasca Bitumen/Aqueous Surfactant System. *Can. J. of Chem. Engr.*, 61:233–240, 1983.

[66] I.B. Ivanov. *Thin Liquid Films - Fundamentals and Applications.* Marcel Dekker, Inc., New York, 1988.

[67] J.A. Jensen and F. Friedmann. Physical and Chemical Effects of an Oil Phase on the Propagation of Foam in Porous Media. Paper SPE 16375 presented at the California Regional Meeting, Ventura, CA, April 8-10, 1987.

[68] A.I. Jimenez and C.J. Radke. *Dynamic Stability of Foam Lamellae Flowing Through a Peridically Constricted Pore.* Number 396. 1989. Oil Field Chemistry.

[69] F.F. Craig Jr. *The Reservoir Engineering Aspects of Waterflooding*, volume 3. SPE of AIME, 1980. 3rd Printing, Monograph in Henry L. Doherty Series.

[70] M. Kanda and R.S. Schechter. On the Mechanisms of Foam Formation in Porous Media. Paper SPE 6200 presented at the 51st Annual Technical Conference and Exhibition, New Orleans, Oct. 3-6, 1976.

[71] A. Kantzas, I. Chatzis, and F.A.L. Dullien. Enhanced Oil Recovery by Inert Gas Injection. Paper SPE 17379 presented at the SPE/DOE Enhanced Oil Recovery Symposium, Tulsa, OK, April 17-20, 1988.

[72] Z.I. Khatib, G.J. Hirasaki, and A.H. Falls. Effects of Capillary Pressure on Coalescence and Phase Mobilities in Foams Flowing Through Porous Media. *SPE Res. Eng.*, 3:919–926, 1988.

[73] D.L. Kuehne, D.I. Ehman, A.S. Emanuel, and C.F. Magnani. Design and evaluation of a nitrogen-foam field trial. *JPT*, 42(504-512), 1990.

[74] G.S. Kular, K. Lowe, and D. Coombe. Foam Application in an Oil Sands Steamflood Process. Paper SPE 19690 presented at the 64th Annual Technical Conference and Exhibition, San Antonio, TX, Oct. 8-11, 1989.

[75] H.C. Lau and J.K. Borchardt. Improved Steam Foam Formulations: Concepts and Laboratory Results. Paper SPE 18783 presented at the California Regional Meeting, Bakersfield, CA, April 5-7, 1989.

[76] H.C. Lau and S.M. O'Brien. Effects of Spreading and Nonspreading Oils on Foam Propagation Through Porous Media. *SPE Res. Eng.*, 3:893–896, 1988.

[77] J.B. Lawson and R.E. Dilgren. Adsorption of Sodium Alkyl Aryl Sulfonate on Sandstone. Paper SPE 6121 presented at the 51st Annual Fall Technical Conference and Exhibition, New Orleans, LA, Oct. 3-6, 1976.

[78] P.C. Liu and G.J. Besserer. Application of Foam Injection in Triassic Pool, Canada: Laboratory and Field Test Results. Paper SPE 18080 presented at the 63rd Annual Technical Conference and Exhibition, Oct. 2-5, 1988.

[79] B.B. Maini and V. Ma. Relationship Between Foam Stability Measured in Static Tests and Flow Behavior of Foams in Porous Media. Paper SPE 13073 presented at the 59th Annual Technical Conference and Exhibition, Houston, TX, Sept. 16-19, 1984.

[80] E. Manegold. *Schaum, Strassenbau, Chemie und Technik.* Heidelberg, 1953.

[81] D.J. Manlowe and C.J. Radke. A Pore-Level Investigation of Foam/Oil Interactions in Porous Media. Paper SPE 18069 presented at the 63rd Annual Technical Conference and Exhibition, Houston, TX, Oct. 2-5, 1988.

[82] K. Mannhardt, L.L. Schramm, and J.J. Novosad. Effect of Rock Type and Brine Composition on Adsorption of Two Foam-Forming Surfactants. Paper SPE 20463 presented at the 65th Annual Technical Conference and Exhibition, New Orleans, LA, Sept. 23-26, 1990.

[83] S.S. Marsden and S.A. Khan. The Flow of Foam Through Short Porous Media and Apparent Viscosity Measurements. *SPEJ*, 6:17–25, 1966.

[84] R.F. Mast. Microscopic Behavior of Foam in Porous Media. Paper SPE 3997 presented at the 47th Annual Fall Meeting, San Antonio, TX, Oct. 8-11, 1972.

[85] E.B. Matzke. The Three-Dimensional Shape of Bubbles in Foam – An Analysis of the Role of Surface Forces in Three-Dimensional Cell Shape Determination. *Am. J. Bot.*, 33:58–80, 1946.

[86] C.A. McPhee, A.D.H. Tehrani, and R.P.S. Jolly. Foam Flooding of Cores Under North Sea Reservoir Conditions. Paper SPE 17360 presented at the SPE/DOE Enhanced Oil Recovery Symposium, Tulsa, OK, April 17-20, 1988.

[87] K.F. Michaels and K.S. Udell. Foam Production During Steam Displacement of Aqueous Surfactants. *SPE Res. Eng.*, 3:897–901, 1988.

[88] L. Minssieux. Oil Displacement by Foams in Relation to Their Physical Properties in Porous Media. *JPT*, 26:100–108, 1974.

[89] S.S. Mohammadi and T.J. McCollum. Steam-Foam Pilot Project in Guadalupe Field, California. Paper SPE 15054 presented at the California Regional Meeting, Oakland, CA, April 2-4, 1986.

[90] S.S. Mohammadi, D.C. Van Slyke, and B. Ganong. Steam-Foam Project in Dome-Tumbador, Midway Sunset Field. *SPE Res. Eng.*, 4:7–16, 1989.

[91] H.M. Muijs, P.P.M. Keijzer, and R.J. Wiersma. Surfactants for Mobility Control in High-Temperature Steam-Foam Applications. Paper SPE 17361 presented at the SPE/DOE Enhanced Oil Recovery Symposium, Tulsa, OK, April 17-20, 1988.

[92] B.H. Nahid. *Non-Darcy Flow of Gas Through Porous Media in the Presence of Surface Active Agents.* PhD thesis, University of Southern California, Los Angeles, 1971.

[93] O.S. Owete and W.E. Brigham. Flow Behavior of Foam: a Porous Micromodel Study. *SPE Res. Eng.*, 2:315–323, 1987.

[94] J.T. Patton, S.T. Holbrook, and W. Hsu. Rheology of Mobility-Control Foams. *SPEJ*, 23:456–460, 1983.

[95] T.W. Patzek and M.T. Koinis. Kern River Steam-Foam Pilots. *JPT*, 42:496–503, 1990.

[96] T.W. Patzek and N.A. Myhill. Simulation of the Bishop Steam Foam Pilot. Paper SPE 18786 presented at the California Regional Meeting, Bakersfield, CA, April 5-7, 1989.

[97] P. Persoff, C.J. Radke, K. Pruess, S.M. Benson, and P.A. Witherspoon. A Laboratory Investigation of Foam Flow in Sandstone at Elevated Pressure. Paper SPE 18781 presented at the California Regional Meeting, Bakersfield, CA, April 5-7, 1989.

[98] J. Plateau. *Mem. Acad. Roy. Sci. Belg.*, 37(49), 1869.

[99] J. Plateau. *Statique Experimentale et Theorique des Liquides Soumis aux Seules Forces Moleculaire*, volume 1. Gauthier-Villars, 1873.

[100] J.F. Ploeg and J.H. Duerksen. Two Successful Steam/Foam Field Tests, Sections 15a and 26c, Midway-Sunset Field. Paper SPE 13609 presented at the California Regional Meeting, Bakersfield, CA, March 27-29, 1985.

[101] C.J. Radke and J.V. Gillis. A Dual Gas Tracer Technique for Determining Trapped Gas Saturation During Steady Foam Flow in Porous Media. Paper SPE 20519 presented at the 65th Annual Technical Conference and Exhibition, New Orleans, LA, Sept. 23-26, 1990.

[102] W. Ramirez, F.F. Friedmann, L.C. Demoyelle, and P.J. Schuler. Adsorption and Interfacial Tension Dynamics of Surfactants in Porous Media. Paper SPE 9280 presented at the Annual Fall Technical Conference and Exhibition, Dallas, TX, Sept. 21-24, 1980.

[103] T.C. Ransohoff, P.A. Gauglitz, and C.J. Radke. Snap-Off of Gas Bubbles in Smoothly Constricted Noncircular Capillaries. *AICHEJ*, 33(5):753–765, 1987.

[104] T.C. Ransohoff and C.J. Radke. Mechanisms of Foam Generation in Glass-Bead Packs. *SPE Res. Eng.*, 3:573–585, 1988.

[105] A.A. Rao. Master's thesis, Illinois Institute of Technology, Chicago, 1980.

[106] K.T. Raterman. An Investigation of Oil Destabilization of Nitrogen Foams in Porous Media. Paper SPE 19692 presented at the 64th Annual Technical Conference and Exhibition, San Antonio, TX, Oct. 8-11, 1989.

[107] S.H. Raza. Foam in Porous Media: Characteristics and Potential Applications. *SPEJ*, 10:328–336, 1970.

[108] Robin. Laboratory Evaluation of Foaming Additives Used to Improve Steam Efficiency. Paper SPE 16729 presented at the 62nd Annual Technical Conference and Exhibition, Dallas, TX, Sept. 27-30, 1987.

[109] J.G. Roof. Snap-Off of Oil Droplets in Water-Wet Pores. *SPEJ*, 10:85–90, 1970.

[110] S. Ross. Bubbles and Foam. *Ind. and Eng. Chem.*, 61(10):48–57, 1969.

[111] S. Ross, A.F. Hughes, M.L. Kennedy, and A.R. Mardoian. The Inhibition of Foaming. V. Synergistic Effects of Antifoaming Agents. *J. Phys. Chem.*, 57:684–686, 1953.

[112] S. Ross and Y. Suzin. Measurement of Dynamic Foam Stability. *Langmuir*, 1:145–149, 1985.

[113] S. Ross and G.J. Young. Action of Antifoaming Agents at Optimum Concentrations. *Ind. and Eng. Chem.*, 43(11):2520–2525, 1951.

[114] W.R. Rossen. Theories of Foam Mobilization Pressure Gradient. Paper SPE 17358 presented at the SPE/DOE Enhanced Oil Recovery Symposium, Tulsa, OK, April 17-20, 1988.

[115] W.R. Rossen and P.A. Gauglitz. Percolation Theory of Creation and Mobilization of Foams in Porous Media. *AICHEJ*, 36(8):1176–1188, 1990.

[116] E. Rubin and C.J. Radke. Interfacial Tension Minima in Finite Systems. *Chem. Eng. Sci.*, 35, 1980.

[117] J.M. Sanchez and R.D. Hazlett. Foam Flow Through an Oil-Wet Porous Medium: a Laboratory Study. Paper SPE 19687 presented at the 64th Annual Technical Conference and Exhibition, San Antonio, TX, Oct. 8-11, 1989.

[118] J.M. Sanchez, R.S. Schechter, and A. Monsalve. The Effect of Trace Quantities of Surfactant on Nitrogen/Water Relative Permeabilities. Paper SPE 15446 presented at the 61st Annual Technical Conference and Exhibition, New Orleans, LA, Oct. 5-8, 1986.

[119] R. Schmidt. Thermal Enhanced Oil Recovery - Current Status and Future Needs. *Chemical Engineering Progress*, 86:47–59, 1990.

[120] H.W. Schwarz. *Rec. Trav. Chim.*, 84:771, 1965.

[121] A.I. Shirley. *Foam Formation in Porous Media: A Microscopic Visual Study.* Number 373. 1987. Surfactant-Based Mobility Control.

[122] F.E. Suffridge, K.T. Raterman, and G.C. Russell. Foam Performance Under Reservoir Conditions. Paper SPE 19691 presented at 64th Annual Technical Conference and Exhibition, San Antonio, TX, Oct. 8-11, 1989.

[123] R.D. Swisher. *Surfactant Biodegradation*, volume 18. Marcel Dekker Inc., New York, 1987.

[124] J.J. Taber. Dynamic and Static Forces Required to Remove a Discontinuous Oil Phase from Porous Media Containing Both Oil and Water. *SPEJ*, 9:3–12, 1969.

[125] P.G. Tait. *Properties of Matter.* Number 12. A. and C. Black, Edinburgh, 1885.

[126] F.J. Trogus, R.S. Schechter, and W.H. Wade. A New Interpretation of Adsorption Maxima and Minima. *J. of Col. & Int. Sci.*, 70(2):293–305, 1979.

[127] F.J. Trogus, T. Sophany, R.S. Schechter, and W.H. Wade. Static and Dynamic Adsorption of Anionic and Nonionic Surfactants. Paper SPE 6004 presented at the 51st Annual Technical Conference and Exhibition, New Orleans, TX, Oct. 3-6, 1976.

[128] A.J. De Vries. Foam Stability. *Rubber Chemistry and Technology*, 5:1142–1205, 1958.

[129] A.S. De Vries and K. Wit. Rheology of Gas/Water Foam in the Quality Range Relevant to Steam Foam. *SPE Res. Eng.*, 5:185–192, 1990.

[130] R.C. Watkins. An Improved Foam Test for Lubricating Oils. *J. of the Inst. of Pet.*, 59(567):106–113, 1973.

[131] S.L. Wellington and H.J. Vinegar. CT Studies of Surfactant-Induced CO2 Mobility Control. Paper SPE 14393 presented at the 60th Annual Technical Conference and Exhibition, Las Vegas, NV, Sept. 22-25, 1985.

[132] A.Y. Zekri. *Interfacial Tension of Surfactant Mixtures Against Hydrocarbon Liquids at Elevated Temperatures and Pressures.* PhD thesis, University of Southern California, Los Angeles, 1981.

[133] V.M. Ziegler. Laboratory Investigation of High-Temperature Surfactant Flooding. *SPE Res. Eng.*, 3:586–596, 1988.

[134] V.M. Ziegler and L.L. Handy. Effect of Temperature on Surfactant Adsorption in Porous Media. *SPEJ*, 21:218–228, 1981.

Appendix A

DATA ACQUISITION SYSTEM

A data acquisition system provides an automatic and error-free method for transferring data directly from measurement intruments to a personal computer for analysis and storage. It takes the signals produced by temperature sensors, pressure transducers, flowmeters, etc, and converts them into a form that the computer can understand. With a data acquisition system (DAS), the computer is used to gather, monitor, display and analyze data. If the acquisition system has output capabilities, the computer may also be used to accurately control processes for maximum efficiency.

A data acquisition software works with the hardware interface. The software is designed to display the data in tables like a spreadsheet, or in histogram charts, pie charts, line plots, and to analyze the data using transforms and curve-fitting.

Basically there are two kinds of interface systems, plug-in and stand-alone. A plug-in system plugs right into the computer. It is designed for a specific computer type, such as the IBM PC or Apple II series. The plug-in card has an external terminal board that attaches it, and that is where all the connections are made for thermocouples, other sensors, and outputs. These cards come with menu-driven software that allows the setup of each input channel for the input type, range, scaling for engineering units, digital input and output capabilities, data logging and control. They can be expanded quickly and easily by just plugging in another card. Depending on the system, one can have up to 240 analog inputs for an IBM. The other type of interface is not dependent upon the computer type. All the computer needs is a standard serial communications port. This "stand-alone" interface can talk to any computer with that port. It is important to note, however, that only the plug-in cards come with software programs.

Lotus Measure, a DAS software produced by Lotus Development Company, allows engineers and scientists to collect measurements directly from instruments and devices into the Lotus 1-2-3 environment for immediate analysis, graphic display and storage. In 1988, National Instruments acquired exclusive rights for support, distribution, marketing and future development of Lotus Measure.

Measure is fully integrated with Lotus 1-2-3; together, the two programs perform as a single software package. Measure and 1-2-3 have the same user interface and the same macro environment, so a macro can incorporate both 1-2-3 and Measure functions. Thus, the user can write a single macro to perform an entire data collection, analysis, display and storage procedure. Measure also has context sensitive help menus.

Measure provides three methods of acquiring data. First, Measure can control test and measurement instruments and accept data from them using the IEEE-488 interface bus. The

second method uses the PC's RS-232C port. Measure's third method of acquiring data is via plug-in data-acquisition boards for the IBM PC. The product supports Metrabyte's DASH-16 board and the IBM Game Card Adapter. The software acquires as many as 64 channels of data simultaneously. It reads in data as letters or in numeric or binary formats. The user writes the code to convert incoming measurements to engineering units. Measure is able to perform conversions on-the-fly as it acquires data.

The product acquires data in stages. Each stage consists of the set of data collected from one starting point, as determined by a trigger, to a stopping time. During a stage, Measure can acquire data collected from channels that are sampled at different rates.It acts as a dynamic driver for Lotus 1-2-3. The user is able to load it by defining it as part of the 1-2-3 hardware set when loading 1-2-3.

To run Measure, the user needs an IBM PC, XT or AT; a Compaq Portable or a Hewlett-Packard Vectra PC with at least 512KB of RAM; and either a Hercules Graphics Card, an IBM Color Graphics Adapter or Enhanced Graphics Adapter. The software required to run Measure is DOS Version 2.0 or higher and Lotus 1- 2-3, Release 2.0 or higher.

The Lotus Measure MBC16.DRV Module has to be added to the 123.SET driver file. Driver sets are updated or deleted using the program provided with Lotus Measure called NEWLIB.EXE. It is important to note that in order to access the context-sensitive Lotus Measure help menu, the file MBC16.HLP has to reside on the Lotus 1-2-3 Program disk for a two floppy computer system user. The driver 123.SET has to be loaded from drive B: as the Lotus Program disk does not have sufficient space for the file. Those using a hard disk do not encounter this problem.

Once Lotus Measure is installed, it is automatically loaded with Lotus 1-2-3. It can be accessed by pressing ALT-F8. The commands in the opening menu perform the following tasks:

- Go: starts a data acquisition run.
- Verify: is used before selecting Go. Verify confirms that you have entered all the necessary settings, a sample number, and a sampling rate. If there is information missing, Verify points this out.
- Observe: presents a screen displaying the current input values of up to 16 of the defined inputs.
- ID-Settings: allows the user to select an analog or digital input channel on the A/D board, and then set up ranges and formulas for the data being collected.
- Stage-Settings: allows the user to define a period of data acquisition, also called a stage.
- Quit: returns the user to the 1-2-3 worksheet.

After selecting the desired set of parameters in the Stage-Settings and ID-Settings menus, a data acquisition run can be performed. When one selects Go, the MBC16 module performs the following operations:

- Evaluates the current settings for interdependencies and missing information.

- Allocates memory according to the number of samples about to be collected.
- Acquires data and stores it in memory.

When the acquisition is completed or interrupted using Ctrl-Brk, the MBC16 module applies the conversion formula as specified and data is placed in the appropriate 1-2-3 worksheet range and the MBC16 main menu appears. When one exits the data acquisition menu, Lotus recalculates the spreadsheet. The data is now ready to be analyzed or graphed.

Further details about the installation and usage of Lotus 1-2-3 and Lotus Measure are available in the reference manuals.

1. Lotus Measure Reference Manual, Lotus Development Corporation, Cambridge, MA, 1986.
2. Complete Data Acquisition and Computer Interface Handbook and Encyclopedia, OMEGA, Vol. 1, 1986.

END

DATE FILMED

10/02/91